UNIVERSITÀ DEGLI STUDI DI PADOVA

Sede Amministrativa: Università degli Studi di Padova

Dipartimento di Ingegneria Industriale

SCUOLA DI DOTTORATO DI RICERCA IN INGEGNERIA INDUSTRIALE

INDIRIZZO: Ingegneria Chimica, dei Materiali e della Produzione

CICLO: XXVI

OPTIMIZATION OF HIGH CARBON AUSTENITIC MANGANESE STEELS FOR COMMINUTION PROCESSES

Direttore della Scuola: Prof. Paolo Colombo

Coordinatore d'indirizzo: Prof. Enrico Savio

Supervisore: Prof. Manuele Dabalà

Dottorando: Rodrigo Lencina

PREFACE

This thesis was submitted to the Doctoral School of Industrial Engineering of the University of Padua in partial fulfilment of the requirements for the degree of Doctor in Industrial Engineering.

The author was granted an Erasmus Mundus BAPE scholarship, from a consortium of Universities that included UNIPD and the University of Catamarca, Argentina.

The research project was sponsored by □□□□□□□□ □□□□□□□□□□ □□□□□□ □□□, of □□□□□ (□□), Italy, that provided financial support and the facilities for the development of the work.

ABSTRACT

Austenitic manganese steels are widely used in mineral comminution processes due to their good wear resistance and high toughness. The classical chemical composition for austenitic manganese steel in these applications is about 12%Mn and 1.2%C, steel first produced by R. Hadfield more than a century ago. Ever since, many efforts to improve its mechanical properties and wear resistance have been made, mostly driven by the continuous demand of the mining industry for bigger crushing equipment and lower production costs.

In this work, two types of austenitic manganese steels containing a relative high content of carbon are investigated. The high carbon content provided the steels good wear resistance, but compromises their mechanical properties. An important deleterious effect observed due to high carbon content was embrittlement due to the precipitation of carbides at grain boundary.

Another important feature of the steels under study was their difference in manganese content, which played an important role in stabilizing carbon in the austenitic matrix. Furthermore, both steels contained titanium, which contributed to increase wear resistance through the formation of a hard phase of stable carbides.

Heat treatments were performed, aimed to solubilize precipitated carbides and to improve quenching conditions, in order to avoid reprecipitation of these carbides, especially in thick castings. The results presented showed a correct selection of the temperature for austenitization and, additionally, a characterization of the kinetics of the re-precipitation phenomenon.

After the improvements of the microstructure, the steels were tested in pilot scale crushers to assess their wear properties. Additionally, field tests were performed as well in industrial applications: in a cone crusher, a horizontal shaft impactor and a hammermill.

The results of the metallurgical and tribological studies demonstrated the need for improvements in the chemical composition of the steels. For this reason, different elements, such as Nb, Al, Ni, Mo, were added to the composition of the steels. Finally, a cost estimation of the industrial production of these new steels was performed, in order to assess their economic feasibility.

The results showed that the phenomenon of carbide re-precipitation is the main reason for embrittlement. Manganese content was the most important variable to stabilize the microstructure. The addition of Ni to this steel resulted in an improvement of mechanical properties, while maintaining the good wear resistance.

Two appendixes are included with original research work that was secondary to the scope of the thesis project. The first, presents a mathematical model that simulates the granulometric curve of the product from a crusher, but taking in consideration the wear in the liners of the machine. The other, presents an ultrasound treatment, which had comminution effects in different types of mineral particles. Ultrasound was tested as well in a leaching process to investigate their kinetic enhancement effects.

SOMMARIO

Gli acciai austenitici al manganese sono largamente utilizzati nell'industria mineraria poiché hanno un'elevata resistenza all'abrasione e un altissima tenacità. La composizione chimica più diffusa nell'attività mineraria è di circa 1.2% C e 12% Mn, composizione che è stata prodotta per prima volta da R. Hadfield più di un secolo fa. Da questo momento, molte ricerche sono state eseguite per migliorare le proprietà meccaniche e la resistenza all'usura di questi acciai. Soprattutto perché la industria mineraria attuale richiede costi di produzione più bassi e frantoi con più grande capacità.

In questo studio, sono presentati due acciai austenitici al manganese, i cui contenuti di carbonio sono considerevolmente alti. Questo contenuto di carbonio fornisce agli acciai buona resistenza all' usura, ma diminuisce le proprietà meccaniche. Un effetto non desiderato del alto contenuto di carbonio è il infragilimento dovuto alla re-precipitazione di carburi a bordo grano.

Un'altra caratteristica importante degli acciai studiati è il loro contenuto di manganese, che ha avuto un ruolo preponderante nella stabilizzazione del carbonio nella matrice austenitica. Anche, entrambi acciai contenevano del titanio, elemento che ha contribuito a incrementare la resistenza all'usura tramite la formazione di carburi duri e stabili.

Sono stati eseguiti dei trattamenti termici allo scopo di solubilizzare delle fasi precipitate e anche a migliorare la condicione di tempra in modo di evitare la re-precipitazione di questi carburi, specialmente nei getti di grosso spessore. I resultati ottenuti forniscono una temperatura ottimale per la austenitizazione degli acciai e anche, caratterizzano la cinetica di re-precipitazione dei carburi a bordo grano.

Dopo le procedure di miglioramento della microstruttura, i due acciai sono stati testati a scala pilota utilizzando dei piccoli frantoi. Anche, sono stati eseguiti test sul terreno, in diverse machine a livello industriale: frantoio a cono, mulino a asse orizzontale e mulino a martelli.

I resultati delle studi metallurgici e tribologici hanno dimostrato la necessita di miglioramenti nella composizione chimica degli acciai. Quindi, diversi elementi sono stati aggiunti agli acciai (Nb, Al, Ni, Mo). Alla fine, è stata eseguita una stimazione dei costi di produzione per gli nuovi acciai, allo scopo di valutare la loro fattibilità economica.

Pertanto, è stato dimostrato che il fenomeno di re-precipitazione è la causa più importante del infragilimento. Il contenuto di manganese è stato la varabile più importante per stabilizzare la microstruttura. La aggiunta di nichel a questo acciaio a permesso la migliora delle proprietà meccaniche, e allo stesso tempo di mantenere la resistenza all'usura.

Se inseriscono due appendici contenenti lavori di ricerca che non apparteneva allo scopo principale della tesi. La prima appendice tratta un modello matematico che simula la curva granulometrica del prodotto appartenete a un frantoio. Il modello prende in considerazione la perdita di qualità dovuta alla usura dei rivestimenti. L'altra appendice parla di un trattamento di ultrasuono eseguito allo scopo di macinare delle diverse particelle di rocce. Anche, questo trattamento è stato impiegato in uno sperimento idrometallurgico allo scopo di verificare l'incremento della cinetica di lisciviazione.

RESUMEN

Los aceros austeniticos al manganeso son ampliamente utilizados en los procesos de conminución de minerales debido a si buena resistencia al desgaste y su alta tenacidad. La composición química clásica de estos aceros, en este tipo de aplicaciones, consiste en un 1.2% de carbono y un 12% de manganeso. Dicha composición fue producida por primera vez por R. Hadfield hace más de cien años. Desde aquel entonces, se han realizado muchos esfuerzos para mejorar sus propiedades mecánicas y su resistencia al desgaste, mas que nada, debido a la demanda continua por parte de la industria minera de maquinas con mayor capacidad y costos de producción mas bajos.

En este trabajo se presentan dos aceros austeniticos al manganeso cuya característica más relevante es el elevado contenido de carbono. Dicha característica permite a los aceros tener una alta resistencia al desgaste, pero al mismo tiempo perjudica sus propiedades mecánicas. En particular, uno de los efectos mas perjudiciales es la fragilizacion del acero debido a la precipitación de carburos en el borde del grano.

Otra característica importante de estos aceros presentados en este trabajo es su contenido de manganeso, que es distinta para ambos, debido a que el manganeso tuvo un rol importante en la estabilización del carbono en la matriz austenitica. Además, los aceros contenían una cierta cantidad de titanio, lo que contribuyo al incremento de la resistencia al desgaste gracias a la formación de carburos duros y estables.

Se realizaron tratamientos térmicos con el objetivo de disolver los carburos precipitados y para mejorar las condiciones de templado de manera de evitar la re-precipitación de dichos carburos, especialmente en el caso de piezas de gran espesor. Los resultados obtenidos muestran una temperatura óptima para la completa austenitizacion de los aceros y también caracteriza la cinética de formación de los carburos a borde de grano.

Una vez realizadas las mejoras en la microestructura de los aceros, se realizaron pruebas en trituradoras de escala piloto de manera de evaluar las propiedades de desgaste de dichos aceros. Además, se realizaron test de campo en industrias mineras que presentaban: trituradoras de cono, molinos de eje horizontal y molinos a martillo.

Los estudios metalúrgicos y tribológicos demostraron la necesidad de mejoras en la composición química de los aceros. Por esta razón, varios elementos fueron incorporados, como ser: Nb, Al, Ni, Mo. Por ultimo, se realizo una estimación de costos de producción de modo de evaluar la factibilidad económica de dichos aceros. Los resultados demuestran que el fenómeno de re-precipitación de carburos es la principal causa de la fragilidad del acero. El manganeso fue la variable más importante para conseguir una microestructura estable. La adición de Ni al acero dio como resultado una mejora de las propiedades mecánicas y al mismo tiempo no perjudico la resistencia al desgaste.

Por ultimo, dos apéndices son incorporados a esta tesis, los cuales presentan resultados de proyectos de investigación que no estaban en línea directa con los objetivos de la tesis. El primer apéndice presenta un modelo matemático que predice la curva granulométrica del producto de una trituradora, teniendo en cuenta el desgaste de los revestimientos. El segundo apéndice presenta un proceso de reducción de tamaño de diversas partículas minerales a través del uso de ultrasonido. También se presentan resultados sobre pruebas hidrometalurgicas usando ultrasonido como catalizados de una reacción de lixiviación.

ACKNOWLEDGEMENTS

I would like to express my gratitude to my academic and research advisor Prof. Manuele Dabalà for his guidance and constant support in helping me to conduct and complete this work.

I would also like to thank Dr. Claudio Maranzana for his generous advice and guidance in the theoretical and practical aspect of this work. By working at his side, I was able to learn many lessons about engineering and, most important, I gained a friend.

In addition, I want to thank Dr. Katya Brunelli for her patience and her constant assistance.

I am indebted to FAR for funding this work and providing research facilities. In particular, I would like to express my gratitude to Sig. Veneroso, Sig. Cervesato, Sig Venutti, Elisa, Giulia, Bil, Pietro, Dario, Mauro, Remo, Alessandro and the entire staff of the company.

Many thanks to all the people I have come to know in UNIPD, whose friendship and companionship I will always enjoy.

Finally, I especially want to thank Gwénaëlle for her inspiration, help and continuous encouragement during my studies. We had the exceptional privilege of writing our doctoral thesis together.

TABLE OF CONTENTS

CHAPTER I - GENERAL INTRODUCTION

Austenitic manganese steel (AMS) is essentially a solid solution of carbon and manganese in χ iron. The particular type of austenitic manganese steel presented in this work is also known as Hadfied's steel, named after its 19th century UK inventor and the first alloy steel ever invented.

In literature, it is widely established that the practical limit of carbon in solution is about 1.2%. Indeed, higher carbon contents, about 1.4%, are rarely used since carbon tends to segregate to the grain boundaries as carbides and is detrimental to both strength and ductility, especially in heavier sections. High carbon content in AMS has the purpose of increasing wear resistance. Manganese acts as an austenitic stabilizer in AMS and delays isothermal transformation, also keeping carbon in the austenitic matrix.

Austenitic manganese steel satisfies the requirements of both wear resistance and appropriate toughness. However, the main reason for selecting manganese steel for any particular application is not abrasion resistance, but high toughness. Among these applications, can be cited railway points and crossover components and teeth for earth-moving equipment. Likewise, AMS are widely used in the mining industry, particularly in comminution processes were mineral ore, rock or inert materials undergo particle size reduction.

Mining is a primary industry that produces raw materials for the production of most of the goods found in modern society. Mining is a wide term that includes the extraction and processing of metallic ores, industrial minerals and fuel minerals, such as coal and oil sands. In addition, quarrying is a type of mining that produces low added value materials such as aggregates for construction applications. Finally, in the last decades, recycling has been established as a new source of raw materials, "mining" in waste dumping sites and scrap yards instead of mineral deposits. All these industries described require some kind of comminution process, in which AMS may be used.

Crushing is a primary process in the production chain of many industries and is performed in a wide range of applications, consequently worldwide figures of crushing material are difficult to find. According to the USGS, the production of crushed stone for the construction industry in USA, the biggest market in the world, was 1.11 billion tons in 2011, and it can be fairly stated that most of the material passed through some kind of crusher using AMS liners.

Abrasive wear conditions in crushing operations range from heavy impact and gouging (primary crushing) to high-stress abrasion (tertiary crushing and impact crushing). During crushing operations, the material is reduced from a maximum of approximately 1500 mm in diameter to about 6 - 10 mm maximum diameter. Two or three stages of crushing are usually involved in a comminution operation. Crushing is generally accomplished by squeezing the ore between two metal surfaces (i.e. AMS liners) with sufficient pressure to fracture the pieces. For softer and less abrasive minerals, such as dolomite or coal, an impact-type crusher can be used, in which the ore pieces are struck with a rotating bar with enough velocity to cause fracture. Typical materials used in crusher liners are all castings; such as AMS, low-alloy martensitic steel and chrome white iron. The final selection of the material is made on the basis of abrasion resistance and toughness.

Similarly, production figures of AMS for comminution applications are hard to come by. Among the main worldwide producers, can be mentioned Columbia Steel of USA, Magotteaux of Belgium, Sandvik of Sweden, Metso of Finland, and many Chinese foundries; nonetheless, there is also a significant production in many countries for the local market.

Two grades of AMS are presented in this work, one with 12-13% Mn content and another with 16-18% Mn. The commercial names of these steels cannot be published in order to preserve the intellectual property of the sponsor of this work, thus are termed arbitrarily H12Ti and H16Ti respectively.

H12Ti and H16Ti possess two important characteristics; firstly, a carbon content of about 1.40 – 1.45%, which is relatively high and unusual for the crushing liner market and secondly, a certain amount of titanium. Both elements, albeit with different physical mechanism, provide the steels with a high wear resistance.

Maranzana [1] in his doctoral thesis has already characterized H12Ti and explained the role of Ti in increasing wear resistance of the is steel in comminution applications. In the last years, H16Ti was developed using a higher Mn content, mainly to keep as much carbon as possible into the austenitic matrix, thus increasing wear resistance.

Nevertheless, both steels have presented irregular performances in the field. In particular, fractures occurred in thick castings during service, which is the most critical failure that a liner can present. Consequently, the requirement of optimization H12Ti and H16Ti was established, chiefly by enhancing their mechanical properties while keeping wear resistance as high as possible.

As a consequence, the optimization process presented in this work had the scope of increasing toughness of both steels, mainly by improving the heat treatments applied to them. The key variable of the optimization was casting thickness, and the main constrains was that the wear rate of both steels should not decrease.

As previously mentioned, one of the main features of both H12Ti and H16Ti is a high carbon content, which tends to form carbides; therefore, experiments were focused firstly on improving the austenitization or solution heat treatment in order to maintain carbon in the austenitic matrix. Secondly the efforts where concentrated on treatments to prevent microstructural embrittlement. Chapter 2 presents a series of characterizations of the mechanical properties of H12Ti and H16Ti as well as several experiments aimed to improve their microstructures.

As mentioned before, wear rate is an important constrain of the optimization process. Although, simulation of wear conditions in laboratory are very difficult for crushing, much efforts were made to reach conditions as representative as possible; consequently, mostly pilot scale tests and field tests were performed. Chapter 3 covers the wear tests performed to the steels with already enhanced toughness.

The results presented in Chapter 2 and 3 demonstrated that chemical compositions should be considered as a variable in the optimization process. Chapter 4 deals with the modification of the original recipe used to prepare the steels, as well as testing to assess wear resistance. Finally, Chapter 5 presents an economic estimation of the performance of the steels presented in Chapter 4. The estimations allowed assessing the economic feasibility of the technical improvements.

This work also includes two Appendixes that present side research projects that deals with some aspects of comminution. Appendix A presents a mathematic simulation of a comminution process. Appendix B, in turn, presents a comminution process using ultrasound techniques.

Figure 1 presents a schematic representation of the complete research work carried out during the doctoral course.

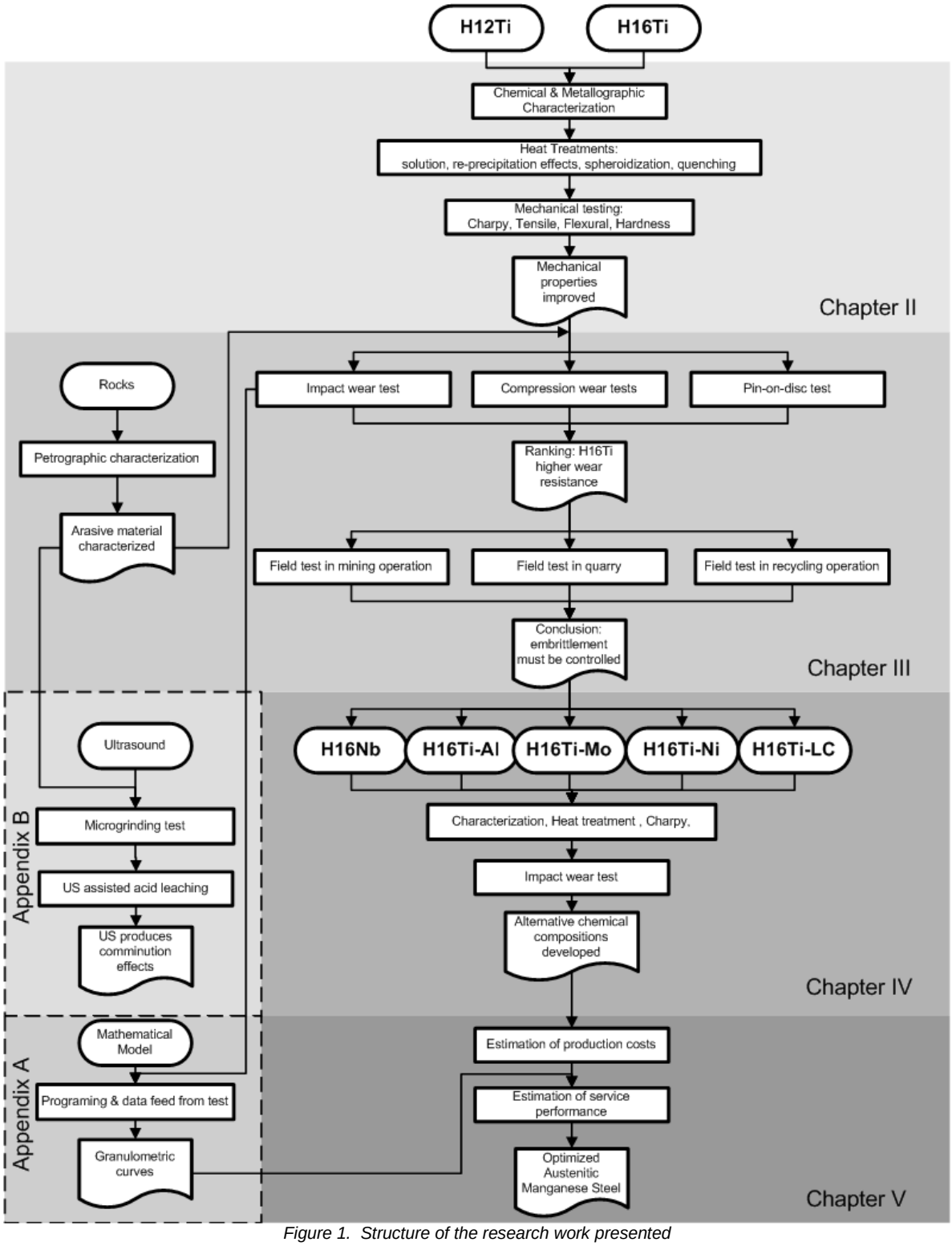

Figure 1. Structure of the research work presented

CHAPTER II - ENHANCEMENT OF THE MECHANICAL PROPERTIES OF AUSTENITIC MANGANESE STEELS USING THERMAL TREATMENTS

2.1. GENERAL CHARACTERISTICS OF AUSTENITIC MANGANESE STEELS

The properties of austenitic manganese steel are influenced by heat treatment, pouring temperature, chemical composition with respect to casting thickness. These are the main controlling factors for optimum performance of austenitic manganese steels. In this chapter, a characterization of the mechanical properties of H12Ti and H16Ti is presented. Furthermore, possible alternatives to the current heat treatment are investigated in order to maximize these mechanical properties of both steels.

2.1.1. Chemical composition of Austenite Manganese Steel.

Chemical composition of AMS is a determinant factor in its resulting mechanical properties, carbon and manganese being the most important components. In general, AMSs used in mineral processing industry have a hypereutectoid composition (carbon content from 0.83% to 2.06%). Table 2.1 shows the ASTM Standard Specification for Austenitic Manganese Steel Castings suitable for abrasive applications [2] [3].

Table 2.1: Chemical requirements of ASTM A 128

Grade	Composition (%)						
	C	Mn	Cr	Mo	Ni	Si	P
A	1.05-1.35	11.0 min				1.0 max	0.07 max
B1	0.90-1.05	11.5-14.0				1.0 max	0.07 max
B2	1.05-1.20	11.5-14.0				1.0 max	0.07 max
B3	1.12-1.28	11.5-14.0				1.0 max	0.07 max
B4	1.20-1.35	11.5-14.0				1.0 max	0.07 max
C	1.05-1.35	11.5-14.0	1.5-2.5			1.0 max	0.07 max
D	0.70-1.30	11.5-14.0			3.0-4.0	1.0 max	0.07 max
E1	0.70-1.30	11.5-14.0		0.90-1.20		1.0 max	0.07 max
E2	1.05-1.45	11.5-14.0		1.80-2.10		1.0 max	0.07 max
F	1.05-1.35	6.0-8.0		0.90-1.20		1.0 max	0.07 max
G*	1.00-1.50	15.0-18.0	3.0				

* grade G from [2]

Carbon forms interstitial solid solutions in χ-iron and is the largest contributor to the strain hardening capacity of austenitic manganese steel. Therefore, only by increasing carbon to the highest practically possible level where it can be kept in solution after quenching, significant performance improvement of austenitic manganese steels can be achieved [4] [2].

There can be two ways to increase carbon content; the first alternative is to increase the cooling rate from 950°C to 500°C during quenching to such an extent so as to surpass the speed of precipitation of carbides from austenite [5] [6]. It may be possible in laboratory to simulate this situation, but does not appear feasible in shop floor, especially with heavy section castings [7]. The remaining alternative is to make the transformation of austenite more sluggish and slow so that the excess carbon is not allowed to precipitate even with standard quenching practice. It appears to be the best possible way to achieve this, is to increase the manganese content along with carbon, as

manganese contributes the vital austenite stabilizing effect without effecting mechanical properties up to a level of 20% [4] [8]. As mentioned before, the reason of the development of H16Ti, was, in part, to respond to carbide reprecipitation by increasing manganese content by 4-6 % with respect to H12Ti.

Manganese contributes a vital austenite-stabilizing effect. It sharply depresses the austenite-ferrite transformation and thus helps to retain 100% austenite structure at room temperature after water quenching. It is widely held that a Mn to C ratio of 10 was optimum without reference to exact levels [9]. This was probably inherited from earlier steel making limitations as it is apparent that the fixed ratio has no basic significance. Manganese within the range of 10 to 14%, has almost no effect on yield strength, but it does benefit tensile strength and ductility. Below 10% Mn the tensile properties decline rapidly to perhaps half the normal level at about 8% Mn. For crusing requirements, 11% Mn is desirable as a minimum, but the maximum is rather arbitrary and probably depends more on the cost of the alloy than on metallurgical results, since acceptable properties may be produced up to at least 20% Mn [10] [8].

Carbon and Manganese content in AMS are not only interrelated, they are related to casting thickness as well. As such, the choice of carbon content will depend on the ductility to be retained and the casting thickness. Current literature published would recommend for safety purpose to maintain carbon between 1.15 to 1.25%: thus, the higher the thickness lower the carbon, to take care of the inadequacies of industrial heat-treatment furnaces. Therefore, H12Ti and H16Ti contain carbon levels that would normally be considered too high to maintain good toughness [9] [4].

Chromium increases yield strength and flow resistance, which can be useful in certain applications: however, on the other side of the ledger, chromium is very detrimental to toughness and is extremely sensitive to section size variation, so chromium misuse may generate huge losses for both liner manufacturers and users. Published data on effect of chromium is misleading since interaction with section size and carbon content are omitted. For instance, a 25 mm test bar data indicates no significant loss in toughness up to 2% Cr, whereas the actual sacrifice in a casting is considerable. Even these data do not tell the whole story since chromium greatly inhibits the heat-treatment response, which further compounds the problems. For a 2% Cr, AMS at a typical carbon content of 1.20%, an austenising temperature in the region of 1125°C to 1150°C is required to ensure complete carbon solution. Thus, when this requirement is coupled with the limitations of industrial heat-treatment equipment, it is easy to visualise the potential danger with the Cr content, especially at higher carbon contents. Only a slight deviation in any of the critical processing steps can destroy the remaining toughness and the result will be a cracked casting or one which will eventually fail prematurely [10] [2].

Titanium has been added to conventional AMS in amounts ranging from 0.03% to 0.24% in order to refine grain size of crusher liner castings and consequently increase their life by minimizing cracking. In heavy sections the grain refining effect is not prominent, but the titanium ties up carbon and in effect, makes the steel equivalent in ductility and yield strength to a lower carbon grade of manganese steel [11] [12]. The carbon content of H12Ti and H16Ti have been purposely increased in order to partly replace that is used in titanium carbide formation, without depleting the carbon content

of the matrix [13] [14]. Maranzana has described in detail the benefits of Ti in H12Ti, however it has been not possible to determine the quantity of carbon involved in TiC formation yet.

Titanium addition may be interpretated as some kind of metal-matrix composite, that consist of metal as the matrix and usually ceramics (e.g.,TiC, NbC) as the reinforcement [15] [16]. The composite materials offer such property combinations and performance profiles, which are not available in any conventional engineering materials [17]. Particle-reinforced metal-matrix composites as a wear resistant material have been paid increasingly more attention, owing to the low cost and good mechanical properties as well as the physical properties. This is because the particle phases can strongly resist the abrasive wear. Interfacial bonding between hard ceramic reinforcements and the matrix was verified to be a control factor whether a remarkable improvement of wear resistance of the composites could be acquired or not. The hardness of the reinforcement should be higher than that of the abrasive material for obtaining good abrasion resistance. In addition, the matrix hardness should be as high as possible. The incorporation of ceramic particles into AMS matrices can lead to a dramatic improvement in the abrasive wear resistance [17] [17] [18].

The chemical effects of other elements such as silicon, phosphorous, sulphur, aluminium, nickel, molybdenum, vanadium and niobium are presented in Chapter 5.

2.1.2. The melting of Austenitic Manganese Steels.

Induction furnaces are the most commonly used melting furnaces for making steel castings. Additionally, fuel fired rotary furnaces, with 10 t capacity, can be used for the production of AMS. Raw materials for the production of AMS are usually steels scrap of manganese steels, pig iron and regular steel scrap. Besides, ferroalloys are used for the adjustment of the final chemical composition. The smelting temperature in plant ranges from 1480°C to 1580°C, in order to dephosphorize the steel. The bath is then transferred into a ladle, where final adjustment of the chemical composition is performed [8] [2]. Finally, the ladle pours the molten steel into moulds of olivine sand, bounded with sodium silicate.

Pouring temperature is an important variable of the production process. It is well known from both practical experience and published literatures that high pouring temperatures, resulting in large grain size and alloy segregation, are detrimental to the strength and ductility of AMS [10] [4].

The freezing range of AMS is about 1371°C to 1260°C. In-plant cracking problems and inferior mechanical properties can be anticipated if pouring superheat exceeds 120°C. Moreover, it will be much more pronounced as the casting thickness and carbon content increases. Thus in the production of heavy section castings, pouring temperature control becomes extremely important if adequate toughness is to be preserved in finished casting [5]. After the pouring, moulds are left at room temperature for at least 48 hour before opening.

The pouring temperatures of all castings presented in this work were kept as low as possible. The exact value of the pouring temperature cannot be published in order to protect intellectual property of the sponsor of this work.

2.1.3. The heat treatment of Austenitic Manganese Steels

After solidification, AMS are brittle due to the presence of precipitated phases (eutectic carbides, grain boundary carbides and pearlite colonies) [19] [3]; and a treatment to solubilize these phases is necessary to increase mechanical properties, usually at temperatures ranging from 1050°C to 1150°C [9].

When casting cools inside the mould, it cools very slowly. This allows the austenite to decompose to carbide and ferrite. The quantity of decomposed products is dependent on cooling rate which in turn depend on section thickness and mould material. The purpose of heat-treatment as such is to retain 100% austenite at room temperature with all the carbon dissolved in it [20].

The heat treatment of Manganese Steel is simple in principle, consisting of heating to a fully austenitic condition and rapidly quenching in water. Soaking should be performed above the carbon solubility line A_{CM} as shown in Figure 2.1. The A_{CM} should be exceeded by 10 to 37°C to compensate for carbon microsegregation [2].

The austenitization or solution treatment must end with an effective quenching in order to avoid re-precipitation of the dissolved phases. In industrial conditions, carbide re-precipitation could be an undesirable result of an inefficient thermal treatment ending, which may lead to failure of the final product, especially for cast pieces with large sections [21] [7].

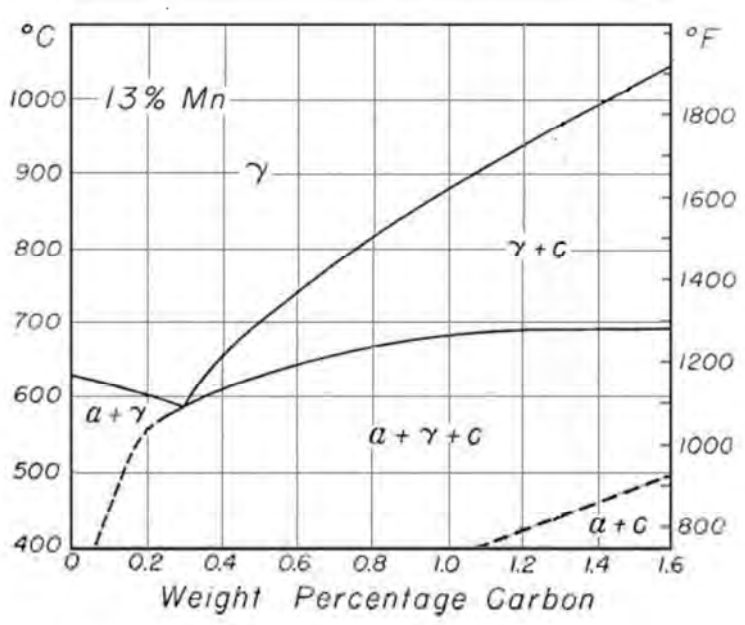

Figure 2.1. Pseudo-binary diagram of the Fe-Mn-C system at 13% Mn [2].

In addition, the embrittling effect of high heat-treatment temperature upon AMS must be considered. At high temperatures incipient fusion occurs at the grain boundaries producing, in severe cases, a continuous network of a ledeburitic type structure. The severity of this defect and the degree of embitterment is strongly influenced by increasing section thickness, carbon and phosphorous content. The molybdenum grades of manganese steels are particularly sensitive to incipient fusion, especially at higher carbon level [10] [22].

2.1.4. The problem of embrittlement

Manganese austenites, when treated in isothermal conditions, undergo transformation between the upper critical temperature A_{cm} and 300°C, range where cementite starts to form because of its ejection from austenite. The transformation or decomposition of the austenite (i.e. γ → γ + carbides) begins with the formation of intergranular carbides, which tends to develop into a continuous network that embrittles the steel. Figure 2.2 presents the transformation of a typical AMS (1.28%C, 12.4%Mn, austenitized at 1050°C for 30 min) in isothermal conditions. The diagram shows that between 300° and 700°C, precipitation of intergranular carbides begins after an incubation time of a few seconds. Moreover, the acicular carbides form after an incubation period described by a C-like curve, which nose is located at 600°C and 1 min incubation time. Finally, pearlite appears after a longer incubation time (slow transformation kinetics) and in a narrower temperature range than that of the acicular carbides [2] [3].

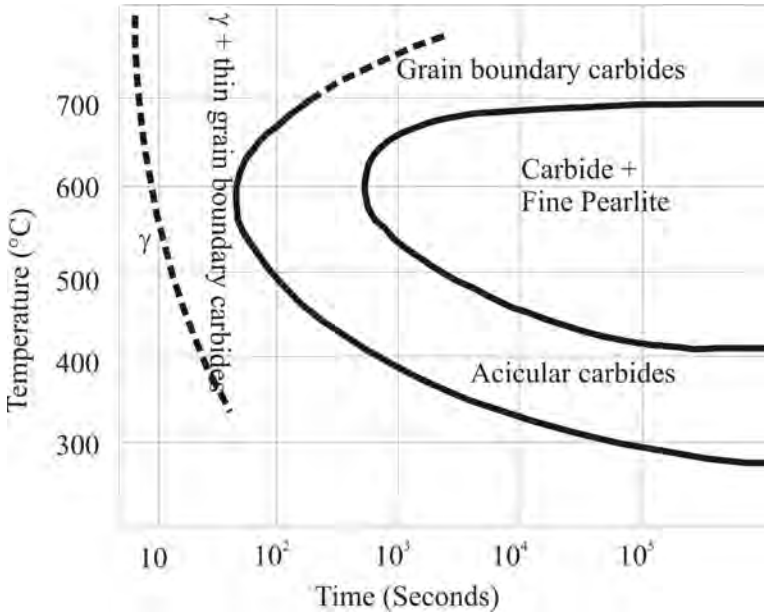

Figure 2.2. Isothermal Transformation Diagram of AMS with 1.28% C and 12.4% Mn. [2]

As mentioned before, chemical composition strongly influences transformation kinetics of the manganese austenites. On one hand, when the carbon content decreases from 1.27 to 0.94%, at temperatures of 600°C, the incubation time of intergranular carbides increases from a few seconds to 2 minutes, for steels with 12% Mn content. On the other hand, when manganese content varies in the order of 3%, there is little modification on the incubation time of the intergranular carbide re-precipitation. Chromium reduces as well the incubation time of the intergranular carbides re-precipitation [2] [21] [23].

Published research work showed that an increase in carbon content on the austenites at 6% Mn shortens the incubation time for acicular carbides precipitation, displaces the temperature of the nose of the transformation curve to a higher one, and widens the domain of the carbide precipitation. The incubation time of the pearlitic transformation of AMS is reduced by an increase in carbon content, and extended by an addition of molybdenum, chromium and vanadium [2].

The reasons for embrittlement in AMS can be found in interdendritic, intergranular and sometimes transgranular mechanisms. AMS embrittle when the austenite grains loose cohesion due

to the presence of carbides, such as grain boundary carbides. These carbides can be divided into two classes: thin grain boundary carbides (less than 0.2 µm thickness) and thick g.b.c. (thicker than 0.2 µm). There are other phases that embrittle the microstructure, such as phosphide eutectic and aluminium nitride inclusions. Nevertheless, due to the low content of these elements in the steels investigated, those last mechanisms of embrittlement were considered negligible for the purpose of this work. Embrittlement impact on the steel depends on the percentage of grain boundary covered by the carbides, and the loss of cohesion with the austenite matrix. Thin carbides or "carbide delineations" do not decrease impact toughness. However, thick carbides (of around 1 µm) do decrease toughness. It was reported that thin carbides do not gradually grow, or get thicker, but rather, thick carbides appear locally and extend along the grain boundary. However, in chromium bearing steels, gradual thickness of grain boundary carbides has been observed. [3] [21].

In order to improve wear resistance properties, some AMS steels are currently produced with the addition of micro-alloying elements, such as niobium, titanium or vanadium, that form stable carbides or nitrides, either singly or in any combination. These stable carbides or nitrides are not affected neither by the solution treatment usually applied to AMS, nor by common isothermal treatments, therefore, they should not contribute to the phenomenon investigated [11].

Heat treatment at high temperature causes surface decarburisation and some loss of manganese. This decarburisation layer can be as much as 3 mm and can be slightly magnetic as well. This is not usually a problem, as most liners contact surfaces are machined by either milling or grinding, which removes most of this decarburized layer. Nevertheless, the decarburization layer represents a loss of material. This is one of the reason why excessively long heat treatments are generally avoided in industry [4].

The dispersion hardening treatment consist of transforming part of the austenite to pearlite by heating to 600°C, followed by re-austenising between 980 to 1010°C which dissolves the as cast carbides together with some of those present in pearlite. The undissolved carbide form a fine dispersion of spherodised particles and in this condition the steel has better yield, tensile strength and ductility than plain 12%Mn steel. [8] The process is known as spheroidization of carbides may have two effects, decrease the embrittlement and increase wear resistance in applications where low stress abrasion is predominant. However, from a metals research perspective, the claim that microstructural development via heat treatment may determine wear performance of crushing liners seems far-fetched.

2.1.5. Casting thickness

Casting thickness is correlated to design of the liner. AMS steels have good gouging abrasion wear resistance and strain hardening characteristics, but their main feature is high toughness. Therefore, embrittlement mechanisms such as grain boundary precipitation are important phenomena to be considered during production of large cast pieces (e.g. cone and gyratory crusher liners), especially when thicknesses are larger than 100 mm. Nowadays, crushing equipment manufacturers

(such as Sandvik, Metso, Krupp and others) design and build larger equipment in respond of the market's demands. Consequently, liners need to be thicker and tougher. [2] [24].

2.1.6. Quenching conditions

Quenching is accomplished by immersion in an agitated water tank, as agitation reduces the tendency for the formation of a vapour coating (known as the Leidenfrost effect) on the casting surfaces, and therefore a uniform rate of cooling is obtained. The speed of quench is an important factor in the final mechanical properties. The maximum rate of quench is fixed by the heat absorption from the casting surface by agitated water and by the rate of thermal conductivity of the AMS [9].

AMS has low thermal conductivity. A lower rate of quench, results in lower mechanical properties in the centre of heavier section. This results in a practical maximum thickness for castings of about 150 mm. Another reason for limiting casting size to 150 mm is that castings larger than this value develop large residual stresses upon cooling in the mould. Such stresses acting on a brittle steel structure are prone to cause cracking in heavier sections prior to heat treatment [7] [20].

Great emphasis is given on the importance of quenching speed. Thus, foundries have invested heavily in the equipment necessary to provide for a rapid transfer of hot castings to a large water tank equipped with propellers for vigorous agitation and cooling tower to maintain cool water temperature. In spite of these precautions, a poor microstructure is still one of the primary causes of premature field failures, as is the case of H12Ti and H16Ti.

It is true that slower cooling rates will aggravate toughness due to grain boundary carbide reprecipitation, especially in heavier sections. Nevertheless, all the undesirable constituents which form below the Acm involve nucleation and growth, hence diffusion and time. It has been shown that retarded cooling down to 950°C before quenching has no big deleterious effect on ductility [5].

Rather, it is the cooling rate over the range of 950°C to 500°C, which is important. However, the speed of quenching becomes immaterial if measures are not taken first to ensure that the carbon is in solution in the austenite. The majority of heat treatment related field failures are caused by poor temperature control rather than poor quench [6].

Regarding temperature of water in the quenching tank after quenching, it is sufficient to see that water does not continue steaming after quenching. It can be taken care by ensuring that the volume of water in the tank is sufficient enough so that temperature does not rise beyond 50°C. It is also to be noted that some amount of vapour will, in any case, form and, if they remained attached to the body of the casting as they are non-conductor of heat, will prevent the casting from transferring heat to water. As such it is recommended that the water is agitated just after quenching to drive away the steam bubbles from the tank [2] [8].

2.1.7. Mechanical properties

AMS has yield strength between 392 MPa to 460 MPa. Although stronger than low carbon steel, it is not as strong as medium carbon steel. It is however, much tougher than medium carbon steel. Yielding in AMS signifies the onset of work hardening and accompanying plastic deformation. The ultimate tensile strength of AMS varies but is generally taken as 893 MPa. At this tensile strength,

AMS displays elongation in the 25 to 40% range. The fatigue limit for manganese steel is about 269 MPa. Nevertheless, the mechanical properties of AMS listed above vary significantly with section size. Properties affected are tensile strength, elongation, reduction of area and impact toughness. For example, a 1 inch (25.4 mm) thick section properly heat treated, will display higher mechanical properties than 4 inch (102 mm) section. Grain size is the primary reason for these mechanical differences. Fine-grained specimens exhibit tensile strengths and elongations up to 30% greater than course grained specimens [9] [10].

The ability of AMS to work harden up to its ultimate tensile strength is its main feature. In this regard, AMS has no equal. The range of work hardening of AMS from yield to ultimate tensile is approximately 200%. This however is accompanied by large dimensional instability [9] [8].

To most people, toughness means the ability to withstand severe impact conditions without fracturing. If impact & shock is absent, white cast iron is a better choice. For light or moderate impact, a hardened steel is justified. For heavy impact or for large safety factor, AM is the logical choice. Even in applications where other materials possess sufficient toughness for normal conditions, AMS may be chosen because of the danger of occasional high impact. Work hardening is discussed in the next chapter.

2.2. CHARACTERIZATION OF THE STEELS

2.2.1. Production of samples and specimens

Two batches of steel were produced in the 10-ton capacity rotary smelting furnace. The first batch was of H12Ti steel and the second batch was of H16Ti steel. The steels were produced by smelting manganese steel scrap. Besides, ferroalloying elements were used to adjust the final chemical composition.

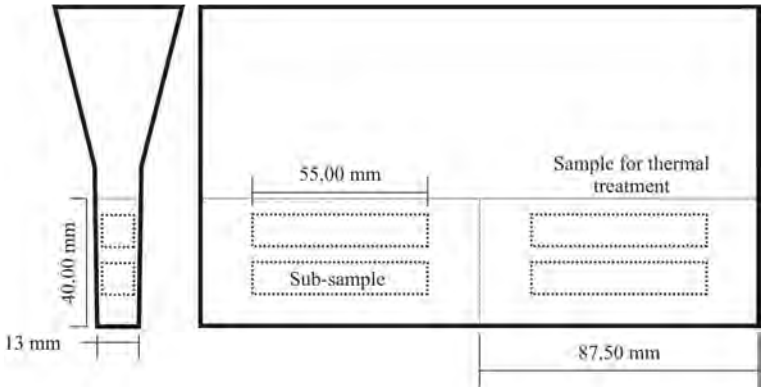

Figure 2.3. Schematic representation of the Y-block produced in H12Ti and H16Ti. The position of the samples and specimens used in this work are represented. The bottom part of the block was used, and the top part was discarded.

The steels were poured into several moulds made with olivine sand bonded by sodium silicate. The moulds had the form of Y-shape blocks, according to the dimensions featured in ASTM A536. (see Figure 2.3) The quantity of Y-shape blocks produced for each steel was enough to provide samples and specimens for the heat treatments and mechanical tests presented in this work.

Furthermore, liners were casted from the same batches of H12Ti and H16Ti, to be used in the wear tests presented in the next chapter.

2.2.2. Chemical characterization

The chemical compositions of H12Ti and H16Ti, in as-cast condition, were characterized using a Thermo ARL 3460 Metals Analyser optical emission spectrometer. The results, shown in Table 2.2, were compared with the ASTM standards, shown in Table 2.1. H12Ti composition matched the Grade C by its Mn content, but was above specifications in terms of carbon content. However, H16Ti was in accordance with Grade G in terms of carbon content, but below specifications in terms of Chromium content. The content of titanium is only shown as range (0.3 - 0.7) in order to protect intellectual property of the sponsor of this work.

Table 2.2. Chemical composition of the steels

(%)	C	Mn	Cr	Mo	Ni	Si	P	S	Al	Ti
Steel H12Ti	1.46	12.50	1.46	0.10	0.20	0.53	0.030	0.00	0.13	0.3 – 0.7
Steel H16Ti	1.41	16.68	1.53	0.08	0.13	0.48	0.034	0.003	0.025	0.3 – 0.7

2.2.3. Metallographic characterization in the as-cast condition

Samples of dimension 87 mm x 40 mm x 13 mm were cut from the top part of the Y-shape blocks for the microstructural characterization and impact toughness testing. The samples were polished using conventional polishing techniques and etched with Cogne Unico, in order to observe the carbides' morphology and to evaluate the continuity of the precipitated carbides in the grain boundaries. Based on UNI3135-65, this reagent was prepared with: 2 g of picric acid, 6 cm^3 of acetic acid, 10 cm^3 of chloridric acid and 100 cm^3 of ethylic alcohol. Etching lasted 30 - 60 seconds, and was performed at room temperature. Samples were observed by optic microscopy (OM), Zeizz axiotech reflected light microscope, in order to characterize the microstructure. Afterwards, carbides' morphology and composition were characterized using a scanning electron microscopy (SEM) Cambridge Stereoscan 440 instrument equipped with a Phillips PV9800 EDAX micro-probe, for EDS (energy-dispersive X-ray spectrometer) semi-quantitative analysis.

As-cast microstructures of H12Ti and H16Ti steels are presented in Figure 2.4. The presence of precipitated phases within the austenitic structure was observed. The most visible phases were attributed to eutectic carbides, pearlite colonies and the carbides at grain boundary.

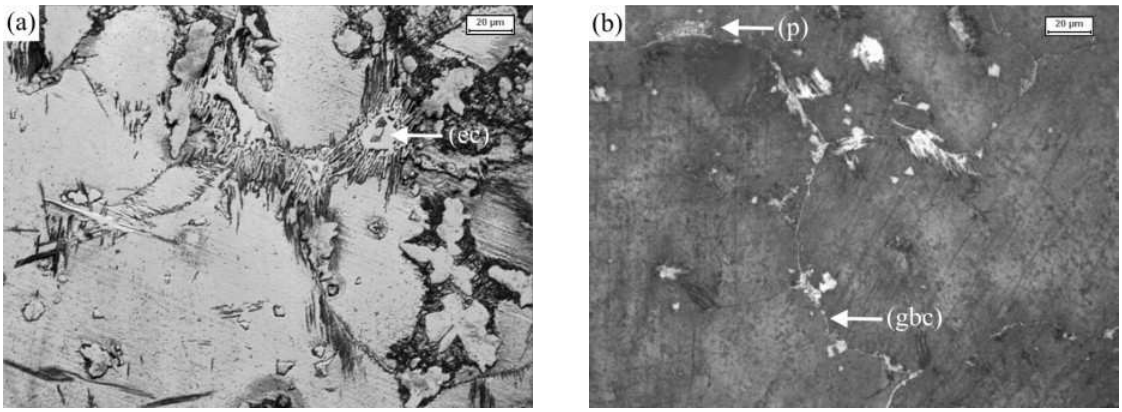

Figure 2.4. Micrographic images of the samples in as-cast condition. (a) H12Ti, (b) H16Ti. The microstructure presented eutectic carbides (ec), grain boundary carbides (gbc) and pearlite colonies (p). (Magnification 500x. Etched with Cogne Unico).

Figure 2.5 shows the microstructure of the as-cast sample of H16Ti steel, where grain boundary carbides and pearlite colonies can be observed. The results of the EDS analysis showed that the pearlite contained a higher proportion of Mn and Cr, in comparison with the analysis presented in Table 2.2.

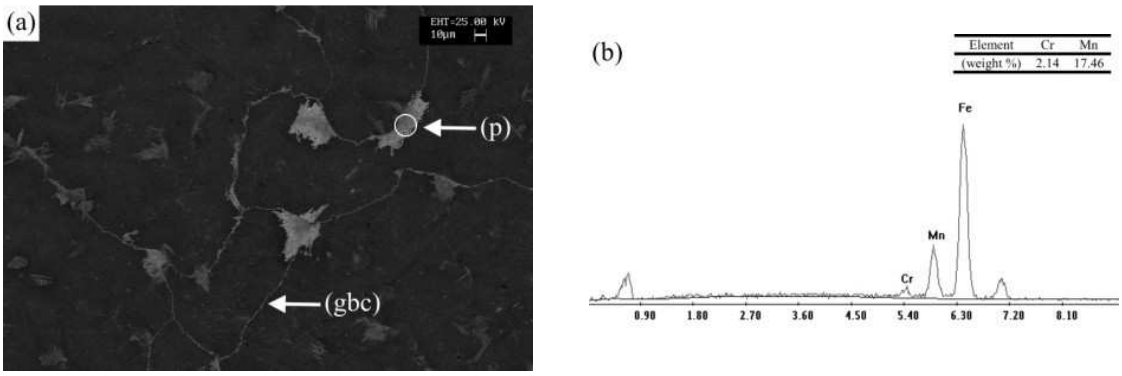

Figure 2.5. (a) SEM image of the sample H12Ti in as-cast condition. (b) EDS spectrum on region inside the circle.

2.3. SOLUTION HEAT TREATMENT

2.3.1. Introduction

Solution heat treatment at the industrial process was usually carried out at 1050°C during 60 min for H12Ti and H16Ti steels. However, metallographic observations showed that this treatment was not effective to solubilize all precipitated phases present in the microstructure, especially when treating thick castings (above 100 mm). Consequently, an investigation was carried out in order to determine the optimal temperature and holding time for complete solubilisation.

2.3.2. Experimental

The experiments were performed using an electric furnace, where samples of H12Ti and H16Ti were introduced at room temperature and heated with a 3.66°C/min ramp.

The variables of the experiments were temperature (1050°C, 1090°C, and 1130°C) and holding time (60, 120 and 180 min). Figure 2.5. shows the curves of the nine treatments performed.

Finally, samples were quenched in water at room temperature and characterized.

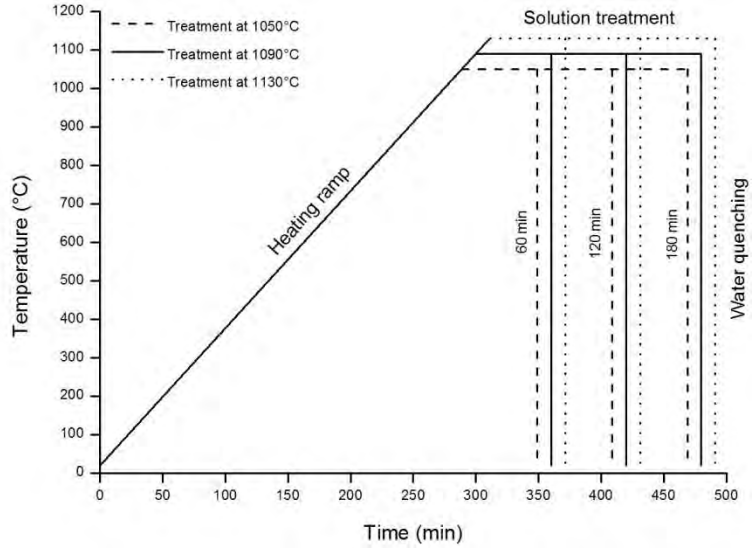

Figure 2.6. Solution heat treatments performed.

2.3.3. Results and discussion

Treatments performed at 1050°C for 60, 120 and 180 min showed the presence of grain boundary carbides in the microstructure. Evidently, temperature is not enough to reach complete solution of primary carbides.

Samples treated at 1090°C for 60 min showed a very fine phase of carbides at grain boundary. Samples treated at 1090°C for 120 and 180 min presented a microstructure free of grain boundary carbides. The temperature seems to be enough to dissolve the carbides. A thin face of carbides is usually considered not harmful to the mechanical structures, thus the results of the 60 min treatment could had been considered acceptable. However, the 120 min treatment presented the conditions of good austenitization at a relatively reasonable amount of time. The 180 min treatment presented also good results in terms of microstructure. Nevertheless, a 180 min treatment was considered to be too long for a hypothetic application in industrial scale. Therefore the 1090°C and 120 min was selected as the best result.

Samples treated at 1130°C for all holding times presented a structure free of precipitated phases. However, a small evidence of liquefaction was detected at the grain boundary for all three holding times. Furthermore, macroscopic observation confirmed the production of high amount of scale on the surface of the sample. The 1130°C temperature was therefore considered too high for the solution treatment of H12Ti and H16Ti. At industrial scale, high temperatures may also produce superficial cracking, a defect that would be only detected after grinding of the casting surface.

The micrographs presented in Figure 2.7, showed the microstructure of H12Ti and H16Ti steels after a solution treatment at 1090°C for 120 min and immediate quenching. The heat treatment dissolved all the as-cast precipitated phases into the austenitic grains, leaving the microstructures

apparently clean, at 500x magnification. Only the carbides of Ti were present. However, as mentioned earlier, these phases have high smelting point and do not contribute to the re-precipitation phenomenon. Moreover, the microstructure of both steels, H12Ti and H16Ti are alike, which facilitated the comparison between both types.

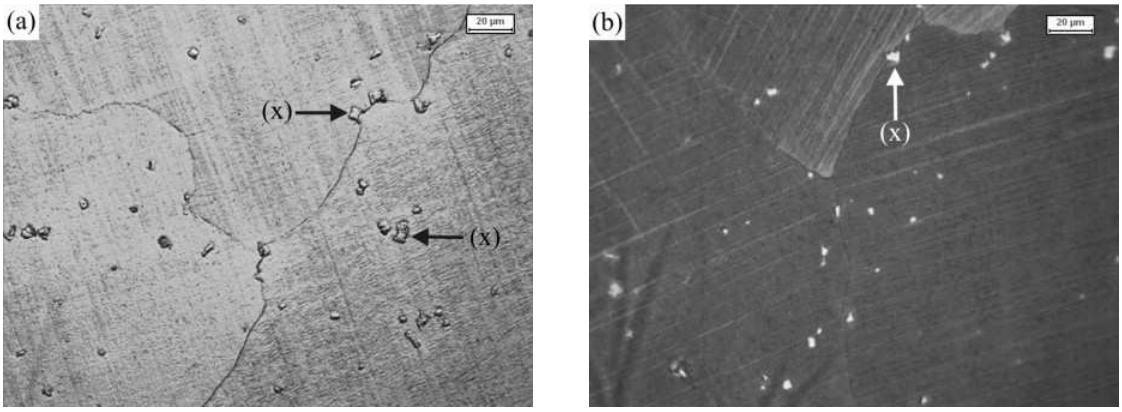

Figure 2.7. Micrographic images of the samples after solution heat treatment at 1090°C for 120 min and immediate quenching. (a) H12, (b) H16. The grain boundaries were free of carbides. Only TiC were present (marked with X). (Magnification 500x. Etched with Cogne Unico).

SEM images of the 1090°C/120 min sample presented a microstructure clean of pearlite, and coarse grain boundary carbides. However, fine grain boundary carbides, of approximately 0.1 µm thick remained for both M12Ti and M16Ti. The image (a) of Figure 2.8 shows the sample of H16Ti after the solution treatment, where all pearlite colonies and thick grain boundary carbides were dissolved. Only the thin grain boundary carbides (0.1 – 0.2 µm thickness) remained, as a film around the austenite grain.

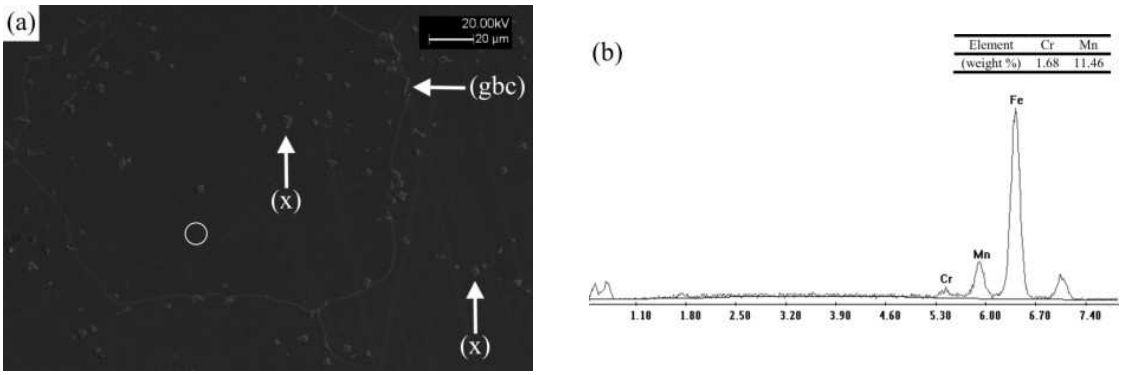

Figure 2.8. (a) SEM image of the H12Ti sample in the solution condition; thin grain boundary carbides are visible (gbc). (b) EDS spectrum on region inside the circle (austenite matrix).

According to OM characterization, a solution treatment at 1090°C for 120 min was the best condition to obtain a structure free of embritling phases such as pearlite, acicular carbides and thick grain boundary carbides. However, SEM observations confirmed that thin grain boundary carbides remained in the microstructure of both steels H12Ti and H16Ti. Thin grain boundary carbides are not considered to be source of embrittlement. Therefore, the temperature of 1090°C and the holding time

of 120 min was confirmed as the optimal condition for the solution treatment. For further experiments, the 1090°C – 120 min heat treatment was adopted as the standard for austenitizing samples.

For industrial applications, the solution treatment was adapted, due to constrains in the operation of the furnaces. The heating ramp varies between 2.1 to 2.8 °C/min, depending on the mass and the dimensions of the pieces charged. The holding time remains 120 min and the quenching is performed in an 83 t capacity thank with agitated water and 4% salt content.

2.4. MECHANICAL TESTING

2.4.1. Introduction

Tests of the mechanical properties were conducted in order to determine the effectiveness of the solution heat treatments.

2.4.2. Flexural test

The test was performed using an industrial press, with a very capacity high pressure capacity (> 1500 kN). The dimensions of the specimens were 85x70x360 mm. The parameters were b=300 mm, h=85 mm and h=70 mm. The variables of these test were heat treatment: 1050°C/60 min treatment and the 1090°C/120 min treatment, and also steel: H12Ti and H16Ti.

Table 2.3. Results of flexural test

	Stress in outer fibres at midpoint σ_{max} (MPa)	Strain in the outer surface ε (mm/mm)
H12Ti (1090°C)	2376	0.16
H16Ti (1090°C)	3324	0.26
H12Ti (1050°C)	1598	0.24
H16Ti (1050°C)	1409	0.21

Although the tests were not performed using the standard equipment, but rather an industrial press, the results were considered to be enough representative to rank the best steel considering the variables under study (i.e. steels and heat treatments)

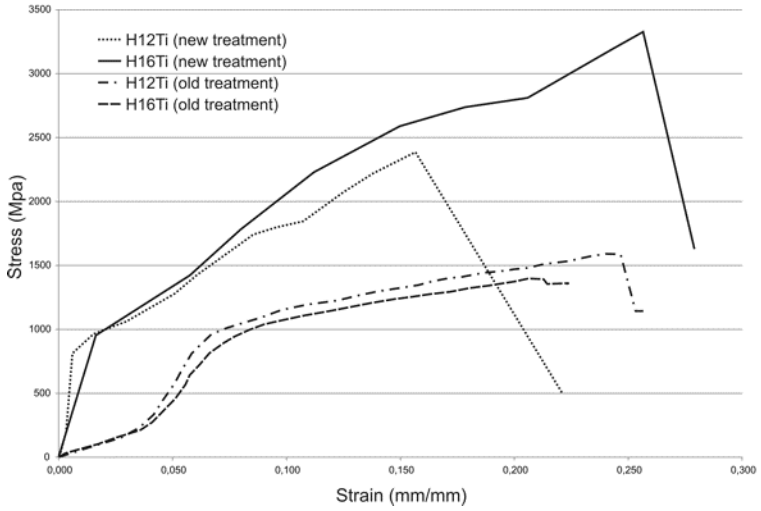

Figure 2.9. Results of flexural tests, strain – stress curves
New treatment = 1090°C /120 min
Old treatment = 1050°C / 60 min

Figure 2.9 presents the curves plotted using stress and strain observed in the specimens. The results show that the 1090/120 min heat treatment had an overall positive impact in both steel clearly improving the their modulus of elasticity in bending, which was around 5300 MPa for both steels with the old treatment (1050°C – 60 min). Furthermore, with a modulus of elasticity of 21632 MPa, H16Ti clearly outranked H12Ti, that presented 15281 MPa.

The improvements in mechanical properties were largely attributed to a good austenitization of both steels.

2.4.3. Charpy Impact Toughness

Samples were machined to obtain specimens for the Charpy impact test, according to ASTM E23 type A. Samples in the as-cast condition and samples in the solution treated condition (both using the “new” and “old” treatment) were tested for both H12Ti and H16Ti steels. Test were carried out in duplicate. Mean value of absorbed energy in Joules (J) is presented together with the corresponding standard deviation (SD). Figure 2.3 shows the position from where the specimens were extracted for the tests. The test were performed by duplicate; the results are presented in Table 2.4.

Table 2.4. Results of Charpy impact tests.

Sample treatment	H12Ti		H16Ti	
	Mean (J)	SD	Mean (J)	SD
As-cast	15.0	4.1	18.8	3.8
Solution 1090°C	215.0	10.7	298.1	11.3
Solution 1050°C	120.2	21.4	184.8	16.2

As expected, as-cast specimens showed very low impact toughness, for both H12 and H16, whereas the values observed in the solution treated specimens represented improved mechanical conditions.

The solution treatment of 1050°C – 60 min showed better results for H16Ti but not yet satisfactory impact toughness for crushing applications. While the 1090°C – 120 min heat treatment presented an increase in the impact toughness of above the 78%.

Impact toughness was considered to be the most representative indicator of the mechanical properties of the steels used in crushing applications.

2.4.4. Tensile test

Samples of H12Ti and H16Ti in solution condition were prepared mechanically into specimens 10 mm in diameter and 125 mm in length. The results are presented in Table 2.2 and Figure 2.8.

Table 2.5. Results of tensile tests

		H12Ti	H16Ti
Modulus	(MPa)	35712.6	34439.5
Stress at Offset Yield	(MPa)	376.5	363.7
Stress at Yield	(MPa)	543.9	495.7
Peak Yield	(MPa)	543.9	495.7
Break Stress	(MPa)	187.4	488.2
Strain at Break	(%)	5.71	2.74

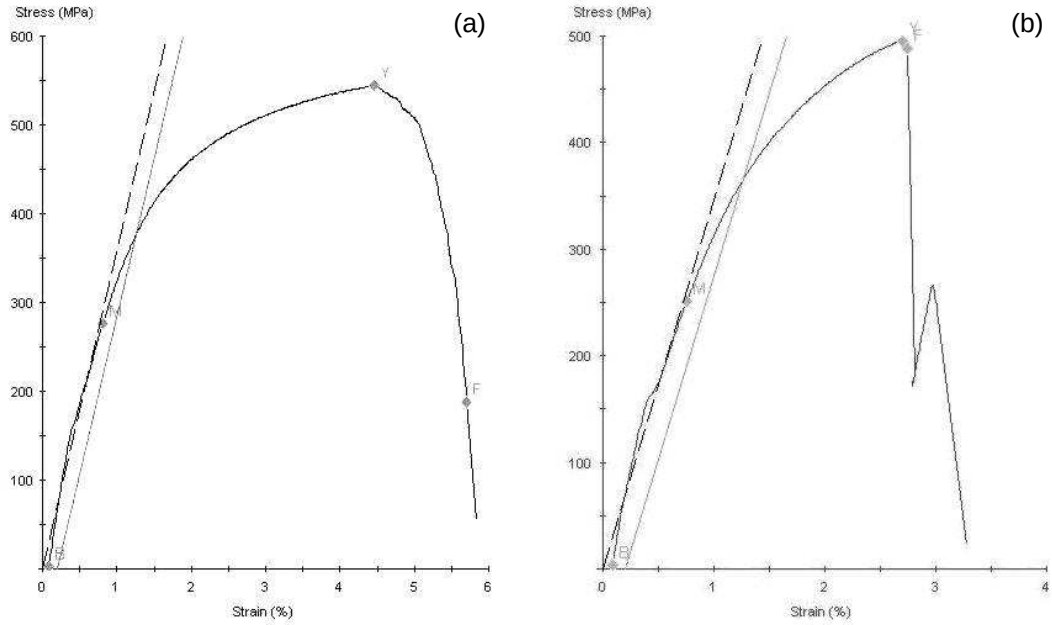

Figure 2.10. Strain – stress curves for (a) H12Ti, (b) H16Ti

Figure 2.11 presents the fracure surface of the specimens, where the dendritic structure of the materials was clearly observed. In general H12Ti and H16Ti presented lower yield in comparison with data from literatures, mostly because published data correspond to steels with 1.20% C.

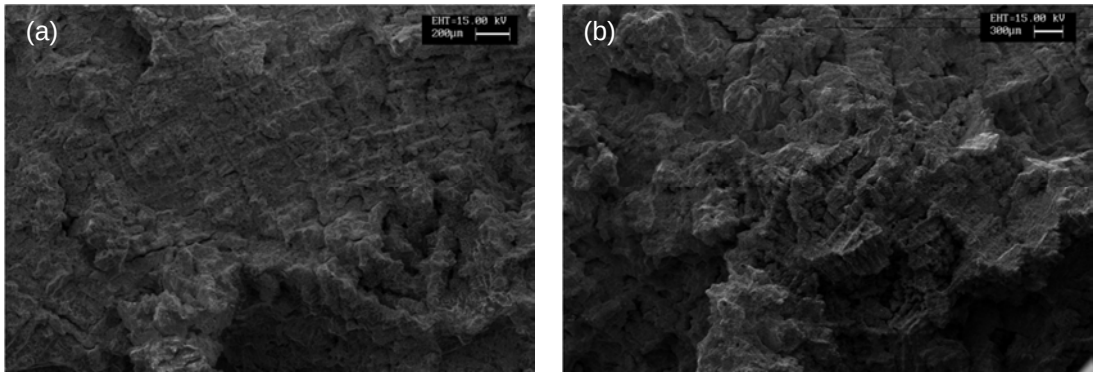

Figure 2.11. SEM images of the fracure surface of the specimens (a) H12Ti, (b) H16Ti

2.4.5. Hardness

Microhardness was measured using a Shimadzu micro hardness tester with a 200 g weight. Table 2.6. presents the results before and after work hardening (crushing operation) for both steels with the 1090°C - 120 min heat treatment.

Table 2.6. Micro-Hardness.

	Mean (HV_{200})	SD
H12Ti without work hardening	310	25.5
H16Ti without work hardening	325	31.7
H12Ti with work hardening	598	40.6
H16Ti with work hardening	625	36.8

Table 2.7. Hardness Brinell.

	Mean (HB)	SD
H12Ti	203.7	1.2
H16Ti	192.7	1.3

Hardness Brinell was also measured. The results show no significant difference between both steels. The test were performed before work hardening. Table 2.7 presents the results.

For the scope of this work, microhardness was selected as the most representative indicator to study work-hardening phenomenon.

2.5. EFFECT OF CARBIDE RE-PRECIPITATION ON THE IMPACT TOUGHNESS

2.5.1. Introduction

The aim of this investigation was to study the correlation between the degree of carbide re-precipitation and the toughness of H12Ti and H16Ti. The 1090°C – 120 min solution heat treatment was performed on both steels in order to dissolve precipitated phases during the solidification of the cast. Subsequently, an isothermal heat treatment was performed in order to produce re-precipitation at different temperatures and incubation times; conditions were selected in order to simulate poor quenching (freezing) conditions in the microstructure, generally occurring in large castings. Finally, samples were water quenched to effectively freeze the microstructure. Impact toughness was determined using the Charpy impact test. The microstructure of samples was characterized by optic microscopy (OM) and scanning electron microscopy (SEM). Results are presented in the form of comparative curves.

2.5.2. Experimental

Twenty-eight samples were tested for H16Ti steel and another twenty-eight for H12Ti. Samples were prepared according to section 2.1.1.

Thermal treatment consisted of three steps: (i) solution treatment at 1090°C for 120 min, (ii) isothermal treatment and, (iii) water quenching. Figure 2.12 shows a schematic representation of the succession of these steps. In step (ii), the samples were quickly extracted from the furnace and quenched into a salt bath with temperatures that varied according to treatment: 1000°C, 950°C, 875°C, 800°C, 750°, 700°C and 650°C; and for holding times of 5, 10, 15 and 20 min. Finally, the step (iii) was the quenching of the samples into a 1 m^3 tank containing water at room temperature. Figure 2.13 shows the time-temperature curves for all three steps.

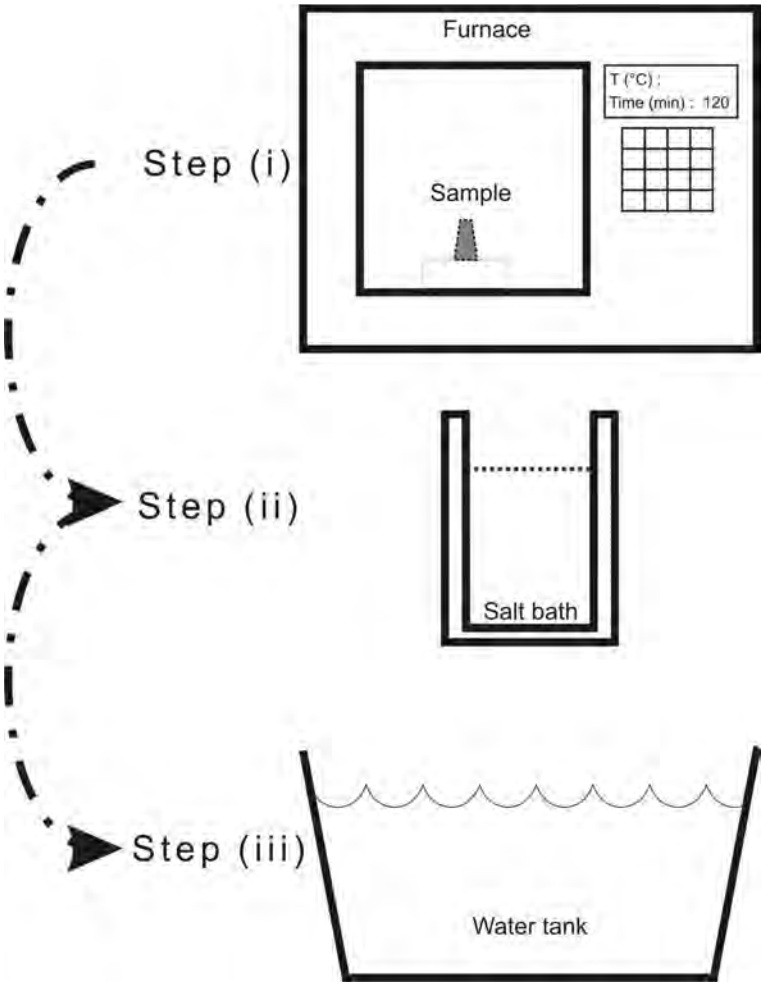

Figure 2.12: Schematic representation of the three steps of the heat treatment presented in this section.

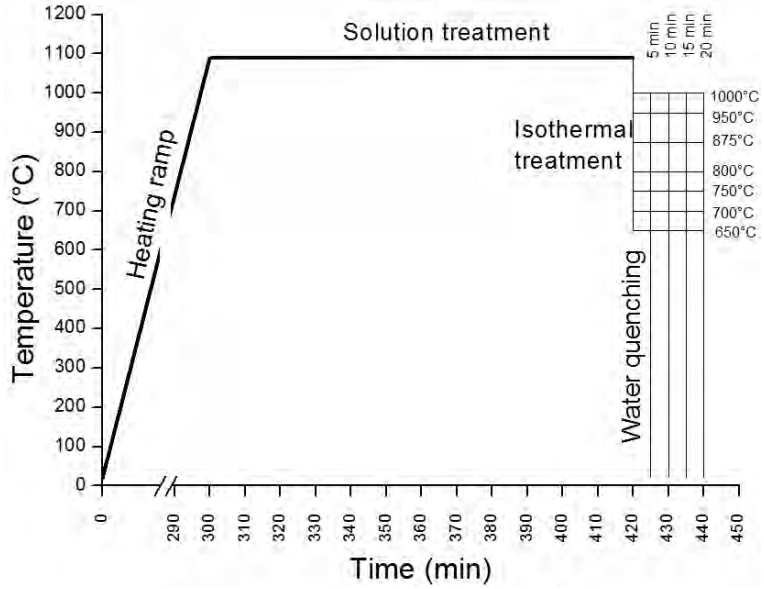

Figure 2.13. Curves of the treatments: 28 samples treated for H12Ti steel and 28 samples treated for H16Ti steel.

Using the 500x magnification micrographics for all samples, and in combination with the ImageJ 1.47v image analysis software, the area of re-precipitated phases at grain boundary was quantified. The amount of pixels containing carbides from each micrograph was measured and their proportion calculated in reference to the total quantity of pixels in the micrograph. The data collected and processed allowed the construction of phase transformation curves from austenite to austenite plus carbides. The boundary limit to define the change of phases was the dramatic loss of toughness presented in the results section. Charpy impact test for samples isothermally treated for 5 and 10 min were performed.

2.5.3. Results

Starting point is the as cast condition presented in (2.2.3), the goal was to obtain microstructures 100% austenitized, or mostly free of grain boundary carbides (gbc).

The samples isothermally treated at 1000°C (steps i, ii and iii) did not showed evident signs of re-precipitation; the microstructure was similar to those observed in the solubilized condition (Figure 2.7). Therefore, micrographs of these samples are not presented.

Samples isothermally treated at 950°C for 5 min are shown in Figure 2.14. The first signs of carbide re-precipitation were observed at grain boundary, as discontinuous morphology. The re-precipitation was more evident in H12Ti microstructure, whereas in H16Ti microstructure carbides were isolated near the junction of three grains.

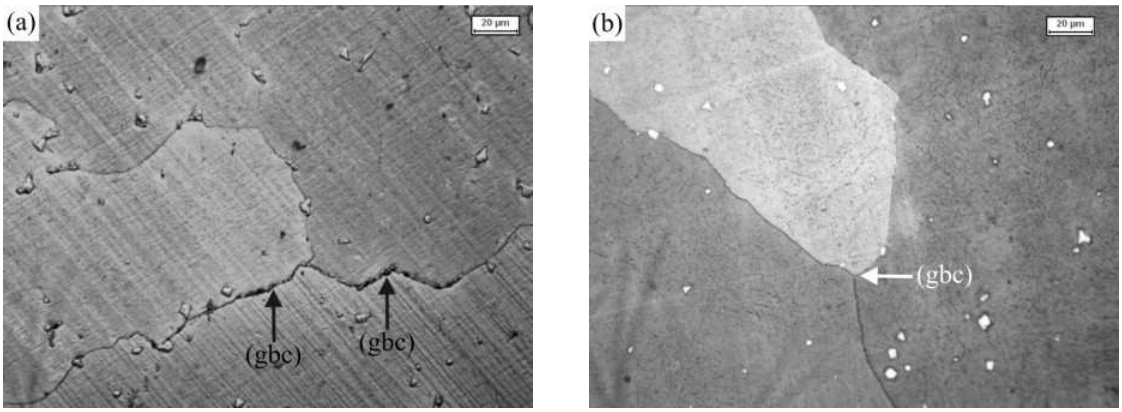

Figure 2.14. Micrographs of samples isothermally treated at 950°C for 5 min. (a) H12Ti, (b) H16Ti. The microstructures presented small quantities of grain boundary carbides (gbc). (Magnification 500x. Etched with Cogne Unico).

Figure 2.15 shows the micrographs of samples isothermally treated at 950°C for 15 min, where the effect of longer holding time can be appreciated. Clearly thick grain boundary carbides had developed along the grain boundary. In particular, the microstructure of H12Ti steel presented grain boundary carbides with a continuous morphology, whereas H16Ti microstructure maintained isolated grain boundary carbides. Samples treated at 950°C for 10 min (not shown) presented an intermediate structure between 5 min and 15 min treatment, while samples treated at 20 min (not shown) presented a network of carbides along the grain boundaries, comparable with what was shown in Figure 2.15.

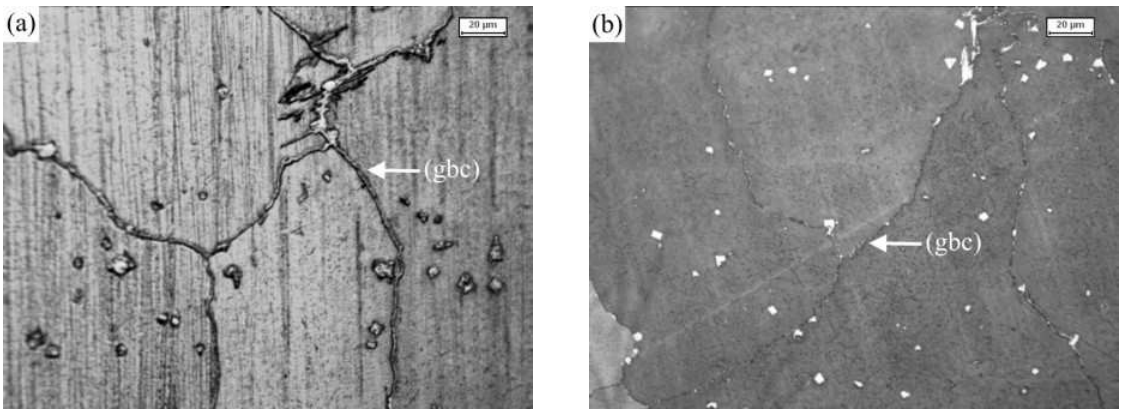

Figure 2.15. Micrographs of samples isothermally treated at 950°C for 15 min. (a) H12Ti presented a continuous phase of grain boundary carbides, (b) H16Ti presented a less developed phase of grain boundary carbides. (Magnification 500x. Etched with Cogne Unico).

Samples isothermally treated at 800°C for 5 min are shown in Figure 2.16. Thick grain boundary carbides of almost 1 µm thickness had developed along all the grain boundary for H12Ti steel. In contrast, H16Ti presented thick grain boundary carbides with an isolated morphology.

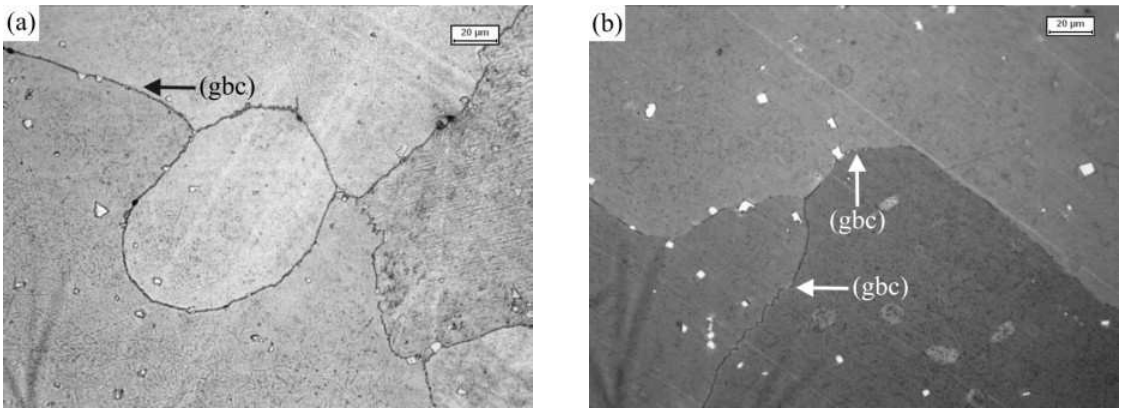

Figure 2.16. Micrographs of samples isothermally treated at 800°C for 5 min. (a) H12Ti presented a microstructure with continuous grain boundary carbides, (b) H16Ti presented a microstructure with still isolated grain boundary carbides. (Magnification 500x. Etched with Cogne Unico)

Figure 2.17 shows the micrographs of samples isothermally treated at 800°C for 15 min, where the effect of longer holding time can be appreciated. Acicular carbides appeared for the first time in H12Ti steel, which were observed as a fully developed thick grain boundary carbide network. H16Ti steel microstructure differed from the H12Ti steel as it only presented the thick grain boundary carbide network. Samples treated at 800°C for 10 min (not shown) presented an intermediate structure between 5 min and 15 min treatment, while samples treated at 20 min (not shown) presented a microstructure similar to that shown in Figure 2.17.

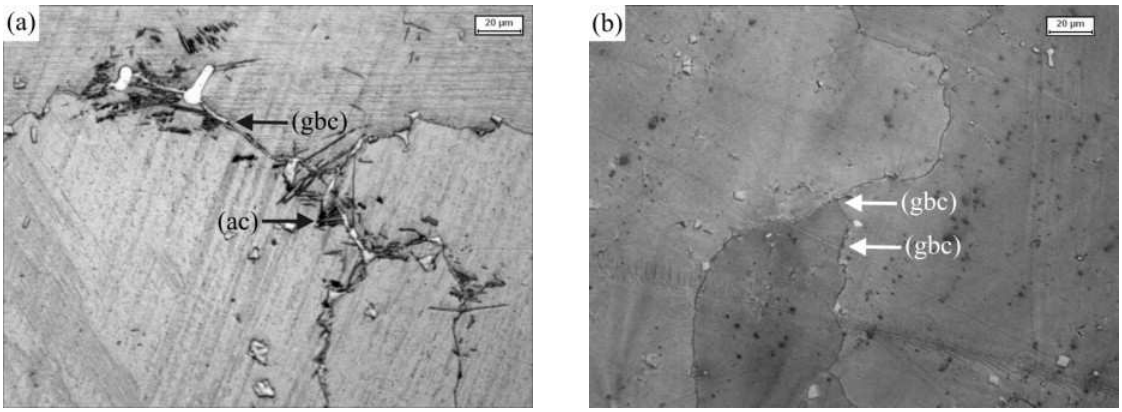

Figure 2.17. Micrographs of samples isothermally treated at 800°C for 15 min. (a) H12Ti showed acicular carbides (ac) and grain boundary carbides, (b) H16Ti showed only grain boundary carbides (gbc). (Magnification 500x. Etched with Cogne Unico)

Samples isothermally treated at 700°C for 5 min, are shown in Figure 2.18. The occurrence of thick grain boundary carbides and acicular carbides was dominant for H12Ti steel. In the case of H16Ti steel, there was no evident sign of acicular carbides, but there was a fully developed network of grain boundary carbides.

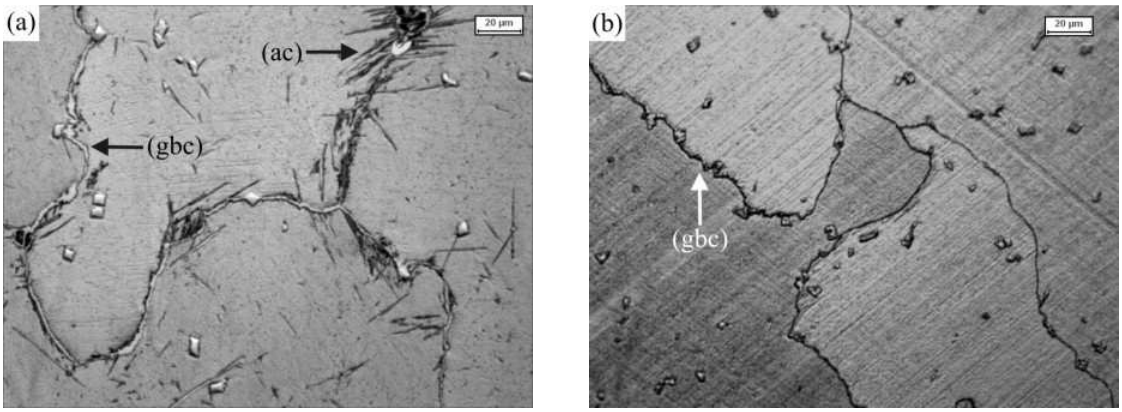

Figure 2.18. Micrographs of samples isothermally treated at 700°C for 5 min. (a) H12Ti showed the presence of acicular carbides; (b) H16Ti did not showed the presence of acicular carbides. (Magnification 500x. Etched with Cogne Unico)

In the samples isothermally treated at 700°C for 15 min, the presence of a network of thick grain boundary carbides was observed, accompanied with acicular carbides for both steels, as shown in Figure 2.19. Samples treated at 700°C for 10 min (not shown) presented a structure intermediate between 5 min and 15 min treatment, while samples treated at 20 min (not shown) presented a microstructure similar to that shown in Figure 2.19. Samples of both steels, H12Ti and H16Ti, treated at 650°C displayed a fully developed network of thick grain boundary carbides and acicular carbides. The images are not presented.

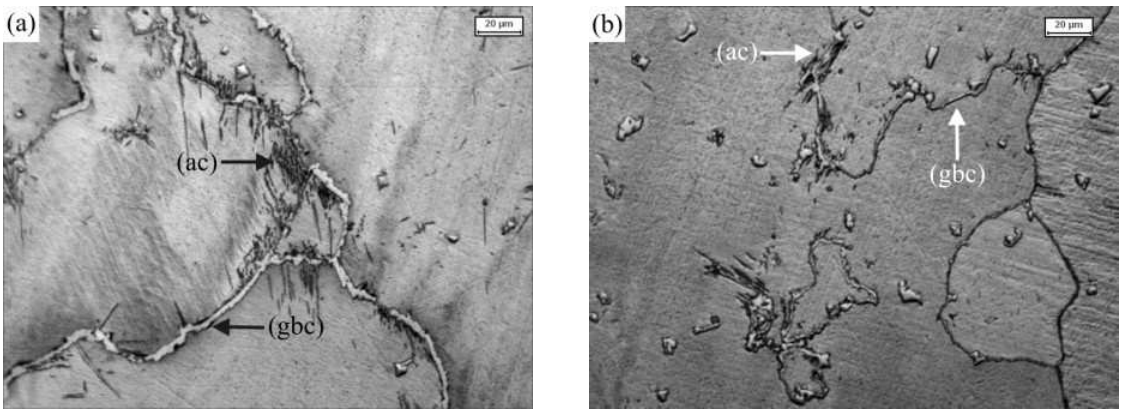

Figure 2.19. Micrographs of samples isothermally treated at 700°C for 15 min, both steels showed microstructures with thick grain boundary carbides and acicular carbides. (a) H12Ti; (b) H16Ti. (Magnification 500x. Etched with Cogne Unico)

Characterization with SEM revealed that the re-precipitated grain boundary carbides phases observed in the micrographics, presented similar composition in both steels. Acicular carbides also presented a similar composition in both steels. EDS microprobe analysis allowed semi-quantitative characterization of these phases. Figure 2.20 shows the SEM image of thick grain boundary carbides in H12Ti steel isothermally treated at 800°C for 10 min. The carbides formed a continuous film between the austenite grains. EDS spectrum showed that the grain boundary carbides were rich in chromium.

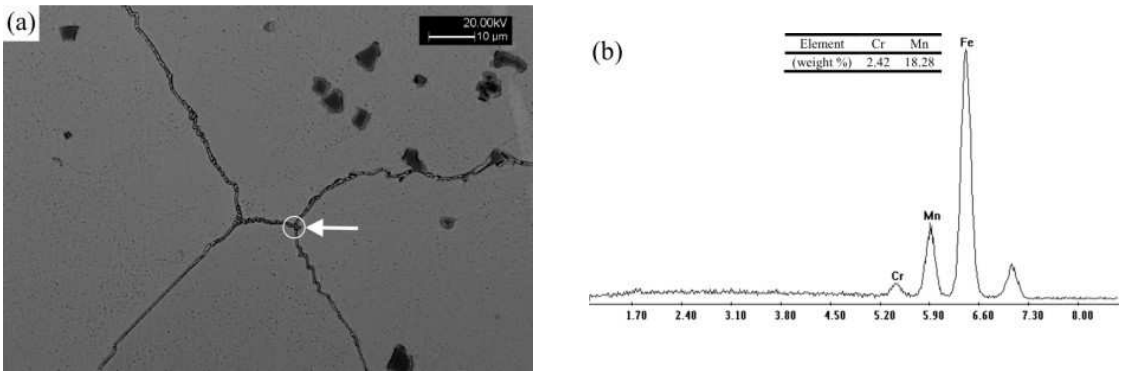

Figure 2.20. (a) SEM image of the H12Ti sample isothermally treated at 800°C for 10 min, where grain boundary carbides were visible along all the perimeter of the austenitic grains. (b) EDS spectrum on region inside the circle.

Figure 2.21 shows the SEM image of acicular carbides developed in H12 steel isothermally treated at 650°C for 20 min. The EDS analysis presented Cr content analogous from that of the austenite matrix.

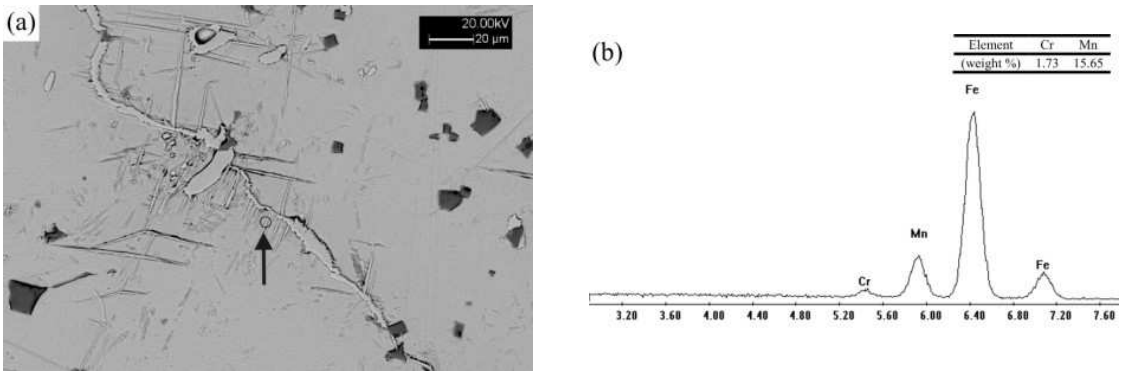

Figure 2.21. (a) SEM image of the H12 sample isothermally treated at 650°C for 20 min, where acicular carbides were present. (b) EDS spectrum on region inside the circle.

The results of the Charpy impact tests for the samples isothermally treated are shown in Table 2.8. The mean values of the isothermally treated specimens, for both steels, ranged between the as-cast and the solution treated. According to the results of the microscopic characterization, the majority of samples treated for 15 and 20 min presented structures characterized by a fully developed network of grain boundary carbides, which was already known to decrease impact toughness; therefore, only the samples treated for 5 and 10 min were tested.

Table 2.8: Results of Charpy impact tests for samples isothermally treated for 5 and 10 min.

Temperature	H12Ti				H16Ti			
	Time 5 min		Time 10 min		Time 5 min		Time 10 min	
(°C)	Mean (J)	SD	Mean (J)	SD	Mean (J)	SD	Mean (J)	SD
1000	191.0	13.2	137.3	9.4	291.5	12.2	275.9	8.9
950	183.7	8.2	132.1	11.1	278.2	9.5	267.5	10.2
875	95.4	5.6	45.8	6.7	195.9	5.9	185.4	7.6
800	31.5	7.4	34.6	7.7	121.2	6.9	112.4	8.4
750	17.9	6.0	18.4	4.8	123.5	5.7	81.8	6.8
700	19.4	4.6	22.7	6.7	71.5	4.9	40.2	4.9
650	21.5	7.1	24.1	8.1	24.4	9.4	19.4	8.5

Figure 2.22 shows the fracture of Charpy test specimens observed with OM. In micrograph (a) the fracture of the H12Ti specimen treated at 1000°C for 5 min is presented: the fracture was ductile and with trans-granular features. However, in the specimen of H12Ti treated at 750°C for 10 min (b), the fracture was fragile with inter-granular characteristics; grain boundary carbides were observed on the fracture line. SEM images of the surfaces of the fractures are presented in Figure 2.23 for the same specimens.

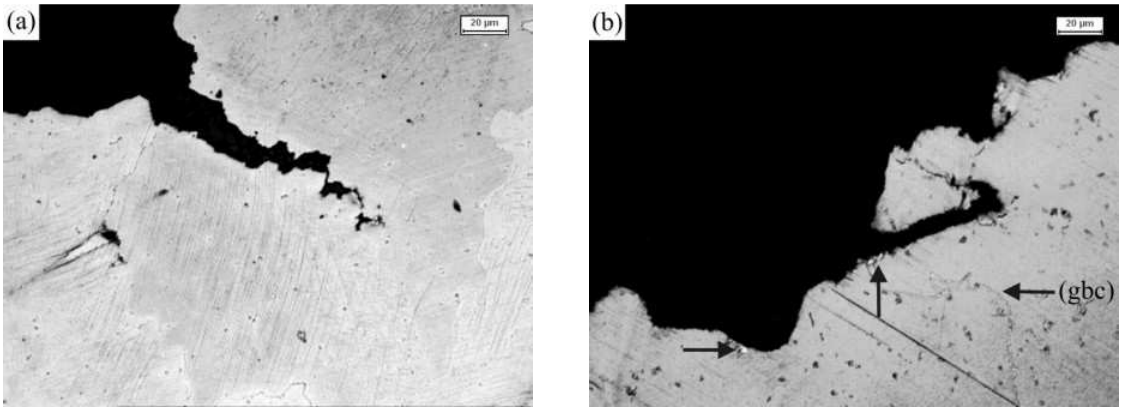

Figure 2.22. (a) Micrographs of H12Ti specimens in the regions near the fracture of the Charpy impact tests (a) isothermally treated at 1000°C for 5 min; (b) isothermally treated at 750°C for 10 min. (Magnification 500x. Etched with Cogne Unico)

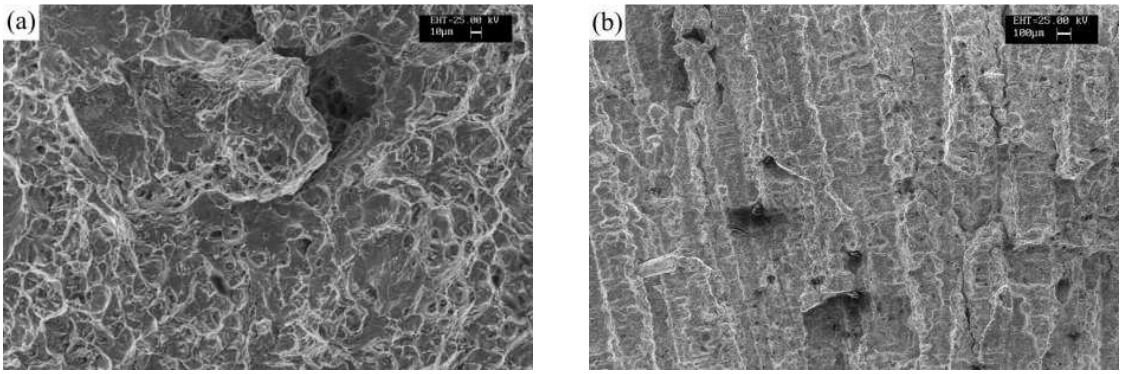

Figure 2.23. (a) SEM image of the fracture surface of H12Ti specimens (a) isothermally treated at 1000°C for 5 min, (b) isothermally treated at 750°C for 10 min.

2.5.4. Discussion

Austenitic manganese steels H12Ti and H16Ti presented different responses to isothermal treatment (steps i, ii and iii). H12Ti steel always presented the first signs of re-precipitation earlier than H16Ti steel. Grain boundary carbide re-precipitation started to be apparent at 950°C and 5 min treatment in H12Ti steel, whereas H16Ti steel showed only small evidence of carbides precipitation for the same treatment conditions. With the increment of holding time, H12Ti steel showed a fully developed network of carbides, while H16Ti steel presented only isolated carbides at grain boundary.

A similar behaviour was observed for the treatment at 800°C, where H12Ti steel showed developed grain boundary carbides at 5 min, whereas H16Ti steel presented less amount of carbides with isolated morphology. Finally, at 700°C the trend continued with the H12Ti steel with more developed carbides. At this temperature, thick grain boundary carbide networks were fully developed,

usually accompanied with acicular carbides. The different behaviour observed between the two steels investigated was be due to the 4% higher content of manganese in H16Ti steel, which may contribute to keep carbon inside the austenite matrix.

Taking in consideration the TTT diagram presented in Figure 2.2, it is possible to hypothesize that in the case of H12Ti and H16Ti steels, higher carbon content shifted the re-precipitation curves of grain boundary carbides and acicular carbides to higher temperatures and shorter times for both steels.

The EDS microanalysis showed that grain boundary carbides composition was richer in chromium than the austenitic matrix, which is in accordance with the results presented in literature [3]. Acicular carbides, however, presented an amount of Cr similar to the austenite matrix.

The Charpy impact tests results are presented as a graph of temperature vs. absorbed energy in Figure 2.24. The results were plotted according to steel type and isothermal treatment time. The results of the tests for solution treated and as-cast specimens are included (higher and lower values). The H16Ti sample showed clearly higher values of impact toughness than the H12Ti sample, this might confirm the correlation between the degree of re-precipitation phenomenon and loss of mechanical properties. The data obtained fitted exponential function curves, and showed that there was critical range of temperatures where absorbed energy values decreased rapidly. This range was approximately located between 925°C and 850°C for both steels.

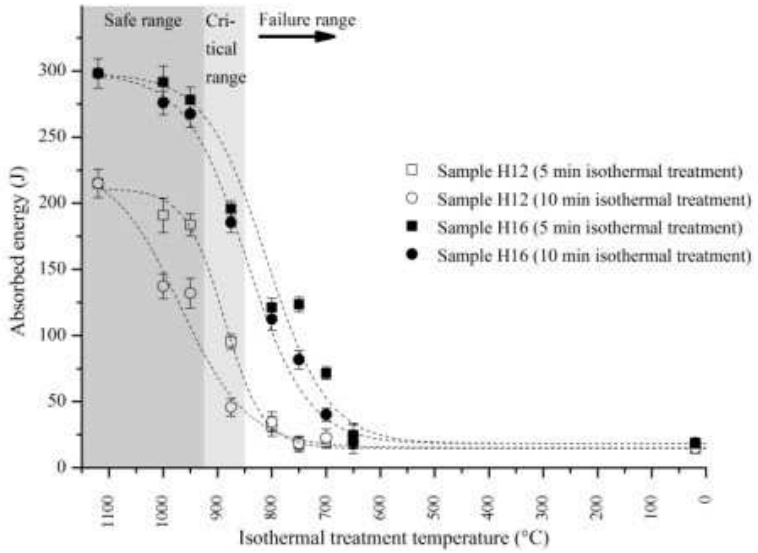

Figure 2.24. Impact toughness values vs. isothermal treatment temperature curves for H12 and H16 steels isothermally treated at 5 and 10 min.

Finally, Figure 2.25 presents two isothermal phase transformation curves: from austenite to austenite and re-precipitated carbides. The curves represent approximately the boundary conditions at which impact toughens starts to decrease rapidly (i.e. critical range of Figure 2.24). Utilizing the areas occupied with carbides in each micrograph (by counting pixels), and establishing a critical value of impact toughness, interpolations and extrapolations were performed for each temperature investigated. The resulting curves show the temperature-time conditions at which embrittlement became critical. The curve of H12Ti steel in particular, revealed a higher sensitivity of the re-

precipitation phenomenon; it started at higher temperatures and shorter holding times and extended for a wide range of temperatures. Whereas the H16Ti steel curve revealed a more traditional C-like behaviour. The curves allowed assessing of the impact of manganese content in the re-precipitation phenomenon.

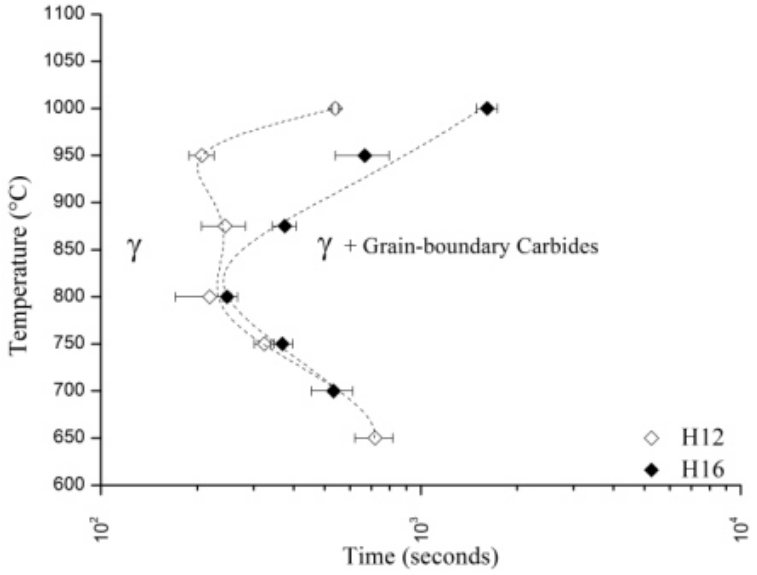

Figure 2.25. Isothermal phase transformation diagram, showing boundary limit conditions for carbide precipitation, based on impact toughness critical range.

2.6. CARBIDE RE-PRECIPITATION AT LOW TEMPERATURES

2.6.1. Introduction

H12Ti and H16Ti were tested with low temperatures heat treatments in order to study the re-precipitation of carbides that may embrittle the structure. Steel may be exposed at low temperature heating during the montage of the liners into the crusher. Therefore, the understanding of the sensibility of the steels to low temperatures may explain some failures occurring during operation.

2.6.2. Experimental

Samples of both H12Ti and H16Ti in already solution state underwent a heat treatment consisting on heating with a 3.57°C ramp to 300 or 500°C for 60, 120 or 180 min. Afterwards, they were quenched and characterized. Figure 2.26 shows the curves.

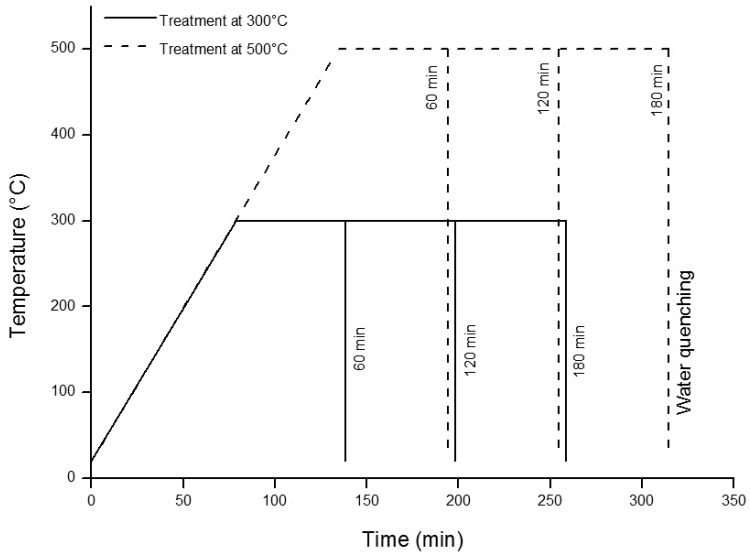

Figure 2.26. Thermal treatment curves

2.6.3. Results and discussion

The samples treated at 300°C did not show signs of reprecipitation, the micrographs showed a structure fully austenitized, similar to that observed in Figure 2.7.

Samples treated at 500°C instead, showed clear signs of re-precipitation in the form of acicular carbides. Figure 2.27 shows the acicular carbides presents at the internal of the grain as well as at grain boundary. Time had small influence, at 60, 120 or 180 min the density of carbides observed was approximately similar. In addition, for H12Ti and H16Ti the approx. same density of acicular carbides was found.

There seems to be a temperature around 500°C where re-precipitation starts. The kinetics seems to be fast, since at 60 min the major quantity of carbides was already developed. There is no significant difference of this phenomenon with different Mn content.

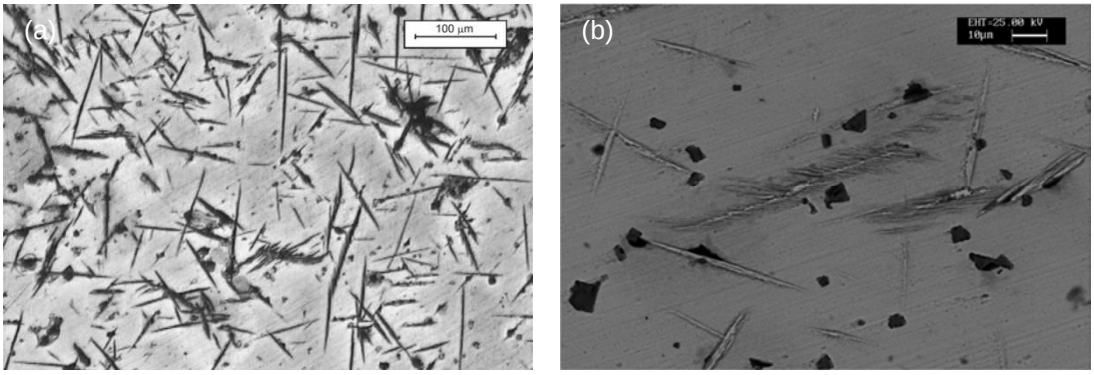

Figure 2.27. Sample of H12Ti treated at 500°C for 120 min (a) Micrograph (b) SEM image.

Reprecipitation of this type may occur during the heating of the pieces undergoing solution treatment. In industrial furnaces, due to the great mass of material treated, heating ramps are usually performed at stages, with intermediate holding times introduced in order to homogenise the temperature of the complete charge. According to the results presented, 500°C is a threshold for the phenomenon of reprecipitation. If the intermediate holding times of the heating ramp were performed

after 500°C, the reprecipitation of acicular carbides may be stimulated, which in turn may difficult the austenitization at 1090°C, especially in thick castings. Therefore, temperature homogenization during heating must be performed below the critical temperature.

2.7. SPHEROIDIZATION OF CARBIDES

2.7.1. Introduction

To avoid re-precipitation, it was tested the speroidization of carbides. The as-cast condition already possessed pearlite formed during the slow cooling in the olivine moulds. The experiment was designed in order to spheroidize this pearlite.

Both steels under study presented some content of pearlite in the microstructure, however H12Ti presented the most, therefore it was selected as the only material for experimentation.

2.7.2. Experimental

Samples in as-cast condition of H12Ti were heat treated using two temperatures as variable: 950°C and 1000°C for holding times of 180, 300, 420 and 540 min. Afterwards they were quenched. See Figure 2.28.

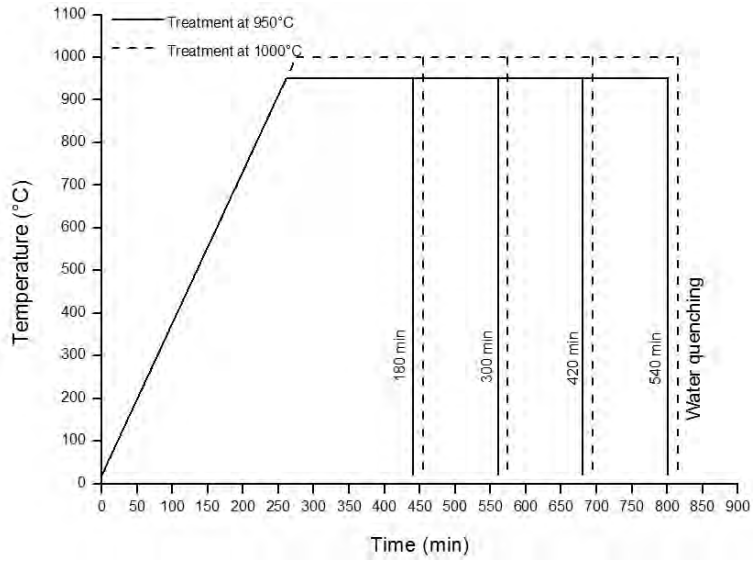

Figure 2.28. Heat treatment curves performed to H12Ti.

2.7.3. Results and Discussion

Figure 2.29 shows the results of the test at 950°C where carbides are neither dissolved nor spheroidized. The fine pearlite remained. The carbides presented a small tendency to become isolated. This meant that that the presence of g.b.c. diminished.

Time was not a relevant variable, the same morphology was observed at 180 min and 540 min, only the density of the network of carbides was smaller in the case of the longer time.

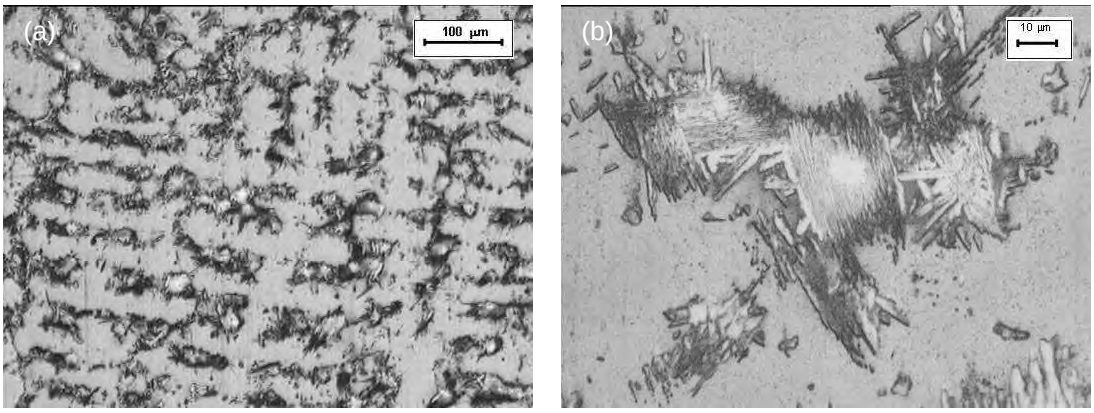

Figure 2.29. H12Ti treated at 950 °C for 540 min

The treatment at 1000°C presented the same structure of pearlite carbides remaining without solubilisation, as can be seen from Figure 2.30.

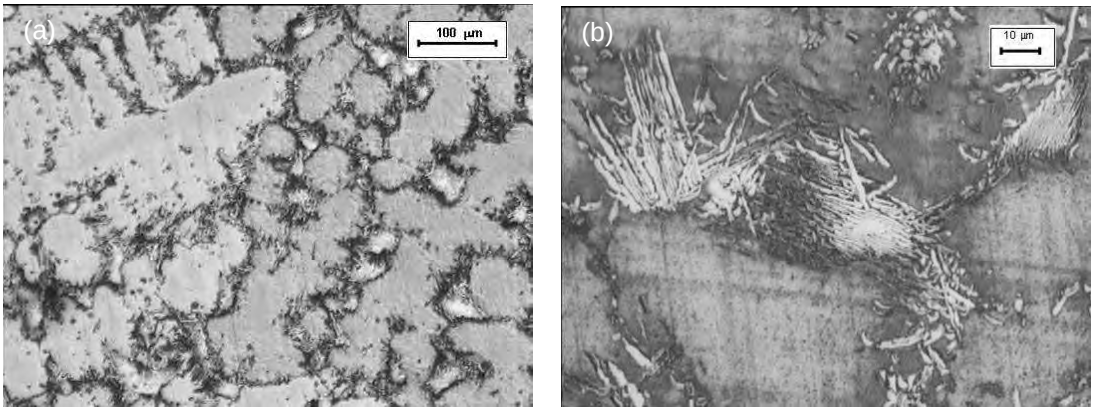

Figure 2.30 H12Ti treated at 1000°C for 540 min

Clearly, the procedure of spheroidization was not successful. One of the possible explanations may be the low Cr content of H12Ti (and H16Ti). Literature mentions the process of spheroidization to be effective in steels with chromium contents superior to 2% [2].

2.8. EFFECT OF QUENCHING CONDITIONS ON CASTING THICKNESS

2.8.1. Introduction

The test were performed in order to understand the relationship between casting thickness and quenching in industrial conditions. A steel ball was used so as to measure the phenomenon at different thickness.

2.8.2. Experimental

Two 300 mm diameter H12Ti steel spheres were casted. They were heat treated into an industrial furnace using the 1090°C-120 min solution treatment. After the heat treatment the spheres were quenched in different conditions. One sphere was quenched at the normal conditions of the water tank. This tank possessed stirrers and was connected to a recirculating systems with a cooling tower. The other steel sphere was quenched with enhanced conditions, which consisted on

introducing a big agitator into the quenching tank to further stir the water. Water temperatures was also controlled, and always kept at values lower than 50°C.

After quenching, a plate of each sphere was cut off from their centre using EDM wire. The dimensions of the plates extracted were 10 mm wide, 65 mm length and the depth was the complete diameter. From these plates, testing probes for Charpy impact test were cut at different depths

Additionally, a 100 mm jaw plate was heat treated and quenched, a thermo couple was attached to the surface of the casting in order to monitor cooling rate. The results of the characterization of a plate with similar geometry and treatment are presented in the next section.

2.8.3. Results and Discussion

The plates extracted from the centre of the spheres, allowed the determination of impact toughness as a function of depth (casting thickness) The results are presented in Figure 2.31. Unfortunately, the spheres also presented internal cracking, due to tensions accumulated during solicitation that were released during heat treatment. The presence of cracking is common in H12Ti and H16Ti, especially in large castings. Specimens for Charpy tests were recovered from the parts of the plates in sound conditions.

The sphere with standard quenching conditions presente a lower impact tougheness, with an average of just 47.6 J. The sphere quenched with enhanced conditions showed a slightly higher average with 53.9 J.

However, the most interesting analysis was the comparison of impact toughness values presented near the surface and in the centre of the spheres. In both cases, there were not important difference between these two regions. These could be explained only be the occurrence of reprecipitation, which had a faster kinetic than the cooling rate of both quenching processes.

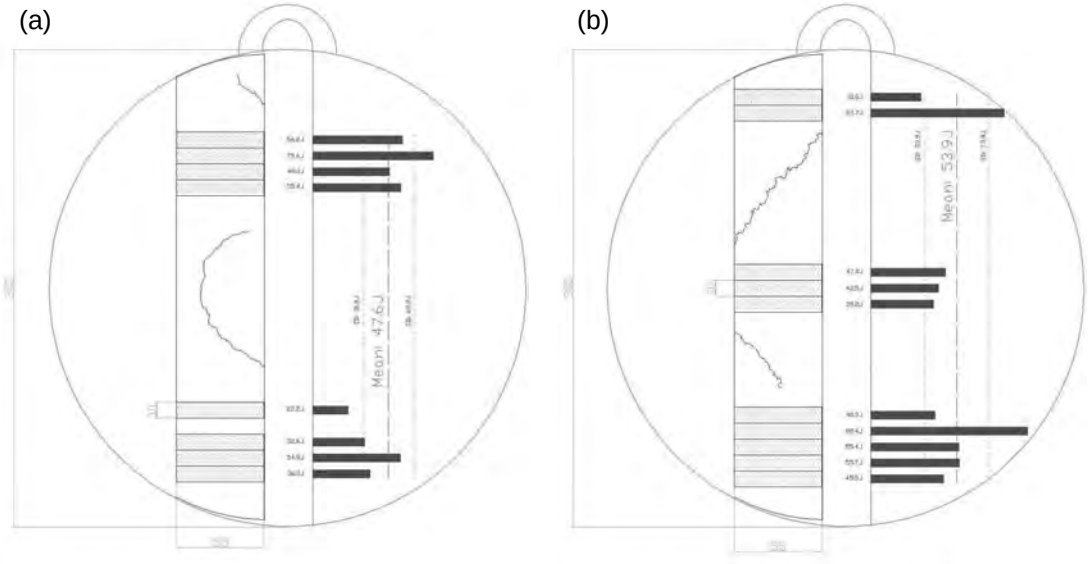

Figure 2.31 (a) Standard quenching conditions (b) Forced quenching conditions (extra stirring)

Figure 2.32 shows the plotting of the cooling curves of the two spheres plus the cooling curves of the jaw plate. Also, the re-precipitation curves were plotted. As can be seen, all curves pass across the re-precipitation curves. There was no great difference between the cooling curves of both spheres. The jaw, however, cross trough a smaller proportion the re-precipitation curves, and for H16Ti is faster. Therefore, thickness is a very important limitation. At thickness of 150 mm the reprecipitation is severe.

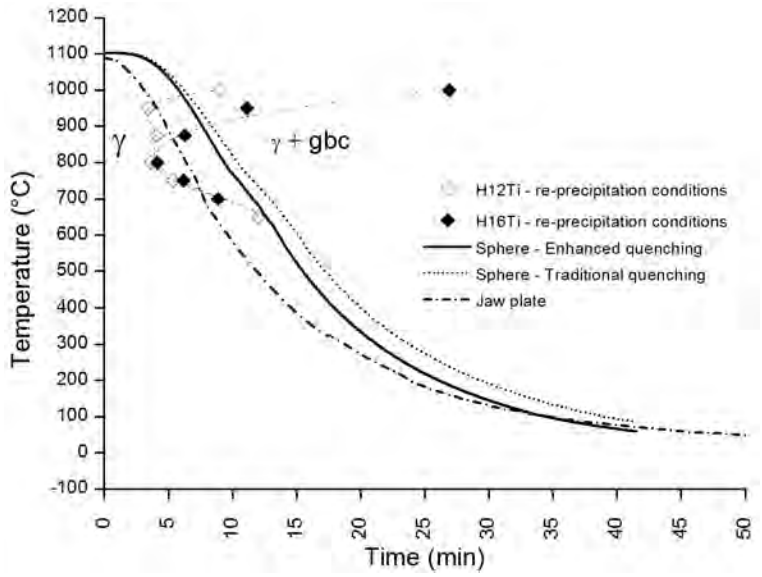

Figure 2.32. Cooling curve of both steel spheres and of a jaw plate overlapped to the re-precipitation curves presented in section 2.5.4.

The cooling rate of the spheres and the cooling rate of the jaw plate are all crossing the threshold of grain boundary carbide. In the case of the 100 mm piece, the period inside the γ+gbc region is smaller, therefore there is a less reprecipitation (see next section)

For the two steel spheres, the variation of the quenching conditions did not reduced significantly the time period inside the reprecipitation zone.

2.9. EFFECT OF QUENCHING CONDITIONS ON CASTING THICKNESS – 100 MM CASE

In order to illustrate the effects of poor solution treatment and ineffective quenching in relationship with casting thickness in industrial scale, a 100 mm piece was characterized of H12Ti steels. The sample was extracted from a crusher liner that failed during service and was recovered from the client and characterized in the laboratory. The thickness of the casting was between 100 and 150 mm. Furthermore, specimens for Charpy impact test were extracted. Figure 3.33 show the piece investigated.

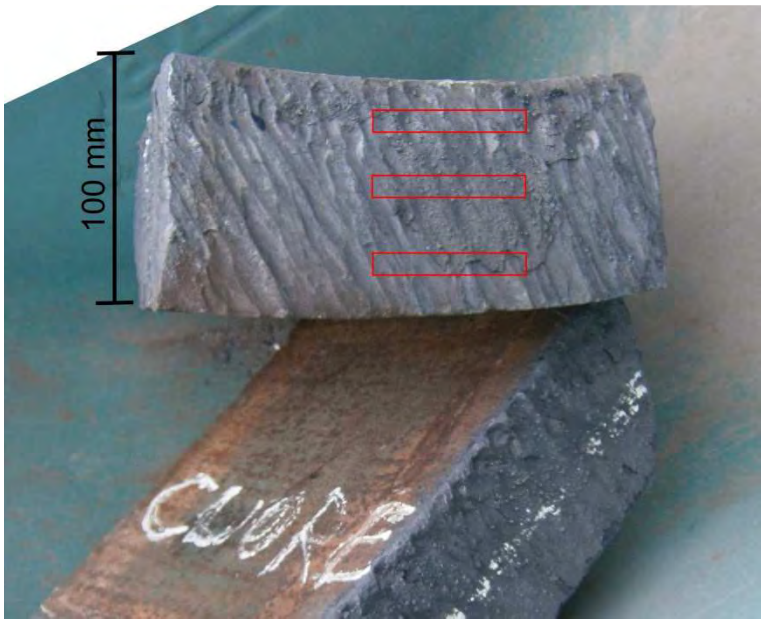

Figure 2.33. Piece of casting cut from a gyratory liner. The rectangles indicate the regions where the specimens were extracted.

The samples extracted at 15 mm depth showed grain boundary carbides reprecipitated, possibly due to poor quenching. However, at 50 mm depth (the centre of the piece), insolubilize carbides were found, probably due to an inefficient austenitizing heat treatment. The impact toughness at the surface was 31.7 J and at the centre was 27.6 J.

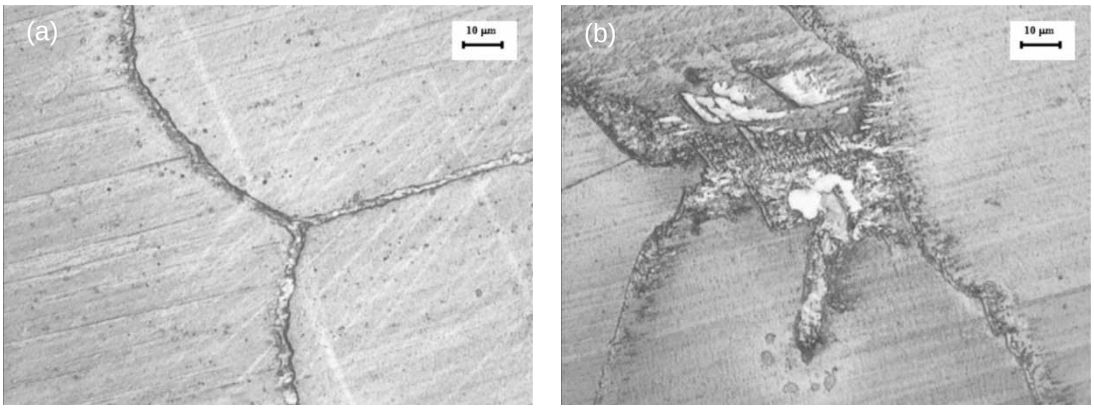

Figure 2.34. (a) Micrograph at 15 mm for the surface. (b) Micrograph at the centre of the piece (50 mm)

2.9. CHAPTER CONCLUSIONS

Solution treatment at 1050°C and 60 min was not appropriate for achieving complete austenitization of H12Ti and H16Ti steels. A new treatment was proposed consisting of a higher temperature and longer holding time. The 1090°C and 120 min treatment rendered the structure of both steels free of pearlite colonies and thick grain boundary carbides. Thin grain boundary carbides remained, although they did not greatly affected impact toughness, which was found to be very good for H16Ti and good for H12Ti. The solution treatment was adopted as the best alternative for enhancing the mechanical properties of both steels.

High carbon content (1.40-1.45%) promoted the formation of grain boundary carbides at temperatures as high as 950°C. Moreover, chromium content was identified as the mayor cause, together with high carbon off course, for carbide reprecipitation at grain boundary. It contributed to the incubation of carbides at grain boundaries.

The presence of discontinuous carbide re-precipitation observed in samples treated at temperatures above 950°C did not critically affect impact toughness. However, and independently of Mn content, samples treated at temperatures lower than 950°C presented a critical decrease in impact toughness.

Manganese content increased the incubation time of carbides (either grain boundary carbides or acicular carbides), and therefore contributed to maintain good values of impact toughness.

Micro-alloying elements, such as Ti, formed of stable carbides (or nitrides) which did not contribute to the carbide re-precipitation phenomenon. They were found to be intact after all heat treatments performed.

Efforts to prevent repecipitation via heat treatment were fruitless. The spheroidization showed to be extremely difficult to achieve for the current conditions presented by both steels.

A strong link between carbide reprecipitation and casting thickness was observed. When the thickness is superior to 100 mm, the reprecipitation becomes critical, and the steel could be considered too brittle for crushing applications.

At this point, it could be fairly stated that H16Ti, thanks to its higher content of manganese, possess the best mechanical properties, in comparison with H12Ti. Additionally, H16Ti showed higher resistance to carbide reprecipitation. Therefore, both steels could be clearly ranked; first H16Ti, as the most reliable for crushing applications, and second H12Ti, with properties much less reliable.

Under the chemical current chemical composition, reprecipitations is difficult to control, therefore variations the original compositions must be considered. H16Ti's chemical composition seems to be the best starting point for a new research orientated on the addition of alloying elements in order to maintain more carbon inside the austenite matrix, or to avoid the carbon to migrate to the grain boundary and form carbides.

The results and conclusions presented in this chapter dealt with the improvement of the mechanical properties of the steels and their microstructure. However, these is only represents half of the scope of this work. The next chapter will present the results of experiments that assess wear rate of H12Ti and H16Ti.

CHAPTER III – AUSTENITIC MANGANESE STEEL WEAR IN COMMINUTION PROCESSES

3.1. INTRODUCTION

3.1.1. Comminution processes in the mining industry

In the mining industry, because most minerals are finely disseminated and intimately associated with the gangue, they must be initially liberated before separation can be undertaken. This is achieved by comminution in which the particle size of the ore is progressively reduced until the clean particles of mineral can be separated by different methods such as floatation, gravitational, magnetic, among other. In the case of quarry products, such as aggregates for concrete, comminution processes are used to produce material of controlled particle size. In general, the desired particle size is achieved through successive stages of comminution processes and classification, or screening processes [24].

Explosives are used in mining to remove ores from their natural deposits, consequently blasting can be regarded as the first stage in comminution. Comminution in the mineral processing plant, takes place as a sequence of crushing and grinding processes. In the aggregate industry, instead, crushing is the only comminution process utilized. Crushing reduces the particle size of run-of-mine material to such a level that grinding can be carried out until the mineral and gangue are substantially produced as separate particles. Liners and other wear parts made of AMS are usually employed in crushing processes, and in some occasions in grinding [25] [26].

Crushing is accomplished by compression of the ore against rigid surfaces, or by impact against surfaces, for instance AMS plates, in a rigidly constrained motion path. This is contrasted with grinding which is accomplished by abrasion and impact of the ore by the free motion of unconnected media such as rods, balls, or pebbles. Crushing is usually a dry process, and is performed in several stages, with reduction ratios being small, ranging from three to six in each stage. The reduction ratio of a crushing stage can be defined as the ratio of maximum particle size entering to maximum particle size leaving the crusher (*i.e.* $F80/P80$). Grinding is usually performed "wet" to provide pulp feed to the concentration process, Mills with either steel rods or balls, or sized ore as the grinding media, are used in the last stages of comminution [27].

Rock particles are irregularly shaped, and loading force is not uniformly distributed in its entire surface, but is achieved through points, or small areas, of contact. Breakage is achieved mainly by crushing, impact, and attrition, and all three modes of fracture (compressive, tensile, and shear) can be discerned depending on the rock mechanics and the type of loading [27] [26].

When an irregular particle is broken by compression, or crushing, the products fall into two distinct size ranges: coarse particles resulting from the induced tensile failure, and fines from compressive failure near the points of loading, or by shear at projections (Figure 3.1). The amount of fines produced can be reduced by minimizing the area of loading and this is often done in compressive crushing machines by using corrugated crushing surfaces [24].

Another mechanism of rock crushing is by impact. In impact breaking, due to the rapid loading, a particle experiences a higher average stress while undergoing strain than is necessary to achieve simple fracture, and tends to break apart rapidly, mainly by tensile failure. The products are often very similar in size and shape [28].

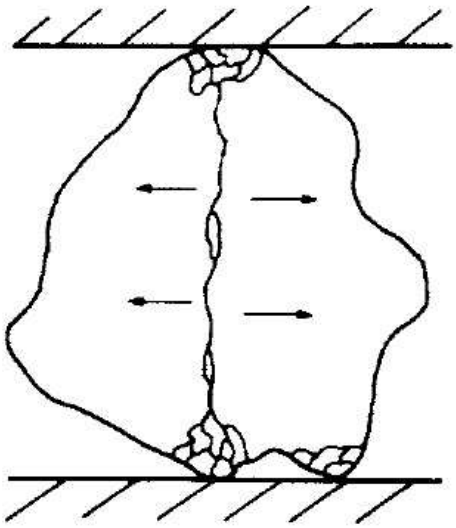

Figure 3.1. Comminution by crushing [24]

Crushing is the first mechanical stage in the process of comminution and is usually performed in two or three stages, as can be seen in Figure 3.2. The crushing forces have to be intense so that the elastic limit of the material being crushed is exceeded. Crushers tend to be massive and rugged (although sometimes portable), requiring large drive motors. They are energy intensive and expensive, both to construct and to operate [24].

In primary crushing, lumps of run off mine ore, or rocks from the quarry can be as large as 1.5 m across to 10-20 cm, feeding heavy-duty machines, which in turn feed the secondary crushers or AG/SAG mills. Usually, gyratory and jaw crushers are used in this stage [27] [26].

Secondary crushing includes all operations for reclaiming the primary crusher product from ore storage to the disposal of the final crusher product, which is usually between 5 and 2 cm in diameter. Cone crushers, HSI, HPGR can be considered secondary crushers [24].

Tertiary crushing deals mostly with already fine material as feed, and delivers products ranging from 20 mm to 6 mm. Sometimes there is a quaternary stage, but it uses the same principle. Hammermills, roll crushers and cone crushers are among the machines used in this stages.

Crushing may be in open or closed circuit depending on product size. In open-circuit crushing, undersize material from the screen is combined with the crusher product and is then routed to the next operation. If the crusher is producing material for ball grinding or final product in quarrying, it is good practice to use closed-circuit crushing in which the undersize from the screen is the finished product. The crusher product is returned to the screen so that any over-size material will be recirculated. One of the main reasons for closing the circuit is the greater flexibility given to the crushing plant as a whole. Closed-circuit operation also allows compensation for wear which takes place on liners, and generally gives greater freedom to meet changes in requirements from the plant [27].

Circuit configuration has an important role in liner wear; specifically the role of screens inside the crushing circuit is determinant to the performance of liners. Screening removes from the feed of the crusher material that is too fine for the process. The presence of this material in the crushing chamber is only detrimental since it occupies volume and may produce clogging. Also, and most important, fine material produces unnecessary low stress abrasion on the surface of the liners [26].

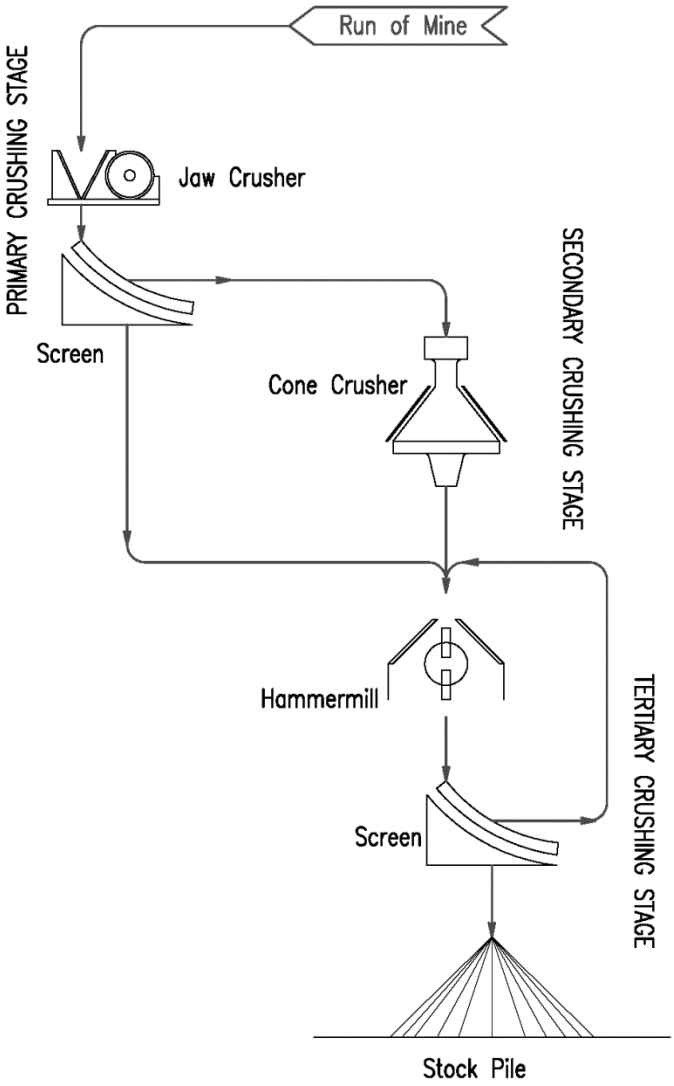

Figure 3.2. Flowsheet of a comminution process. Cone crusher is in open circuit configuration. Hammermill is in close circuit configuration.

Crusher design is another import factor considering liner wear, and it is one area that has not kept pace with new material developments, with jaw plates, cone liners and blow bars design being without major design modification for many years. The gyratory, jaw, cone, and roll crushers crush rock by applying high compressive forces to each rock, consequently high toughness is the most important required for the liners.

The Jaw crusher consist of jaws, or liner plates, which are set at an acute angle to each other, and one jaw is pivoted so that it swings relative to the other fixed jaw. Material fed into the jaws is alternately nipped and released to fall further into the crushing chamber. Eventually it falls from the discharge aperture, or closed side setting (CSS) [24]. AMS is used almost exclusively in the manufacturing of plates for jaw crushers due to the great forces involved in compression crushing.

The gyratory crusher consists essentially of a long spindle, carrying a hard steel conical grinding element, the head, seated in an eccentric sleeve. The spindle is suspended from a "spider" and, as it rotates, normally between 85 and 150 rpm, it sweeps out a conical path within the fixed crushing chamber, or shell, due to the gyratory action of the eccentric. AMS is the predominant

material for manufacturing liners for this type of crushers, although, there are new materials being used such as white cast high chromium iron for the shell or concave [24].

The cone crusher is a modified gyratory crusher; the essential difference is that the shorter spindle. Cone crushers tend to produce more elongated particles because of their high reduction ratios and ability of such particles to pass through the chamber unbroken. AMS is almost exclusively used for the manufacturing of liners (mantle and concave) of cone crushers for the same reasons of jaw crushers.

The horizontal shaft impactor comminutes by impact rather than compression, by sharp blows applied at high speed to free-falling rock. The moving parts are beaters, which transfer some of their kinetic energy to the ore particles on contacting them. The internal stresses created in the particles are often large enough to cause them to shatter. These forces are increased by causing the particles to impact upon an anvil or breaker plate. The hammers are made from AMS or, more recently, chrome white iron. The breaker plates are made of the same material. However, due to the high velocities of the hammer, the wear rate is very high. Impact hammers are, therefore, typically used to crush softer ores such as coal, limestone, and cement plant feed [27].

The hammersmills use the same principle of crusing by impact. Apart from the blow bars, or hammers, they have a casing in both sides and a grid at the bottom discharge. Hammermills tend to be used on smaller impact crushers or for crushing soft material. The exit from the mill is perforated, so that material which is not broken to the required size is retained and swept up again by the rotor for further impacting. The speed of the rotor varies between 500 and 2000 rpm, this type of machine is designed to give the particles velocities of the order of that of the hammers. Fracture is either due to the severity of impact with the hammers or to the subsequent impact with the casing or grid. Since the particles are given very high velocities, much of the size reduction is by attrition, i.e. breaking of particle on particle, and this leads to little control on product size and a much higher proportion of fines than with compressive crushers. In the last decades AMS has lost terrain to other alloy such as Low-alloy martensitic steel for this application. Due to the high rate of wear on these machines (wear can be taken up by moving the hammers on the pins) they are limited in use to relatively non-abrasive materials. They have extensive use in limestone quarrying and in the crushing of coal. A great advantage in quarrying is in the fact that they produce a very good cubic product [26].

There is an important difference between the states of materials crushed by pressure and by impact. There are internal stresses in material broken by pressure, which can later cause cracking. Impact causes immediate fracture with no residual stresses. This stress-free condition is particularly valuable in stone used for brick-making, building, and roadmaking, in which binding agents, such as bitumen, are subsequently added to the surface [24].

Impact crushers, therefore, have a wider use in the quarrying industry than in the metal-mining industry. They may give trouble-free crushing on ores that tend to be plastic and pack when the crushing forces are applied slowly, as is the case in jaw and gyratory crushers. These types of ore tends to be brittle when the crushing force is applied instantaneously by impact crushers. Impact crushers are also favoured in the quarry industry because of the improved product shape. In an impact

crusher, all particles are subjected to impact and the elongated particles, having a lower strength due to their thinner cross section, would be broken [29].

There are other types of crushers which not presented in this introduction, such as roller mills, HPGR, and VSI. These process are less common and very specific.

3.1.2. Wear in the mineral processing industry

The dominant wear mechanism in minerals processing is abrasion. Secondary to abrasion, but no less important, is metal-to-metal wear, which in many instances is complicated by abrasion as a result of the environmental conditions in which the machinery operates, such is in grinding processes.

Abrasion is arbitrarily subdivided into broad classifications corresponding to the nature of the wear material/abrasive particle interaction. The abrasive wear classifications usually cited include [26]:

- Gouging abrasion (the removal of large volumes of material per event from the wear surface)
- High-stress grinding abrasion (i.e., the abrasive particle is crushed during the wear interaction)
- Low-stress scratching abrasion (i.e., the abrasive particle remains intact as it moves freely across wear surface)
- Erosion (low-stress scratching)
- Erosion-corrosion (low-stress scratching abrasion in a corrosive environment)

In general, the wear behaviour of materials used in comminution processes is determined by a number of factors, which can be grouped into three main categories [26]:

- the properties of the wear material
- the properties of the abrasive material
- the nature and severity of the interaction between the metal-to-metal wear surfaces and between the abrasive and the wear materials.

These categories are interdependent because the nature of the metal-to-metal contact and the abrasive/ wear material interaction are influenced by the properties of the wear material, and to a great extent, by the properties of the abrasive. Increasing the size, density, or hardness of the abrasive particles, for example, influences the contact stress between the abrasive and wear materials, possibly leading to increases in the wear rate of the wear material. Similarly, if the abrasive particle is sharp, and upon fracture remains sharp, then the cutting or gouging action of the abrasive particle will continue to be effective in removing material from the machine component. Alternatively, in the case of metal-to metal wear, increasing loads place increased stress on contacting parts, which can change the normal mode of adhesive wear to some other damage mechanism (e.g., contact stress fatigue or even plastic yielding) [26].

3.1.3. Wear materials in the mineral processing industry.

The mechanisms of material removal during abrasion are complex and vary with the type of service conditions, consequently no single material can respond optimally in all conditions. By far, metallic wear components are the most prevalent in the mining industries. AMS does have a good

abrasion resistance, but if, abrasion resistance is the only criterion, there are a number of materials available, which are much superior e.g. Low-alloy martensitic steel or Chrome white iron [30]. Table 3.1 shows some of the materials commonly used in the mineral processing industry.

Table 3.1. Materials used in the mineral processing industry for wear applications. [31] [31]

Material Class	Material sub-class	Application area	Perceived advantages	Perceived disadvantages
White cast iron	High chromium	Castings, liners	High abrasion and erosion resistance, high hardness	Moderate impact resistance
Steel	Chromium molybdenum	Wet milling	Corrosion abrasion resistance	Toughness, fabrication and weldability limitations, cost, labour intensive, limited hardness
	Weld-deposited hard-facing	Liners, slurry piping, screen decks.	Excellent sliding abrasion resistance	Labour intensive, limited hardness
	Austenitic manganese	Liner for crushers	High toughness, high work hardenability	Poor sliding abrasion resistance, embrittlement at elevated temperatures
	AISI 1040-45	Slurry piping	Cost, moderate impact-abrasion resistance	Low hardness
	Tempered AR plate	Hopper plates, liners	Moderate to good abrasion and gouging resistance, cost	Toughness, fabrication and weldability limitations
	Martensitic	Blow bars	Good impact-abrasion resistance, weldability	Low hardness
	Pearlitic	Liners	Good under impact abrasive conditions	Poor corrosion -abrasion
Alloys	Ni-Co alloys	High temperature piping	Oxidation and corrosion resistance	Cost, brittle nature
Polyurethanes	Esters, Ehters	Idlers, cyclones, screens	Abrasion erosion resistance	Poor high impact performance
Natural Rubber		belts	Tear, impact and abrasion resistance	Poor ozone resistance
Synthetic rubber	Nitrile, neoprene, silicone	Linings, belts	Good abrasion and tear resistance	Sensitivity to chemicals

Wear rates in crushing and grinding units will be much higher than the wear exhibited in chute linings, screens, and classifiers. Indeed, crushing and grinding operations account for approximately 95% of the material wear in ore processing. These high wear rates arise because crushing and grinding are more energy intensive, and result in more severe impact and abrasive wear [31].

Consequently, the severe impact and abrasive conditions found in crushing and grinding equipment necessitate compromises in material selection criteria in order to minimize the risk of catastrophic failure of these units. Thus, the main reason why AMS are used in crushing processes is for their toughness [26].

Operators of ore processing plants are concerned with wear in terms of the weight loss per tonne of ore processed, especially in crushing and grinding operations. In addition, the energy consumption per tonne of ore processed is also a major concern, especially in the design and construction of new processing plants. There is a direct relationship between the amount of wear of the materials in that operation and the energy consumed by that operation. Therefore, by controlling the amount of wear in the various unit operations of an mineral processing plant, the energy consumed can also be controlled [30].

3.1.4. Wear resistance of Austenitic Manganese Steels.

The wear resistance of this material is a result of the austenitic phase's transformation into martensite because of the friction and impact on its surface. Austenitic manganese steel works well under wear conditions because of the relative speed with which the martensite is created and worn out. [32]. This almost unique ability to work harden rapidly in the locality of sudden deformation is what makes AMS so applicable to comminution processes.

Specifically, the physical mechanism, which causes such hardening, was studied by many researchers who attributed the rapid work-hardening rate in AMS to strain-induced transformation of γ to α or ε martensite, fine mechanical twinning, stacking fault-dislocation interactions, and carbon atom-dislocation interactions. Recently, it was showed that the principal mechanism of rapid work hardening is dynamic strain aging caused by the reorientation of carbon-manganese couples in the strain fields of dislocations [17] [32].

Nevertheless, understanding of this mechanism is not important for practical purpose of either manufacturing or application. Which is important about research on work-hardening mechanisms, is that it suggested that wear resistance might be improved by adding a solid-solution element which increased the solubility of carbon in austenite and simultaneously increasing carbon content [26].

Generally, in AMS, superficial hardness is about 160 – 220 HB after quenching, although the measurement of Hardness Brinell must be taken with caution in the case of these steels. Superficial work hardening of crusher liners maintains surface hardness of 450 to 500 HB over a base of high toughness. This combination cannot be duplicated by heat treatment. The work hardened profile depends on the nature of deforming force. In other words, no heat treatment can increase hardness of the AMS [22].

It is understood that performance of AMS will depend on the type of wear i.e. the wear is associated with heavy or moderate impact or no impact at all because deformation is a necessary pre-requisite for workhardening of manganese steel. Three different types of wear can occur in service of a crushing liner, i.e. Gouging abrasion, Grinding or high stress abrasion, and Scratching or low stress abrasion [22] [26].

In the first case, impact is always involved, such as in case of gyratory crusher or impact crusher. In such cases manganese steel would be able to absorb huge amount of energy and undergo extensive plastic deformation without cracking. Even if crack is eventually developed, manganese steel has such a unique resistance to crack propagation that early detection is possible before equipment damage occurs [26].

In the second type of wear, high stresses results from a crushing action. In such applications, logical choice, so far, has been AMS, mainly to avoid premature failures due to, either mishandling at user's end, or, negligence at manufacturer's end [26].

The third type of wear is no way connected to impact; because the scratching results from loose particles lightly abrading the steels. During this type of low stress abrasion AMS, as there is no chance of deformation, will not harden sufficiently to prevent surface erosion [26].

Gouging abrasion occurs under conditions where abrasive particles indent and move over the wear surfaces under high stress levels. It involves both cutting and tearing types of wear, in which small chips of metal are removed from the wearing surface by the movement of the sharp points of

rock, under considerable pressure, over the wearing surface. This type of action is very similar to machining by a cutting tool. Crushing is the typical operations that involves gouging abrasion. Therefore, wear liners of crushing units are particularly susceptible to gouging abrasion [26].

Gouging abrasion also occurs in impact crushers or almost anywhere where coarse rocks impact a metal surface under considerable pressure or force. Gouging abrasion normally occurs in the crushing and handling of large chunks of rock. It is accompanied by heavy impact and by high bending and compressive forces on the wearing parts, which are made as heavy section castings. As a result, the choice of ferrous alloys that can be used with confidence in these applications is limited. Traditionally, AMS with 12% Mn and 1.20% C are used as material for crusher liners [26].

AMS have fairly good resistance to gouging abrasion. For other applications involving gouging abrasion, such as autogenous mill liners, impactor bars in impact crushers, and earthmoving tools, the manganese steels have been partially displaced by Chrome white irons and Low-alloy martensitic steel.

3.1.5. Abrasive materials found in the mineral processing industry.

A mineral processing plant takes the mined ore and reduces it in size so that the valuable mineral component (metal sulphides and iron oxides, for example) can be separated from the gangue. The gangue in many cases is either silica or silicates, which are relatively hard and abrasive compared to metallic alloys. Each of the mining and minerals processing stages involves two or more wear modes. Selection of the most suitable wear material for the components used in each operation is made on the basis of the most severe one, minimizing the risk of catastrophic failure [25].

The abrasive materials (ore, mineral, or waste material) to be mined and treated can be characterized to some extent by their abrasivity (*e.g.* Abrasion index), and the energy required for comminution in crushing and grinding operations (*e.g.* Bond Index). These two parameters are in turn dependent on abrasive hardness and shape, and its compressive strength and fracture properties [24]. Some of the minerals handled in processing operations may be relatively benign in terms of their abrasivity, in which case they present no substantial wear problems. However, some mineral may contain a small proportion of hard, abrasive material. This is particularly true for coal, which sometimes contains coarse particles of harder minerals such as quartz, or steel slag which contains particles of steel. In general, the presence of the quartz, or another hard mineral, gives rise to significant abrasive wear in the processing equipment, which may not have otherwise occurred [27].

For a successful operation, the comminution process must contemplate the characteristics of the abrasive material. For example, size reduction of hard minerals is usually carried out in gyratory or cone crushers that operate at relatively low speeds and subject the mineral to high compressive stresses. Softer, less abrasive minerals, such as limestone or coal, can be comminuted in impact-type crushers, where a large proportion of the energy required for size reduction is developed through the kinetic energy of the rotating crusher bars and impact hammers [26].

Therefore, to characterize a material in order to predict wear or budget stock may be more difficult than the usual assessment performed to other mechanical parts subject to wear (i.e. bushings). Thus, many companies, and especially manufacturers of crushers and liners, have

developed classifications in base a compound of indexes and tests. Metso's classification is widely accepted in the metallic ore mining industry. Firstly, it classifies the rock according to crushability, be compounding a series of tests such as the Bond index and Los Angeles value. See table 3.2. This classification is used to design or select the appropriate size of a crusher. Also, it can be used for a control of the performance, especially when the ore varies in the operation [26] [33].

Table 3.2. Crushability test classification [34]

Classification	Bond Work Index (kWh/t)	Crushability (%)	Los Angeles value	Ai –8 mm product	Shatter Index
Very easy	0-7	>50	>27	>60	>40
Easy	7-10	40-50	22-27	45-60	35-40
Medium	10-14	30-40	17-22	30-45	30-35
Difficult	14-18	20-30	12-17	15-30	25-30
Very difficult	>18	10-20	5-12	0-15	20-25

Secondly, the classification of abrasiveness is usually employed for the prediction of wear rates of liners. There classification is particularly useful for the selection and optimization of materials, such as AMS grade. See table 3.3.

Table 3.3. Abrasiveness classification [34]

Classification	French Abrasiveness (g/t)	Abrasion Index
Non abrasive	0-100	0 – 0.1
Slightly abrasive	100-600	0.1 – 0.4
Medium abrasive	600-1200	0.4 – 0.6
Abrasive	1200-1700	0.6 – 0.8
Very abrasive	>1700	>0.8

3.1.6. Optimization of wear resistant materials

Development of optimum wear-resistant materials relies on design of the total tribosystem based on the mechanical characteristics of the triboenvironment. Further material refinement is based on knowledge of the wear mechanisms, with material parameters such as composition and microstructure becoming vitally important. Metals have an erodent hardness limit below which they can be useful as wear-resistant materials [31].

In general, this limit stretches up to the point where the hardness of the work-hardened metal equals the hardness of the erodent. Material removal occurs once the capacity to work harden is exceeded either due to strain rate or level of strain that results in fracture rather than yielding. AMS with a high work-hardening capacity can work harden under impact while continuing to yield. Tailoring of composition and microstructure to increase work hardenability is always a good option to start an optimization procedure. One method of increasing hardness is increasing the volume fraction of hard dispersed phase in the metallic matrix, such as TiC or NbC [17].

In some cases, a change in equipment or liner design can be more effective in reducing wear rates than a change to even the most expensive wear-resistant materials. The wearing surfaces of crusher liners are continually subjected to high rates of wear, such that repair and replacement of worn components is a regular maintenance activity. To facilitate easy replacement of worn

components, most crushers make use of components that are designed for easy and rapid replacement and/or repair, but sometimes this can be a disadvantage in terms of wear resistance [24].

Material choice occurs on three levels: first, the selection of the particular material class (metallic, ceramic, elastomeric/polymeric, composite), second, the selection within a particular material class (natural rubber, synthetic rubber, polyurethane), and third, the selection of desired microstructural and compositional features. Thus, under conditions for which a material is most suited, composition and microstructure play critical roles in wear performance. However, if the mechanisms of material removal are known, then composition and microstructure can be tailored for lower wear rate

The driving forces for development new materials and designing new equipment are increase in throughput and decrease in costs. In order to successfully re-engineer existing weak design points as well as optimize materials selection, one must develop a full understanding of the relationship between laboratory based selection tests and field performance [30].

In discussing metallic wear, some researchers have pointed out that wear resistance is not an inherent material property; consequently, there is not a single laboratory test or standard that measures wear resistance. The loading conditions in service must be suitably mimicked by a laboratory test in order for predictive life of a wear component to be estimated.

Standardized test methods are generally inadequate for wear simulation, because these tests are not based on individual tribosystem analysis. It was suggested that there are five important aspects of tribosimulation [30]:

- geometry of the contacting surfaces;
- transmission of force;
- interfacial environment;
- contacting materials;
- operation and failure observations.

The outcomes desired from a tribosimulation can be ranked as follows [30]:

- numerical wear rates in the laboratory test correspond directly with those observed in service
- the ranking and magnitude of the differences between candidate materials is the same in the laboratory and the field
- the relative ranking is the same in the laboratory and field
- the wear mechanisms are the same in the laboratory and field

Due to the expense, time consumption, invasive nature, and difficulty in controlling and quantifying field conditions, systematic studies in the field are relatively rare. [31]. Thus, in practice a range of wear tests must be utilized such that their tribosimulation parameters span the service environment. Such a series of tests can again, at best, only be used to rank material. Table 3.4 presents a list of the laboratory wear test.

Table 3.3. Laboratory wear tests [30]

Wear test	Conditions	Variables
Pin-on-disc	High stress abrasion (two-body abrasive wear)	Abrasive material, size, load, velocity
Dry sand rubber wheel	Low stress abrasion (three-body abrasive wear)	Erodent hardness, size distribution, shape, velocity
Erosion jet	Solid particle erosion	Erodent hardness, size distribution, shape, angle of incidence
Slurry jet	Solid particle erosion	Erodent hardness, size distribution, shape, velocity, slurry pH, temperature
Rotary impact crusher	Impact-abrasion wear	Impact velocity, feed type, size
Jaw crusher	Gouging abrasion	Ore mass, type, size
Slurry pot	Sliding abrasion	Particle velocity, concentration, angle of impact (all hard to control)
High speed impact	Impact gouging	Projectile velocity

Because, in practice, wear of materials involves a combination of two or more wear mechanisms, and materials often rank differently on single wear mode tests, identification of the dominant or synergistic wear mechanisms is vital. The value of the laboratory scale simulation is in its ability to provide data to support decisions on materials selection and design [31].

One of the most illogical, but unfortunately all too common laboratory/field test comparisons arises in situations where the field application involves considerable impact (or repeated Impact), but the laboratory test does not. For example, the pin-on disc test. [35] The net conclusion which can be drawn from these and many other similar types of investigation is that laboratory tests are seldom able to predict with any accuracy the actual wear of materials in the field. Notwithstanding the many conceptual problems which arise in respect of laboratory tests, there is still scope for their use provided that their validity is checked for each field application that they purport to simulate [30] [36].

Another very important factor which must be borne in mind in assessing the utility and validity of laboratory tests is whether they use an ideal “synthetic” abrasive or one which is actually encountered in service. The most widely used standard laboratory tests (the dry or wet sand rubber wheel tests and the pin on abrasive paper test) utilise relatively fine, homogeneous, pure minerals as the abrasive (typically silica sand, garnet, aluminium oxide or silicon carbide), which are very different from the abrasive materials encountered in practice. Since the type of abrasive encountered in the field probably exerts a greater influence on wear than any of the parameters associated with laboratory tests, it is clear that laboratory procedures must employ realistic abrasive species if they are to have any hope of producing meaningful results. It is interesting that laboratory tests developed by some of the mineral processing equipment manufacturers (such as the Bond test developed at Allis Chalmers) do use realistic abrasive species [24] [30].

Field tests do not suffer from the many deficiencies associated with laboratory wear tests. In particular, with appropriate care, real service conditions are exactly duplicated. These are not only those relating to wear but also to other environmental factors, and loading patterns and frequencies. Furthermore, the data need not be comparative, as is the case with laboratory test results. Absolute data can be obtained, which may be used to predict or estimate real component/product life in service [30].

The critical evaluation should include statistical analyses that enable the standard deviation or variance of the measurements to be determined. Lifetime service trials in which an item is used until it

is worn out and then is replaced by items of different materials until improvements eventually evolve, are not proper field tests. However, systematic application of a series of materials for lifetime service measurements can qualify as a proper field test provided that the lifetime of the liner is sufficiently short that parts made of different materials can be tested in a reasonable time. In order to qualify as a field wear test, certain criteria have been proposed [30]:

- the test specimen must constitute all or part of the actual hardware of concern;
- the wear conditions must be those of concern;
- the test specimens must cause little or no disturbance of the wear conditions;
- the time of the test must be relatively short compared with the time for the part to become obsolete.

Variability is usually measured by the standard deviation of a series of test results. The sources of variability in field testing are many, but the following ones are seen as being the most important [24] [27].

- Operating constraints: many components, particularly larger ones such as jaw crusher plates, cone liners, and blow bars can be conveniently changed only at the time of regular maintenance shutdowns. Such components may be discarded before they are fully worn if it is decided that they will not last until the next shutdown. The (incomplete) lifetime of the component will he recorded, not weight loss, and often tonnes of ore processed may not be recorded.
- Variability within ore bodies: It is common for the abrasiveness of the ore to vary within the ore body, thus adding to the variability of lifetimes.
- Equipment effects: such as age and uneven feeding.
- Operator effects: which is small in the case of modern automated crushing plants.

In general, then, field test results will be expected to be more variable than those from laboratory-scale testing. For instance, the ore handled would usually be less homogeneous than the screened and blended rock used in jaw crusher tests.

In some areas, such as primary and secondary crushing, field assessment appears difficult to carry out within a reasonable time frame and the use of realistic laboratory-scale testing methods is indicated. On-site testing of jaw crushers and gyratory crushers presents real problems. The crushers are large and may have relatively long lifetimes dependent on site conditions. Generally, the number of crushers at any one site is very small, so that effective replication (using different crushers as replicates) is not possible. For jaw crushers, the wear on different sections of the jaws may be, markedly different. For instance, one jaw is stationary and the other moves in the crushing operation. High impact wear occurs where the ore strikes the jaws from the feed bins. The feed may be uneven, leading to more wear on one side than the other. In addition, only running time data rather than exact amounts of tonnes crushed may be recorded. The effective lifetimes of the jaws are therefore likely to be very variable. This appears to be one area where realistic pilot scale or laboratory-scale testing

methods are needed. The problems for other types of crushers such as cone crushers and impact crushers are similar [30] [31].

There is a need for realistic pilot-scale testing methods, particularly applicable to components such as jaw crusher plates, blow bars and, cones, where efficient on-site testing is difficult and presents real problems. [30]

3.2. ROCK CHARACTERIZATION

3.2.1. Introduction

The materials for the pilot scale tests presented in this work were sourced from different parts of northern Italy. In total, the material used for all the pilot tests totalized around 30 tons. Additionally, the material processed in the industrial test was also characterized.

3.4.2. Materials and methods

For the pilot scale, the materials used were quartzite, rhyolite, steel slag and granite. The materials processed in the industrial test were andesite, dolomite, and the same steel slag used in the pilot tests.

Samples were observed under transmitted light microscopy and the identification of the phases was carried out by a Siemens D500 X-ray diffractometer (XRD) with CuKα radiation (λ=1.5418 Å, 40 kV and 30 mA). The surfaces of the samples were observed using a Cambridge Stereoscan 440 scanning electron microscope (SEM), equipped with X-EDS (Philips EDAX PV9800).

The specific gravities of each rock were determined using the picnometer method. The Metso classification and the Vickers Hardness Number Rock (VHNR) index were considered good indicators of the rock characteristics for this specific application.

Granulometric analysis were performed according to UNI-933. Shape of granulometric curves and F(80) and P(80) were used as indicators of the comminution performance. The results are presented in the corresponding sections of each test.

The sampling for granulometric analysis was performed using the guidelines of Gy's sampling theory. This theory is widely accepted in the mining industry as the most comprehensive and realistic theory regarding sampling of bulk materials [37] [38].

3.4.3. Results and discussion

Figure 3.3 presents the images of the materials used for the pilot test and Figure 3.4 shows the images of the materials used in the industrial tests.

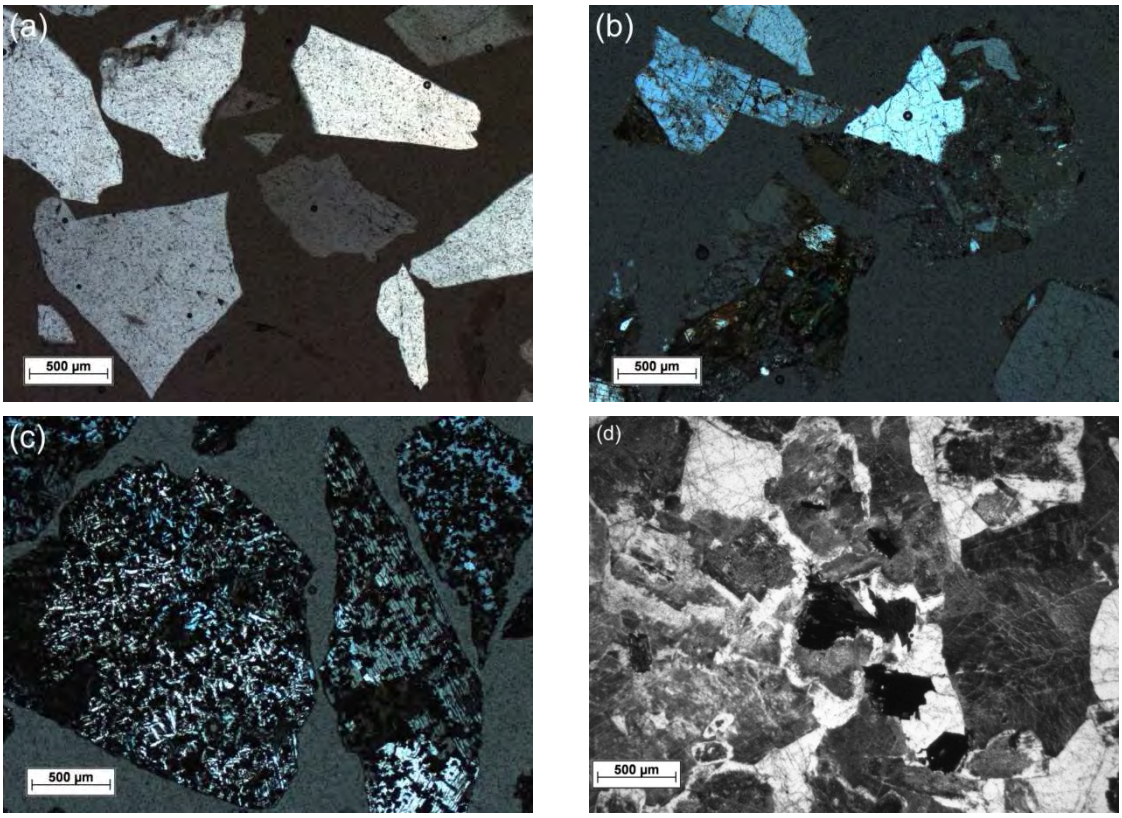

Figure 3.3. Transmitted light microscopy images of (a) quartzite, (b) rhyolite, (c) steel furnace slag, (d) granite, (e) andesite. (cross-polarized light, 25x)

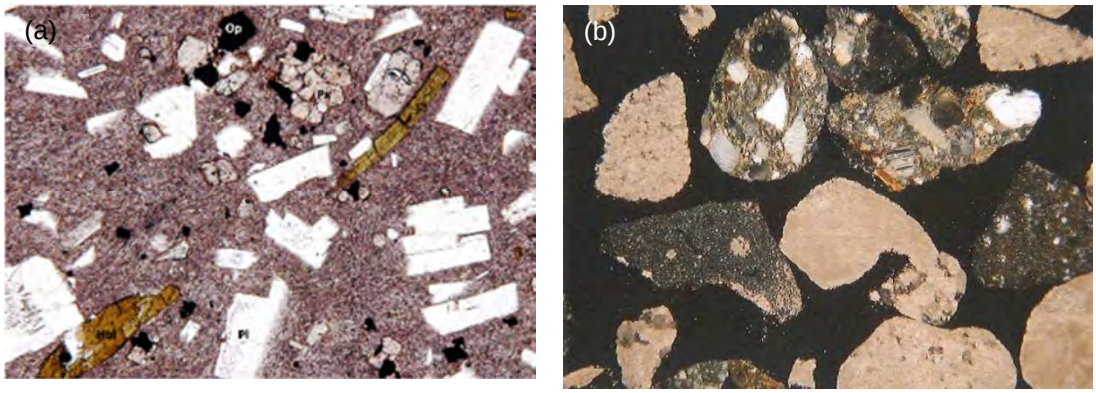

Figure 3.4. Transmitted light microscopy images of (a) andesite, and (b) dolomite. (cross-polarized light, 80x)

Rhyolite, was mainly composed of quartz, alkali feldspar and phyllosilicates, and presented a brown alteration around the grains. The rhyolite texture consisted of crystal grains, immersed into a mostly microcrystalline matrix containing a small proportion of glass. It was characterized by specific gravities of 2.54 g/cm^3 and by a VHNR ranging from 775 to 925 HV. This product may by classified according to the Metso's criteria as having: crushability index, difficult and abrasiveness index medium.

Quartzite presented pure well-formed crystals of quartz. Its specific gravities values was 2.61 g/cm^3 and VHNRs ranged in the intervals from 900 to 1060 HV. This product may by classified

according to the Metso's criteria as having: crushability index, medium and abrasiveness index very abrasive.

The steel furnace slag presented a texture of well-crystalized grains of Gehlenite ($Ca_2Al(AlSiO_7)$), contained a large amount of small crystals of chromian spinel; lime and metal iron were observed as well, but in smaller proportions. One particular feature of this slag was its 12,65% chromium content. Other particular feature of this material was the presence of small pieces of steel retained. It was characterized by specific gravities of 3.27 g/cm^3 and by VHNRs values ranging from 525 to 775 HV [39]. This product may by classify according to the Metso's criteria as having: crushability index, medium and abrasiveness index medium.

The granite presented mainly quartz and plagioclase, slightly altered feldspar to caolinite and mica. The solid density was 2.67 g/cm^3, and VHNRs values ranging from 725 to 925 HV. The Crushability work index of this material was 44.8% (-1.6 mm), and the abrasion index (abrasiveness) 1640 g/t (Ai -8 mm product) [34]. This product may by classified according to the Metso's criteria as having: crushability index, medium and abrasiveness index abrasive.

The andesite was a copper and gold ore with an average work index of 22, a moisture content of approximately 1% and was free from clay. The andesite possess variable mineralogy, but it can be distinguished by the presence of pyroxene, amphibolite and plagioclase. The matrix is dark, hemicrystalline and contains small laths of plagioclase. This product may by classified according to the Metso's criteria as having: crushability index, very difficult and abrasiveness index medium.

The dolomitic rock contained 38.3% dolomite, 36.6% of other calcareous materials, and 25.1% silica and silicates. This product may by classified according to the Metso's criteria as having: crushability index, medium and abrasiveness index slightly abrasive.

3.3. WEAR RESISTANCE CHARACTERIZATION OF THE STEELS

3.3.1. Introduction

Maranzana [1] presented pin-on-disc test results for H12Ti. As mentioned before, H16Ti was invented afterwards, therefore test results for this steel are not available. Consequently, new pin-on-disc test were performed on both steels.

3.3.2. Materials and Methods

Tests were carried out using a adapted pin-on-disc wear-testing machine on a 220 grit SiC abrasive paper stuck to a grinding disk, which rotated at 150 rev min-1. The tests were carried out in air at room temperature, and water was added. The wear rate was defined as the ratio of weight loss in time. Cylinder probes were machined from the two steels with 10 mm diameter and 50 mm length.

3.3.3. Results and Discussion

The results of the tests are presented in Figure 3.5. The final weight loss of H12Ti was 6.9% while the loss of H16Ti was 4.8%. Microhardness measurements were 360HV for H12Ti and 300HV for H16Ti.

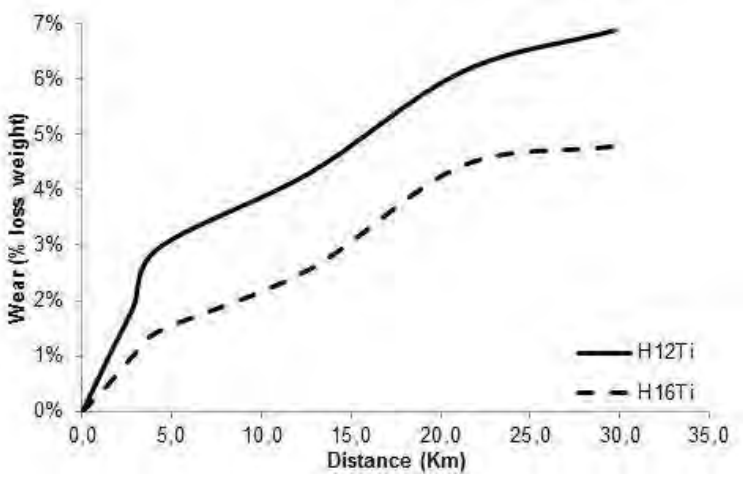

Figure 3.5. results of Pin-on-disk tests.

H12Ti had 43% higher loss of mass than H16Ti, which may lead to conclude that H16Ti is effectively more resistant to wear. The results concur with the results reported by Maranzana [1].

However surface harnesses observed determined low work-hardening. Therefore, the test may not had produced results fully representative of the wear phenomenon occurring in comminution applications. The results may be used, however, as indicative of the relative resistance of both steels in wet-sliding abrasive wear conditions, that sometimes occur when the feed of the crusher contains high amount of fines and moisture, as in the case of primary crushing of ore from open pits.

Therefore, the tests of wear resistance of H12Ti and H16Ti must be carried out using small comminution equipment and not conventional laboratory tests. In this way, the principle of wear will approximate to the actual wear occurring in the real size comminution applications. The following sections present tests that may be considered more representative of the wear mechanisms occurring in real application.

3.4. TEST OF COMMINUTION BY COMPRESSION MECHANISM

3.4.1. Introduction

The test was carried out to assess wear rate of H12Ti and H16Ti under compression crushing. Additionally, the test were carried out using different types of rock in order to study the relationship between rock parameters and steel wear.

3.4.2. Experimental

A Metso Jaw crusher was used for the test. The dimensions of the crusher's feed opening were 4" x 6". Seven sets of plate liners were casted for these tests in both steels. Figure 3.6 shows the drawings of the machine and the liners.

The materials used for the test were quartzite, granite, rhyolite and dolomite. The feed rate was set to 80 – 120 t/h. The quantity of material processes varied from 1000 Kg to 2000 Kg according to the availability of the resource. The steel liners were weighted every 200-300 Kg in order to keep track of the weight loss. The CSS was kept constant at 10 mm throughout the test. In total seven tests

were performed. Particle size of the feed was 20 mm (F80) and the particle size of the product was 3.1 mm (P80).

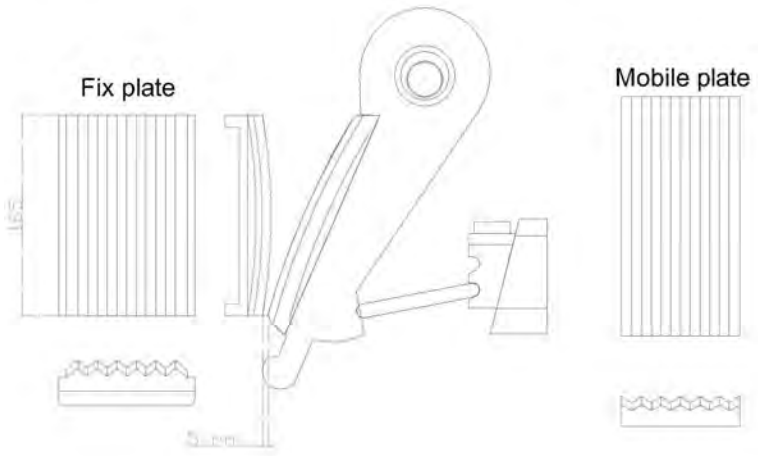

Figure 3.6. Metso jaw chused and the fix and mobile liner plates.

3.4.3. Results and Discussion

The test using dolomite showed a wear ratio of 15 g/t for H12Ti and 20 g/t for H16Ti. However, the wear ratio in the first 500 kg is higher, showing an initial difficulty to workharden. Afterwards the wear ratio becomes linear.

The test of rhyolite presented a wear ratio of 59 g/t for H16Ti. This material was hard but brittle, and thus required high effort of the machine to crush. The power consumption of the machine was higher than in the other tests.

Granite showed very similar wear rate for both steels, with approximately 93 g/t at 1000 kg of material processed. Both steels presented regular and almost linear wear.

Finally, the highest wear ratios were observed in the quartzite with 122 g/t wear ratio for H16Ti and 131 g/t for H12Ti. The particular change of wear rate at different stages of the test could not be explained. Figure 3.7 shows the curves of accumulated weight loss of the steel plates classified by type of steel and rock.

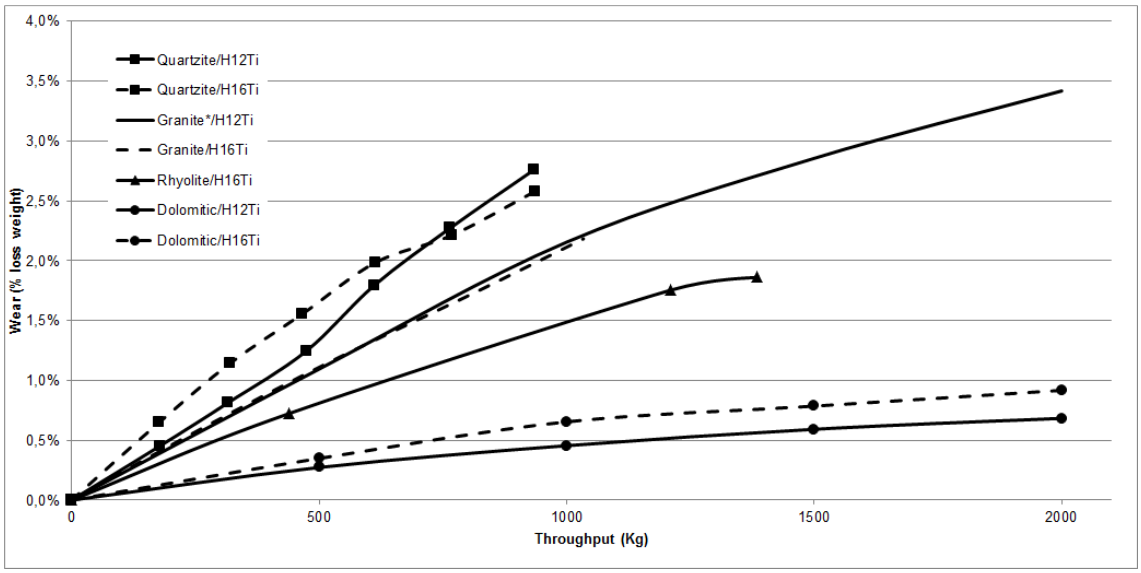

Figure 3.7. Results of wear test of jaw chusher liners according to rock type and steel tested.

Figure 3.8 shows the jaw plates of H16Ti, from granite test. The profile of the plates shows a groove just 10 mm above the bottom. This groove indicated that most of the crushing work was performed in this area, because the P80 value was relatively close to the CSS gap. Also the angle of the plates had some incidence in the forming of this abnormal wear.

Nevertheless, this groove is observed in many jaw crushers in industrial applications. The figure also shows an area of the liner's surface where there is clear sign of gouging abrasion.

H12Ti seems to be superior to H16Ti when treating low abrasive materials, but H16Ti showed equal or better behaviour when treating medium to high abrasive materials.

The test configuration seemed realistic and the results reliable. Furthermore, granite was selected as the abrasive material for future tests, since it showed uniform behaviour in both steels. Granite is also a very representative material as it is widely processed in the aggregate industry.

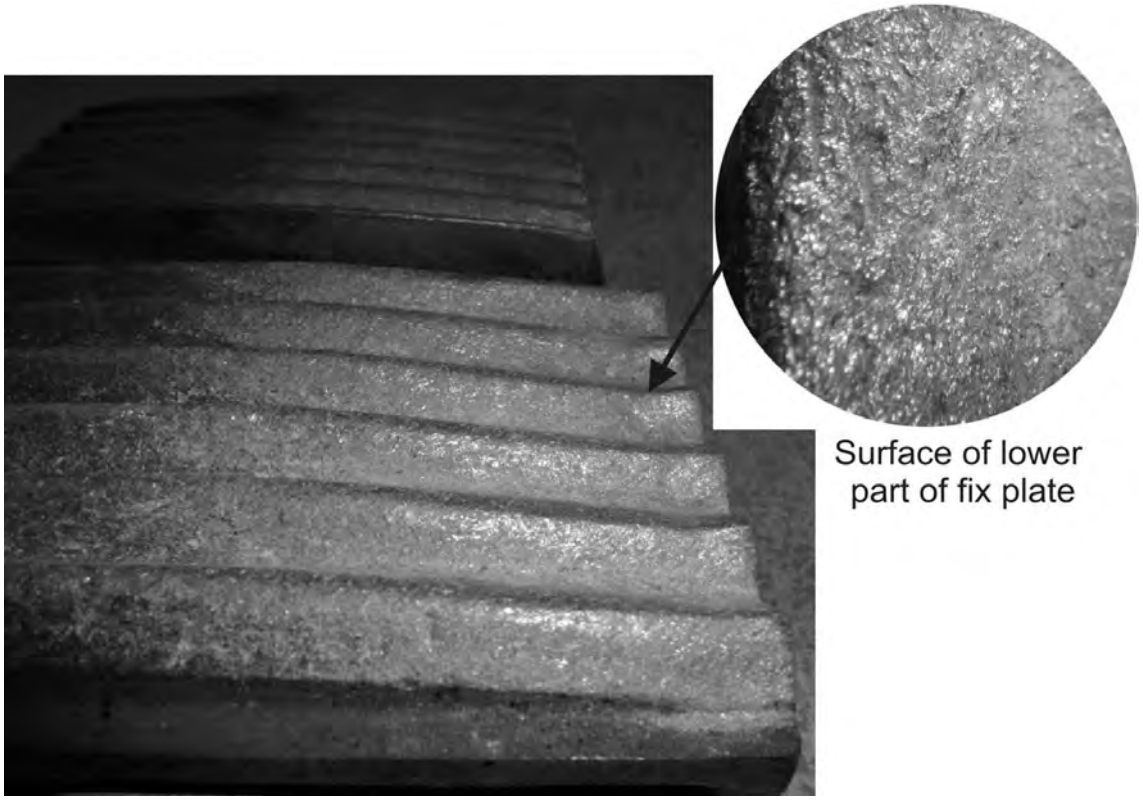

Figure 3.8. Jaw plates after wear test. Top: mobile plate. Botton: fix plate.

3.5. TEST OF COMMINUTION BY IMPACT MECHANISM – VARIABLE HEAT TREATMENT

3.5.1. Introduction

The test was carried out to assess wear rate of H12Ti and H16Ti under impact crushing conditions. For these series of tests, different heat treatments were used. The test were carried out using only one type of rock in order to study only the relationship between steel wear and heat treatment [40].

3.5.2. Experimental

A Hazemag HSI mill with a rotor diameter of 255 mm was used. The rotation speed was 1957 rpm. Five sets of blow bars were casted for these tests. Figure 3.9 shows the drawings of the machine and the blow bars.

The material used for the test was granite. The feed rate was set to 80 – 120 t/h. The quantity of material processed was about 2200 Kg for each test. The steel liners were weighted every 200-300 Kg in order to keep track of the weight loss. The gaps between shield and blow bars were kept constant at 5 mm and 10 mm throughout the test.

The sets of blow bars were treated with the following solution treatments:

- H12Ti solution treatment 1090°C – 120 min (complete solution heat treatment)
- H12Ti solution treatment 1090°C – 60 min (half solution heat treatment)
- H12Ti as-cast (without solution heat treatment)
- H16Ti solution treatment 1090°C – 120 min (complete solution heat treatment)

- H16Ti as-cast (without solution heat treatment)

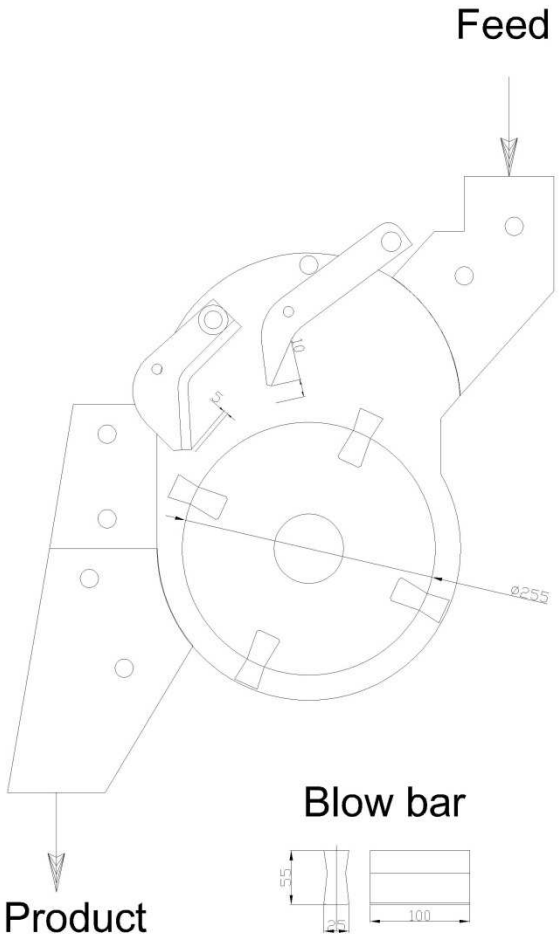

Figure 3.9. Design of HSI impactor and the blow bars employed

After the test, samples were extracted for the blow bars for characterization. Additionally, the microhardness profile was determined.

3.5.3. Results and Discussion

The wear ratio observed was more or less uniform throughout the duration of each tests. In other words, an initial fast wear ratio was not observed.

In general, H16Ti presented the lowest wear ratio, with 244-247 g/t. More specifically, the blow bars in as-cast condition presented slightly higher wear ration than the ones with the complete austenitization treatment.

H12Ti instead, presented the highest wear ratio, with values of 282-307 g/t. In this case, the trend is inverted, because the steel that presented the higher wear was the one with the complete heat treatment.

The trends do not permit to draw clear conclusions about the influence of carbide presence in the microstructure and their relationship with wear ratio.

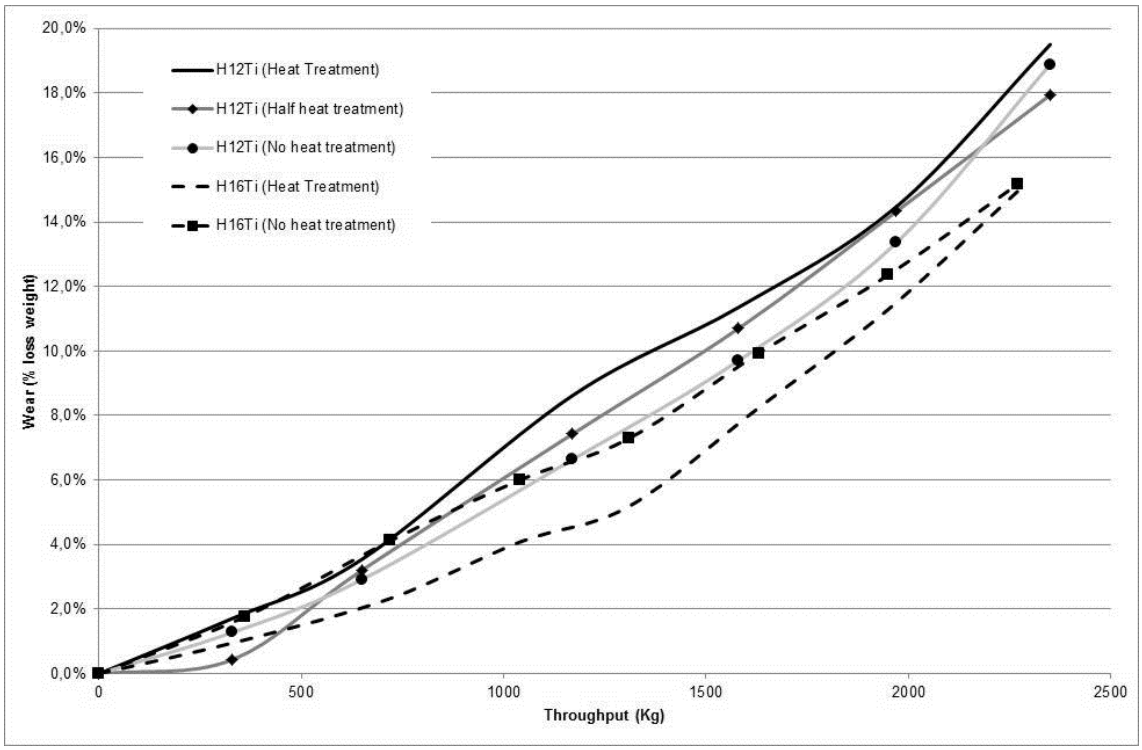

Figure 3.10. Results of wear test for different heat treatments

Good workhardening was observed in both steels. The microhardness profile showed an increase from 300 HV in the matrix to 475 HV for the H12Ti treated and 610 HV for H12Ti without heat treatment. The values of H16Ti were similar.

Figure 3.11 (a) present a micrograph of H12Ti solution treated were a lateral view of the worn surface of the blow bar is presented. The bands of work hardening are clearly observed, they stop at the grain boundary. The picture also shows the place of carbides that were detached from the austenitic matrix.

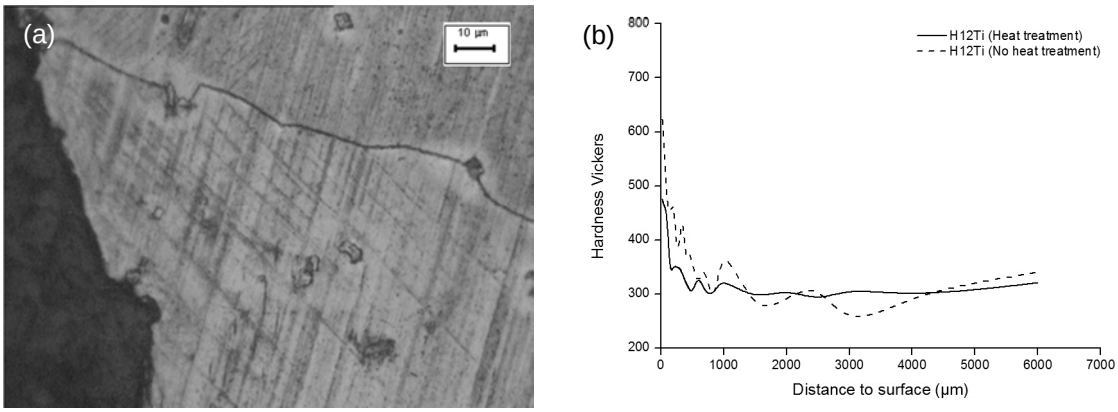

Figure 3.11. (a) Micrograph of H12Ti showing the worn surface, (b) Microhardness profile of H12Ti for different heat treatments.

Figure 3.12. shows a 3D drawing of the blow bar at different stages of wear. The rounding of the shape is observed in the first 1500 kg, afterwards the profile tend to become flat. The loss of shape is correlated to work rate and to the loss of quality in the P80.

The front surface of the blow bar shows the signs of gouging abrasion by impact. There are places were small pieces of metal were removed, and others were a large amount of material was removed. The top surface showed also more microploughing and microcutting. This type of abrasion is to the compression of the rock against the blow bar and the edge of the impact shields.

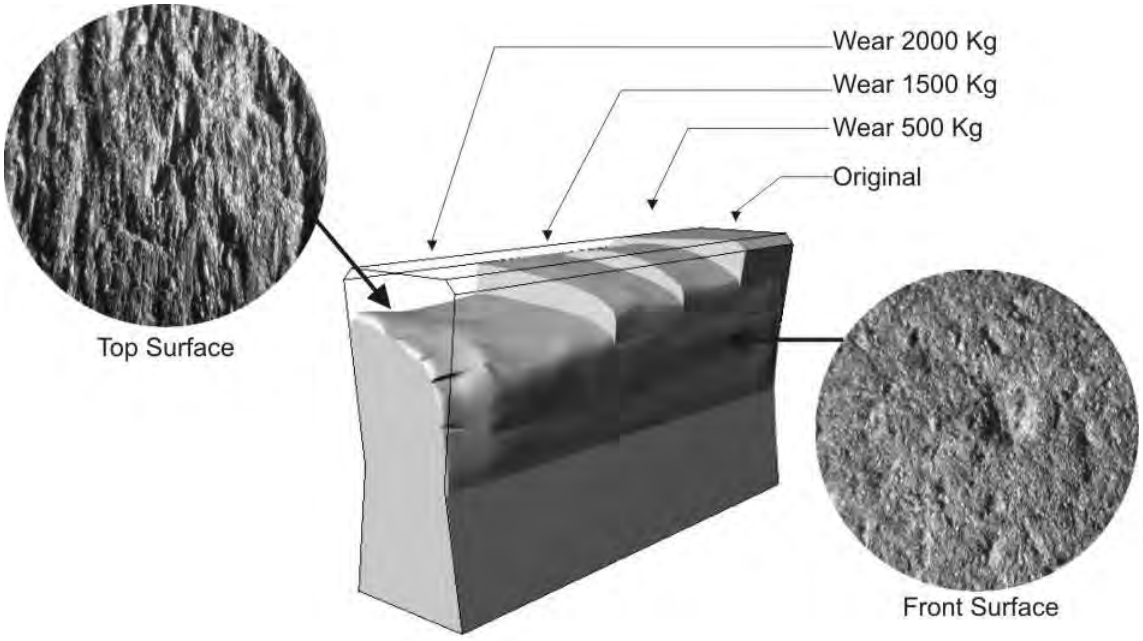

Figure 3.12. Image 3D of blow bar showing the progressive wear, according to quantity of material processed. Also, the type of gouging abrasion is shown on the different zones of the blow bar.

3.6. TEST OF COMMINUTION BY IMPACT MECHANISM – VARIABLE PARTICLE SIZE

3.6.1. Introduction

Andesite was tested using the same conditions as presented in 3.5. The scope of the test was to assess the influence of particle size in the final quality of the product.

3.6.2. Experimental

The abrasive material was the andestite, and the blow bars were made of H16Ti with solution treatment.

The material was separated in different class sizes as following:

- Fraction (+¼''-open)
- Fraction (+¼'' – -3/8'')
- Fraction (+3/8'' – -½ '')
- Fraction (+½ '' – - ¾'')
- Fraction (+¾'' – -1'')
- Fraction (+1'' – -1 ½'')

- Fraction (+1 ½'' – -2'')
- Whole material: P(80) = 25.22 mm
- The fraction of fines, -¼ was removed of the sample, because fines are not efficiently crushed in a HSI.

The total amount of sample processed was about 147 kg. During the processing, product samples were cut for granulometric analysis. The curves can be found in Figure 3.13.

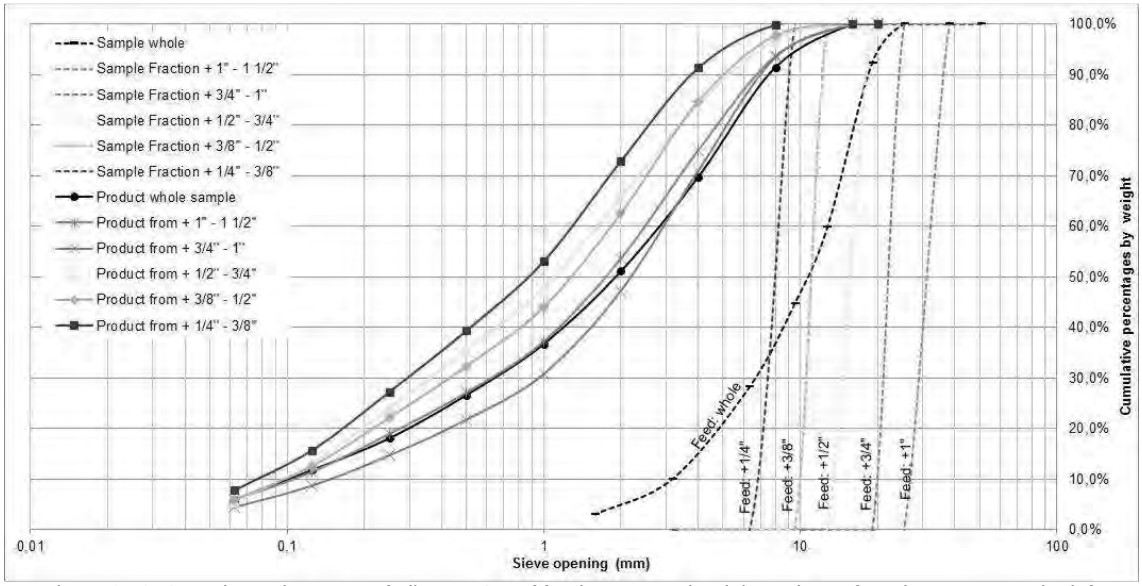

Figure 3.13. Granulometric curves of all tests. Set of feed curves to the right and set of product curves to the left.

3.6.3. Results and discussion

Average P(80) of the seven test was 4,28 mm, with a standard deviation of 1,02 mm. The results show a good response of the material to impact crushing. The products of all the test were uniform, as can be seen in the image, where all the sizing curves were plot together. Wear ratio of the blow bars was 600 g/t (grams of steel per ton of rock processed).

The wear ratio is more or less representative of what is generally found in industry for this type of material.

3.7. FIELD TEST A: METALLIC MINING

3.7.1. Introduction

Three set of liners for cone crusher were tested in a copper-gold mine located in the Andes mountain range in South America. The main scope of the tests was to assess mechanical properties response of both steels in real application; also, the wear rate was characterized in order to compare with the test presented above.

3.7.2. Experimental

The liners tested were 2 sets of mantle and concave in H12Ti and 1 set in H16Ti. They were treated with the solution treatment described in section 2.3.3. The liners were mounted in cone crushers type Sandvik CR660, which were part of a pebble crushing circuit described in figure 3.14. The plant does not have a weightometer to measure throughput been fed to each crusher, therefore only working hours was the parameter used as a measure of the performance.

Table 3.4. Operational Parameters

Crusher throughput (t/h)	350
Re-circulating load	1.4
Crusher net production (t/h)	250
Crusher CSS (mm)	12-14
Crusher Power (kW)	200-275
Crusher Pressure (MPa)	2.4 – 4.8
Screen slot opening (mm)	12

The inverse close circuit presented three crushers, processing between 500 to 800 t/h. Additionally, there were two banana screens, for the classification and re-circulating the coarse fraction back to the crushers. The fresh material processed per crusher was 200-250 t/h with a recirculating load of approx. 1.5. The liners were mounted without re-heating, using epoxy resin as backing material.

The operational parameters are presented in Table 3.4. The liners were visually inspected periodically for fractures and samples of the feed and product were taken in order to assess production quality.

After the test, the liners were removed and samples of steels were extracted and characterized. Furthermore, new thermal treatments were performed to the steel samples in order to assess possible improvements in the microstructure.

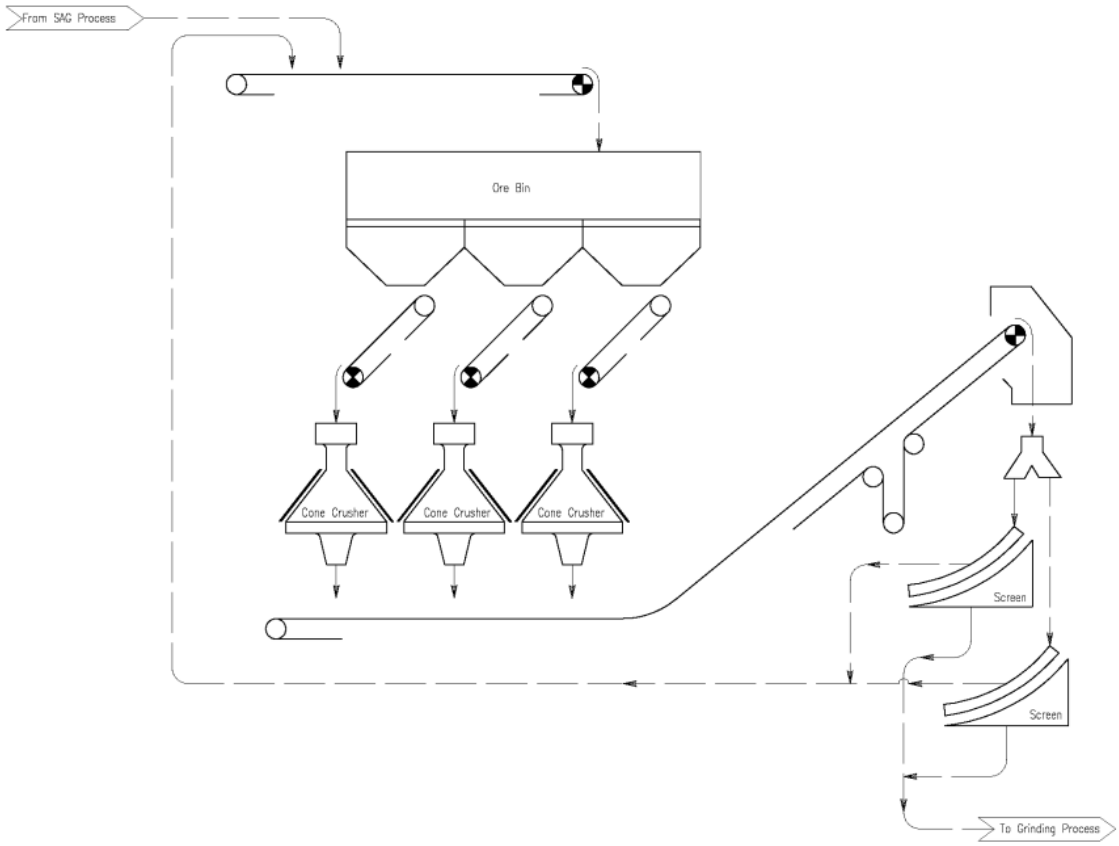

Figure 3.14. Flowsheet of copper mine pebble crushing circuit. The feed origin was a SAG circuit and the product was conveyed to a ball mill circuit. The pebble circuit had inverse closed configuration. The classification was performed with two banana screens, which recirculated the coarse fraction.

3.7.3. Results and Discussion

All three test were ended due to failure of the liners, Figure 3.15. shows pictures of mantles with fractures. Table 3.5. shows the hours of operation of the liners.

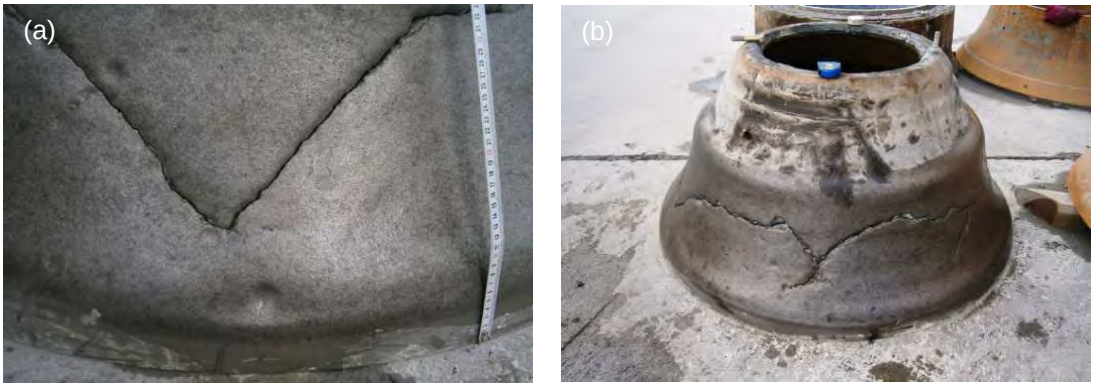

Figure 3.15. Pictures of matles failure. (a) H16Ti wit fracture and marks of hard material (b) H12Ti failure detected late.

Table 3.5. Results of the test in mining

	Weight loss (%)	Productivity	Wear (g/t)	Observations
1° set in H12Ti	32.7	390 h (98-109)	8.31	Fracture of mantle
2° set in H12Ti	27.9	456 (114-128)	6.06	Fracture of mantle
3° set in H16Ti	25.7	435 (109-122)	5.86	Fracture of mantle
A128 –B3 (average)	27-35	250 – 350 (63-98)	9.73	30-50% of the liners are removed due to fracture

The mining company usually mounts liners made in A128B3, which have a service life of approximately 350-500 hours. Therefore, the performance of the liners under testing was considered acceptable in term of tonnage processed, but the values of wear indicated that if the failure had not occurred, the liners would have continued to work, perhaps longer than 500 hours.

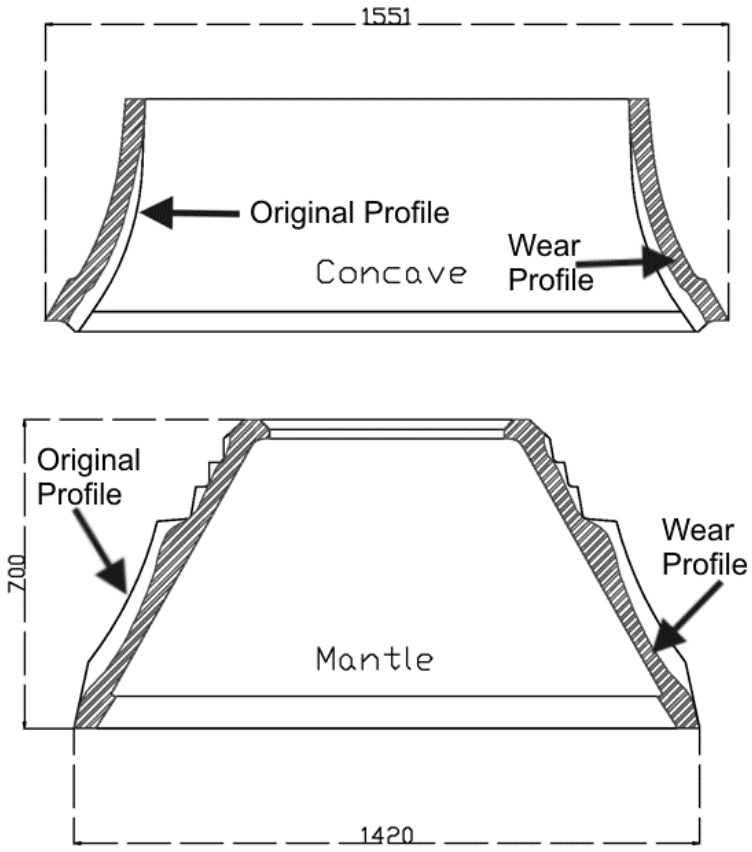

Figure 3.16. Profile of liners before and after the test. Thickness was around 72 to 107 mm.

Figure 3.16. shows the liner's profiles before and after the test. The concave presents the most part of the wear in the lower part. However, the concaves, presented wear in the middle part of the crushing chamber. Thickness at this point reached values of 34 mm, from the 72 mm in the original profile. Wear recommended by original manufacturer of the crushers is around 38% in weight loss. Thus, liners wear resistance have room for improvement. The critical piece of the set is the mantle, which often shows failure.

The product quality is presented in Figure 3.17. show a feed of P80= 63 mm at the beginning of the test a P80= 80 mm at the end of the test, with top sizes of around 90 mm. The products were 17 mm at the beginning and 20 mm at the end. The RR was 3 to 4.

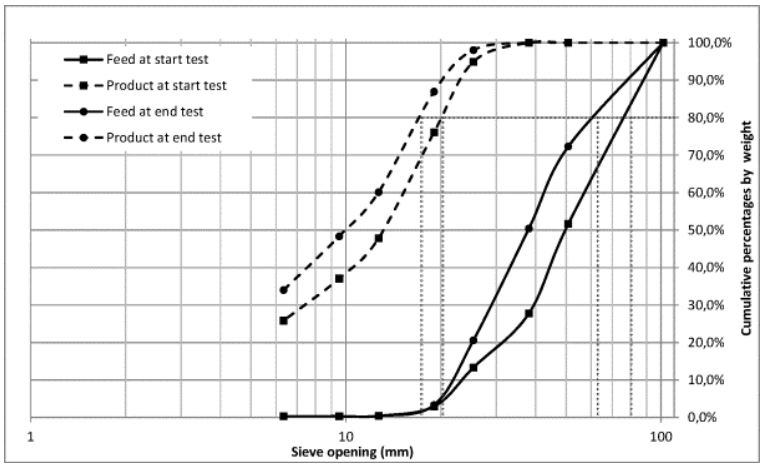

Figure 3.17. Granulometric curves of feed and product of test with H12Ti.

The manufacturer recommends a top size of 60 mm for a CSS of 12-13. Therefore, the process was out of parameter.

The bigger dimension being fed to the crushers originated an abnormal wear concentrated in the middle of the mantle, where most of the work was performed. This unbalanced work originated a weak point in the liner.

However, there are other possible explanations to the failure of the liners. Markings of pinning were observed on the fractures or near them, possible originated from harder materials, i.e. steel balls from the SAG mill that were not properly removed by the magnets)

The chemical analysis did not differed from what was presented in Table 2.1, and therefore are not shown. The metallographic characterization of the steels presented a clearer explanation of the failure. Figure 3.18 presents the microstructure of steel H12Ti extracted from the middle to lower part of the mantle. There are clear signs of carbide non solubilized with isolated and globular morphology. Additionally there were clear signs of thick g.b.c., from an unwanted re-precipitation process.

The impact toughness for the samples of H12Ti were found to be particularly low, with values of around 50 J. H16Ti, however, presented a value of 225 J.

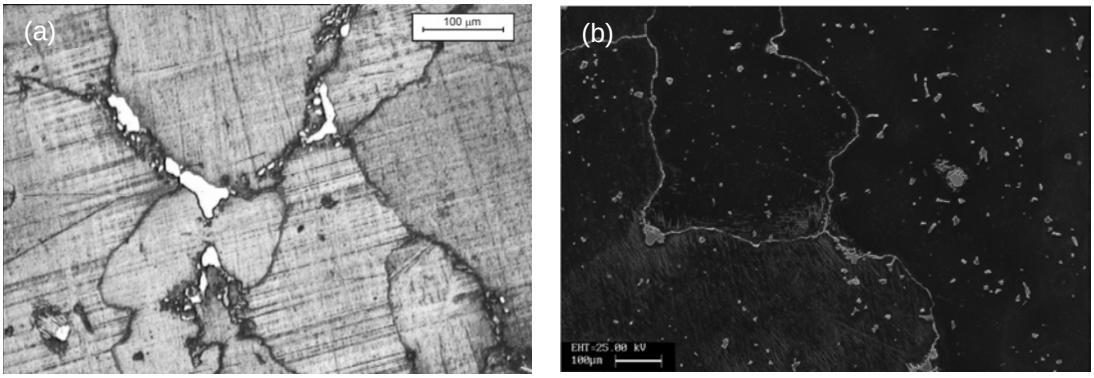

Figure 3.18. (a) Micrograph of H12Ti, with insolubilized carbides (b) SEM image of H12Ti, grain boundary carbides were observed.

The samples of both steels were treated with an additional solution treatment in lab conditions. The treatments had duration of 60 and 120 min in order to assess the degree of carbide solution in the

original heat treatment. The sample of H12Ti treated for 60 min showed an impact toughness of 210 J while the sample treated at 120 min, 250 J. The sample of H16Ti treated at 60 min showed 286 J and for 120 min 300 J. Therefore, the original heat treatment may have presented a lack of solution of primary carbides that kept the microstructure brittle, especially in the case of H12Ti. Perhaps a combination of a 60 min longer thermal treatment at the industrial furnace with better quenching conditions may have avoided failure. Figure 3.19. show the increase of impact toughness with additional heat treatments.

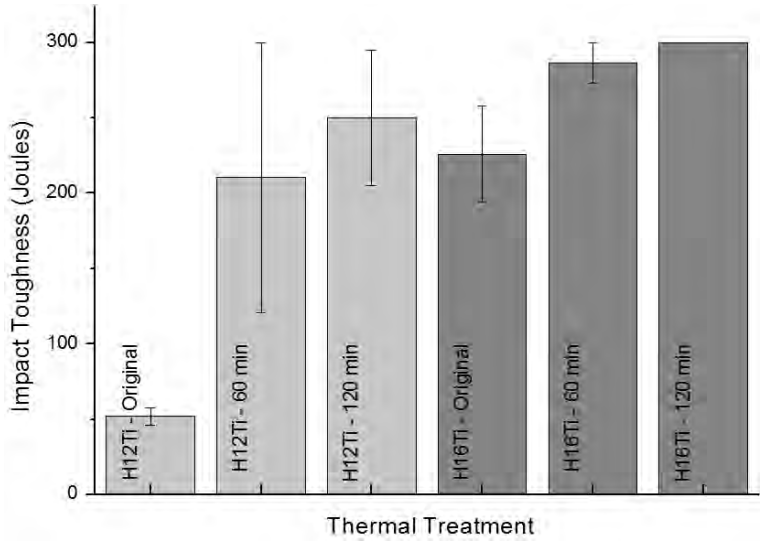

Figure 3.19. Impact toughness increased with heat treatment

Micro hardness profile of both steels showed a good degree of work hardening. Wear resistance of both H12Ti and H16Ti was considered to be more than acceptable. Which is partly justified by the presence of TiC as hard phase in the austenite matrix.

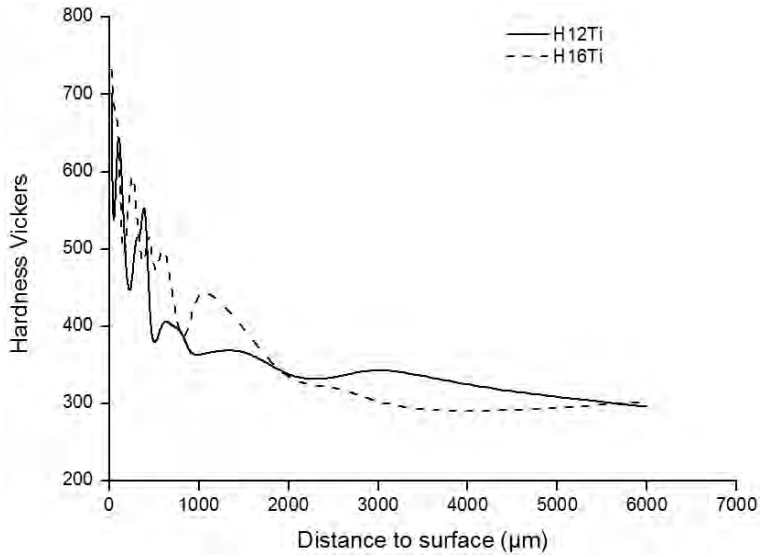

Figure 3.20. Micro hardness profile of H12Ti and H16Ti after service. Good workhardening was observed.

The conditions presented in Field Test A proved to be too hard for the mechanical properties of the H12Ti and H16Ti steel liners tested. The reasons for the failure can be attributed in part to the high crushability of the material. However, there are other important factors to blame, such as the incorrect design of the liner's original profile, which was decision of the mining company, and also the presence of extremely hard materials (steel balls).

3.8. STUDY CASE B: COMMINUTION IN AGGREGATE PLANT

3.8.1. Introduction

Two sets of three blow bars each were tested in an aggregate quarry located in the Udine province. The flowsheet is illustrated in Figure 3.21. The aggregate was dolomite as described in section 3.4. The quarry usually used martensitic steel for their blow bars. Therefore, the scope of the test was to compare the performance of AMS against a material more suitable for this type of applications.

3.8.2. Experimental

Two sets of blow bars were tested in a quarry of dolomitic materials. One set was in H12Ti and the other in H16Ti. Both steel received a complete solution treatment.

The sets were mounted in a Cedarapids 1300 impact crusher. The machine received the feed form a screen with a top mesh of 30 mm. The product was discharged into another screen with a top mesh of 19.6 mm. The oversize re-circulated to the impactor. The bars were weighted before and after the test. The original weigh was 363 Kg. The throughput was calculated to be around 85 t/h. The power draw was approximately 53 -65 Amps.

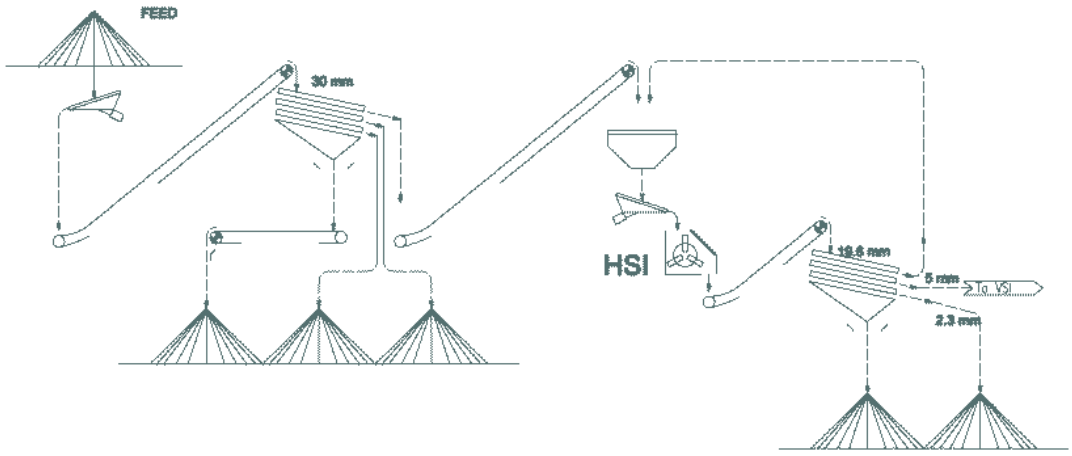

Figure 3.21. Flowsheet of aggregate plant. The material comes from a lake, and it is feed into a three-deck screen. The coarse fraction feeds the HSI. The product is conveyed into another three-deck screen. The top fraction is recirculated into the HSI.

3.9.3. Results and Discussion

The results are presented in Table 3.6. In general the performance of the AMS bars were lower than the martensitic. The wear ratio of H12Ti was 33 g/t, and H16Ti 28 g/t, which allowed to rank

first H16Ti. However, when both steels were compared against the martensitic steel, the wear rates observed turned out to be 50% higher.

Table 3.6. Results of the tests in quarry

	Weight loss (%)	Productivity	
Bars in H12Ti	18%	71 hrs (6035 t)	33 g/t
Bars in H16Ti	20%	93 hrs (7905 t)	28 g/t
Martensitic	20%	161 hrs (13600 t)	16 g/t

The wear profile is presented in Figure 3.22. The power draw increased as the profile changed, but it was within the limits of acceptability. There were no marking or signs for fractures found on the surface of the bars.

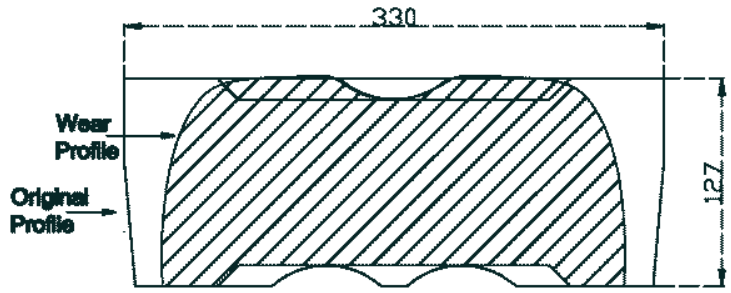

Figure 3.22. Profile of blow bar before and after the test.

Figure 3.23. presents the quality of the product. During the test were no particular problems with the quality of the product that may be attributed to the wear of the impeller bars. The reduction ratio was between 7 to 14.

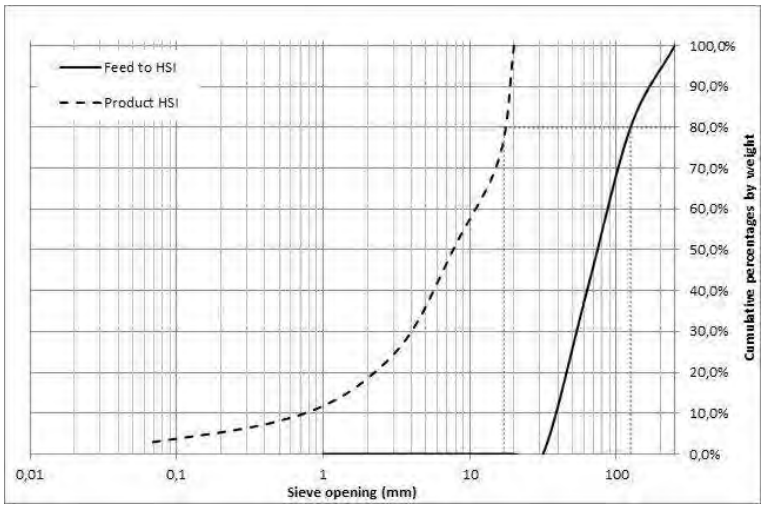

Figure 3.23. Granulometric curves of feed and product of the HSI

The profile of the impeller bar after the test was overlapped with the profile of the blow bar from the test of section 3.7. It was found that both profiles matched, especially in the top part, were the effort of crushing against the plates takes place. This may have meant that the test performed with the Hazemag HSI were representatives in terms of mechanism of wear.

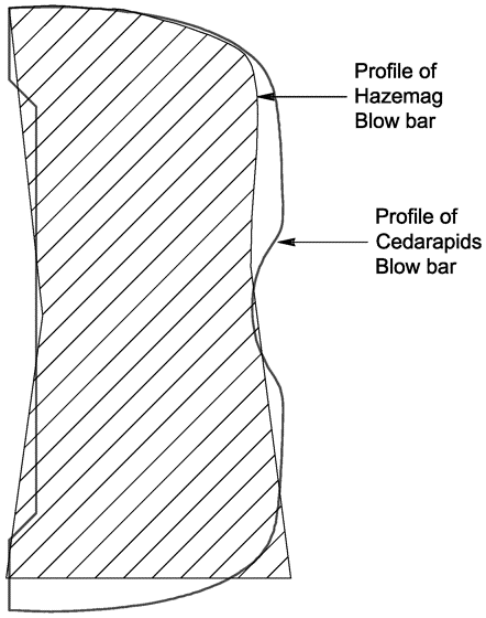

Figure 3.24. comparison blow bar from quarry test and small blow bar from Hazemag pilot scale tests (different scales)

3.9. STUDY CASE C: COMMINUTION IN RECYCLING

3.9.1. Introduction

A set to two blow bars was tested in a Rocky 400 hammermill crushing steel slag. The operation was located in the Udine province. The scope of the test was to assess wear in applications with very fine material.

3.9.2. Experimental

A set of blow bars in H16Ti (with solution treatment) was mounted in a hammermill that processes approximately 40 t/h of steel slag for recycling applications. Figure 3.25 presents the flowsheet of the recycling plant. The plant did not presented weightometers to control feed rates. Furthermore, the plant worked in irregular periods of production, sometimes working one hour per day.

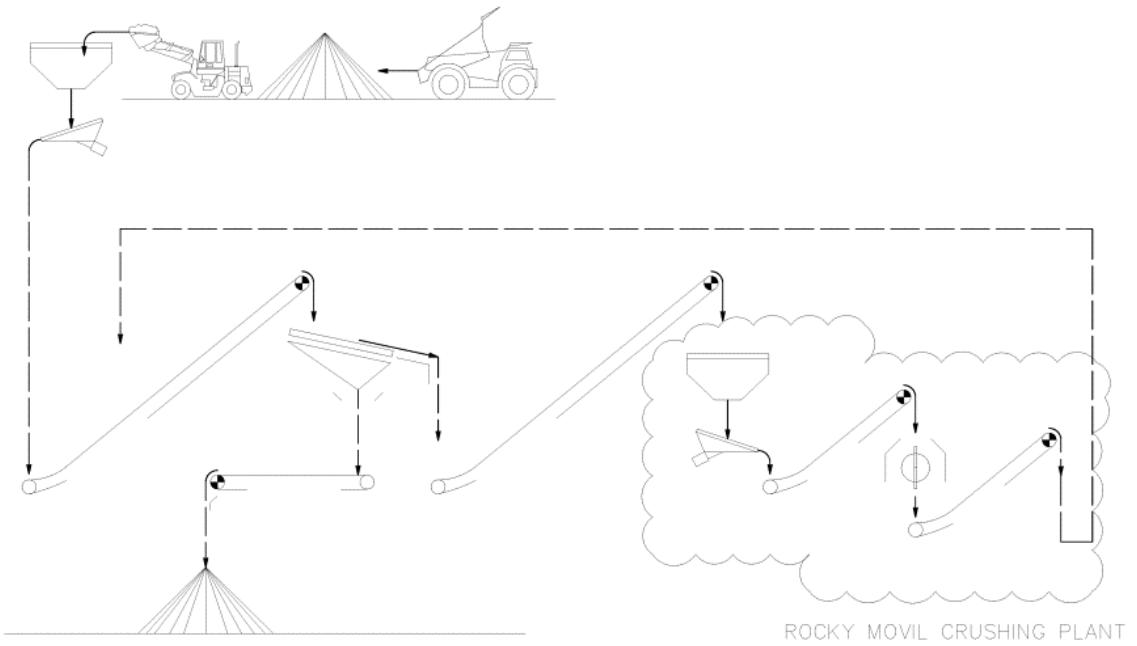

Figure 3.25. Flowsheet of recycling plant. The materials was fed into a screen, the coarse fraction was fed into the hammermill which was in inverse close circuit with the screen.

3.10.3. Results and Discussion

The weight loss was 16,5 Kg from the original 49 Kg of each blow bar. Therefore the loss was 34%. The wear had influence in the quality of the product. Figure 3.27. show that the products becomes coarser in time, this means a loss in the quality.

The circuit is very simple with no reliable control of the weight of material processed. Therefore there is no possible to extract conclusion about the performance of the machine.

The only conclusion was that the wear ratio of the AMS was much higher than the usual material used for this particular application: Chrome white iron.

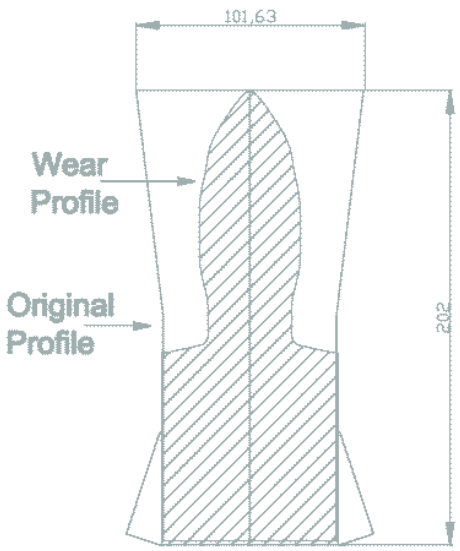

Figure 3.26. Profile blow bar before and after service.

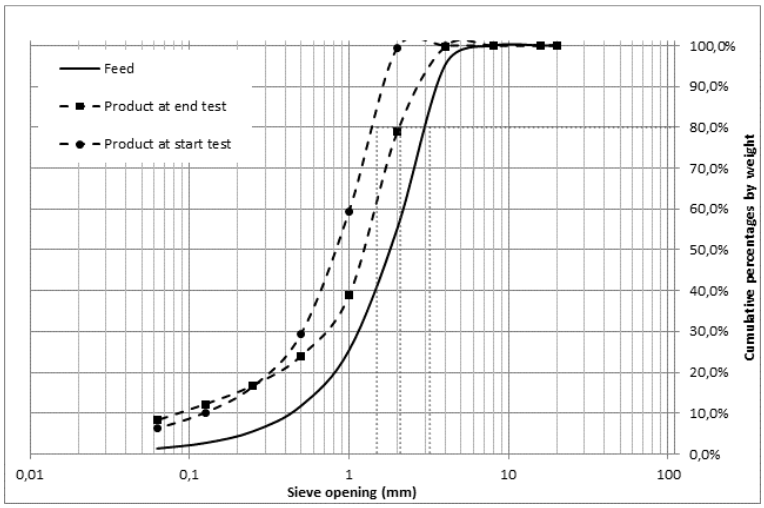

Figure 3.27. Granulometric curves before and after the test.

3.11. CHAPTER CONCLUSIONS

Jaw crusher testing allowed assessing wear ratios of different materials, presenting the influence of abrasion material in the wear rate of the steels. However, steels could not be ranked because they presented different wear ratios according to abrasive material.

The tests using the Hazemag HSI permitted to assess the influence of carbides insolubilized in the microstructure. In general, carbides did not contributed to increase the wear ratio of the steels. The tests also allowed to rank H16Ti as 20%-25% superior in wear rate to H12Ti .

The tests using as a variable particle size permitted to demonstrate that the quality of the crusher's product could be uniform if the blow bars keep their profile, or in other words, quality can be maintained while wear is not too high.

The conclusions drawn from Field test A were that the heat treatment is a critical variable in the manufacturing of the liners. The presence of insolubilized carbides determined the embrittlement in the microstructure. The outcome of the test was determined by the relationship of casting thickness *vs.* heat treatment. There is another conclusion to be drawn from this test, regarding the validity of the results of heat treatments in in laboratory compared with the real process in shop floor. Treatment in laboratory always presented very high impact toughness values, thanks to a good austenitization of the microstructure (i.e. solution of carbides), but these treatment were always performed in small sections, while the real process has many other variables that may affect negatively the solution treatment. A last conclusion may be drawn about the presence of very hard materials, in the feed, that may had determined the failure of one of the liners. This type of anomaly in the system is not as rare as it should, so testing liners' mechanical properties should contemplate these kind of catastrophic events by using many experiments, or the crushing circuit must be prepared to prevent them.

In the case of Filed Test B, H16Ti was clearly superior to H12Ti, mostly due to its higher content of manganese. However, both AMS presented shorter life service than the martensitic.

In the case of Field Test C, wear rate was much higher than chrome white iron, but no quantitative assessment could be made.

Thus, in cases B and C, AMS was not the right material for the conditions. Wear resistance needs to be improved for applications in comminution by impact.

It would also be of benefit if the manufacturers of the AMS could work more closely with the end users in the mining industry (both the mining company and quarry) to enable an accurate assessment of the actual conditions encountered at the crushing plant, and then perform a range of exposure trials to rank candidate materials. This kind of study is rare, though not as rare as successful field trials. For instance:

- In test A: liner design was poorly selected. Also, the presence of steel balls in the feed was impossible to predict in the design of the test.
- In test C: no registers of the operational parameters were available. In addition, there were no statistics available of the performance of the blow bars commonly use, in order to serve as reference.
- In all three tests, the measurements were carried out at the end of the service life.

It needs to be emphasized that as a result of process variables, AMS have a narrow operating window in which they can perform optimally. In other word, the highest of the performance of AMS can only be attained when the other variables of the crushing circuit are set to optimum levels.

In the author's experience, many cases of premature AMS failure in comminution applications are caused by a lack of understanding of the nature of the physical properties of the steel.

CHAPTER IV - DEVELOPMENT OF NEW STEELS

4.1. INTRODUCTION

Chapter two has presented the phenomenon of grain boundary carbides occurring in H12Ti and H16Ti and its embrittlement effects. The unfeasibility of achieving sound mechanical properties in thick castings by means of heat treatments, lead to the conclusion that the chemical formulation of the two steels must be adapted to minimize embrittlement.

Minimize carbon content to levels around 1.2% seems the first logical option, however, the scope of this work in to optimize AMS with contents of 1.4%. Therefore, the challenge is to keep carbon from forming reprecipitated phases.

Previous research work suggested that wear resistance might be improved by adding a solid-solution element which increased the solubility of carbon in austenite and simultaneously increasing carbon content [8] [41]. To increase effectively the solubility of carbon in austenite in AMS, a solid solution element must decrease the activity of carbon in austenite but not interact with carbon so strongly as to form carbides, must not interact with iron and manganese to form intermetallic compounds, must not decrease seriously the castability of the alloy, and must be economical. A survey of the effects of alloying elements on the activity of carbon in austenite indicates that only some elements such as aluminium, nickel and molybdenum meet most part of these requirements [41] [9].

The addition of Aluminium in AMS is usually for controlling phosphorous content during solidification. When aluminium content is around 0.15%, there is a major reduction in the amount of phosphide precipitated along the grain boundaries and the ductility and impact properties are slightly increased. The influence of aluminium after solution treating the steel was found to be equally favourable. If manganese steel is well deoxidized in this way, improvement in wear resistance properties will result [10] [2].

Zudeima and coworkers [41] showed that aluminium reduces the activity of carbon in austenite in AMS. The reduction in carbon activity increases the solubility of carbon in austenite, decreasing the driving force for carbide precipitation by reducing carbon supersaturation. These results also indicate that aluminium reduces the diffusivity of carbon in austenite. Dynamic strain aging data indicate that aluminium raises the temperature range over which dynamic strain aging occurs, also suggesting reduced carbon diffusivity in the presence of aluminium. Together, reduced carbon activity and reduced carbon diffusivity decrease the rate of carbide precipitation in AMS. Additionally, it was presented some data showing Aluminium additions to slightly improve impact toughness [41].

It was shown that adding nickel to plain austenitic manganese steel decreases the tensile strength, slightly increases the ductility but has no effect on yield strength. However, nickel improves the toughness of such steel by inhibiting the precipitation of grain boundary carbides during reheating and cooling. Another beneficial effect of nickel is that it improves low temperature impact strength. [8]

Regarding molybdenum, an important contribution made by molybdenum additions is the significantly improved as-cast mechanical properties and the enhanced resistance to carbide embitterment which occurs if manganese steel is re-heated. In foundry terms, this translate into easier shop handling with reduced propensity for cracking, especially during the removal of gates and risers, arc air flushing and weld repair. For this reason, molybdenum (usually a 1% addition) is a valuable contributor to the production of massive crusher castings. However, it is very important to remember that carbon is the embrittling element and these beneficial effects for large casting production are only of practical significance at lower carbon contents [10] [2].

The ability of molybdenum to suppress carbide embitterment at elevated temperatures is also very useful for castings that encounter re-heating during service. Such application include castings subjected to repeated weld re-building and hard facing and wear castings used at elevated temperatures (up to 500°C) [10].

In the molybdenum grades of manganese steel, at a carbon level above 1.2%, incipient fusion will occur at a temperature below that desired for adequate solution of carbon in the austenite. Thus, molybdenum grades are not suitable for high carbon content in the conventional heat-treatment form [22].

Although phosphorus content of 0.08% is permitted in specifications, experienced foundry men will hold phosphorus to much lower levels. Phosphorus above 0.02% progressively promotes intergranular cracking in manganese steels. Above 0.06%, the high temperature plasticity of manganese steel is severely reduced and the steel becomes extremely susceptible to hot tearing. At such a high phosphorus level, microstructural evidence of grain boundary films of phosphide eutectic can be observed [42].

Silicon is generally added as a de-oxidizer. In heavy section castings, silicon can have a disastrous effect on toughness due to embrittling effects. Even with 0.6 to 1.0% silicon, toughness is adversely affected with increasing carbon content [43].

Sulphur is seldom a factor in 13% manganese steel, since the scavenging effect of manganese, operates to eliminate it by slagging or fixing it in the form of innocuous rounded inclusions of manganese sulphide [2].

Copper acts in a similar manner to nickel and molybdenum and markedly increases the stability of the austenite, though not to the extent as molybdenum. Unfortunately, the abrasion resistance of this steel containing copper are much inferior to those containing 1% Mo [10].

Boron can exert a grain refining action similar to titanium and nitrogen. The presence of boron will accelerate the formation of precipitates at low temperatures and will have a detrimental influence on this respect [2].

Vanadium forms very fine carbides and has been added to austenitic manganese steel in order to increase the initial hardness of the steel and thereby make it more wear resistance under conditions of low stress abrasion [12].

Niobium has high affinity for carbon and nitrogen. It has been used as a scavenger for interstitial carbon and nitrogen in stainless steel, and most important, to avoid chromium carbide

precipitation. This element forms hard carbides that may replace TiC as hard phase in H12Ti and H16Ti [11]. The advantages offered by Nb is that it does not oxidizes, in contrast with Ti, which oxidises rapidly, and almost 50% of the mass added in the charge is lost to the slag.

In order to optimize the AMS preseted in this work, it was decided to test compositions increasing Ni, Mo, Al, in order to stabilize carbon inside the austenitic matrix. In addition, Niobium was selected as a possible replacement for titanium, which may form carbides with higher bonding forces with the matrix. Finally, a low carbon, high manganese steel was casted to check for wear resistance in a completely austenitic structure.

Most importantly, it was decided to use the only H16Ti's chemical composition as the starting point for the optimization. Thus, variations to the original recipe were made to achieve the contents of the new elements proposed.

4.2. EXPERIMENTAL

4.2.1. Experimental of castings made with small induction furnace

The raw materials used for the production of the steels were steel scrap and ferro-alloys. In addition, especial alloys were used to adjust the final compositions of the steels. Table 4.1 presents the different recipes, which used as base the recipe of H16Ti. The exact recipes are could not be published, in order to protect the intellectual property of the sponsor of this work.

All raw materials were exactly weighed to achieve the nominal compositions desired. The smelting of the steels was carried out in a 50 kg high-frequency induction furnace (385 V /600 V and a frequency of 3.06 kHz) in air environment, where the melt was covered with a ceramic cap to protect the melt from the oxidation. The smelting temperature was 1550°C, and the procedure of smelting is presented in Figure 4.1.

Apart from the ferroalloys and alloys, slag-forming materials were added (e.g. 2000 g of lime). FeSi was also added to adjust Si content.

The calculated amount of ferroalloys and alloys were added to the melt by the plunging method. The melt was stirred continuously at temperatures of 1500°C - 1550°C for 15-25 min, until the adjustments of the composition were completed, followed by pouring in an olivine mould.

Table 4.1. Variations of the H16Ti recipe

	Charge modifications	Target
H16Ti-LC	FeMnC (6%C) amount was reduced and replaced by electrolytic FeMn (0.8%C), in this way C content was reduced	Approx. 1.2% C
H16Ti-Mo	FeMo (Mo70%) was added to form small carbides	0.5 – 0.8 % Mo
H16Ti-Ni	Ni (99% purity) was added to stabilize austenite	1.5 – 2.0 % Ni
H16Ti-Al	Al (99% purity) was added to control C activity	1.5 – 3.0 % Al
H16Nb	FeNb (70%Nb) was added in order to replace FeTi (70%Ti)	0.3 - 0.7% Nb

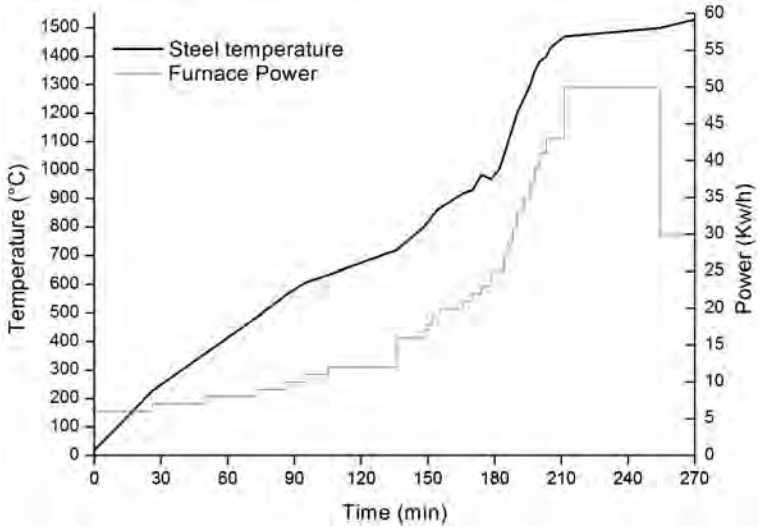

Figure 4.1. Temperature and power of the induction furnace during smelting operation of H16Nb. Above 1000°C the temperature was measured with pyrometer. The pouring temperature was 1500°C.

The moulds had the shape of the Y-block already presented in section 2.2.1. Additionally, blow bars, for wear tests with the impact mill, were also casted (four bars for each steel type tested). The casts were left to solidify and cool down for 24 hours at ambient external temperature before opening the moulds.

Characterization was performed according to sections 2.2.2 and 2.2.3. (Nb content was analysed with Thermo Nilton xlt XRF). Solution heat treatment was performed in an induction furnace using the 1090°C - 120 min treatment.

Specimens were extracted for Charpy impact test. As impact toughness is linked to effectiveness of heat treatment, all samples were treated with the same heat treatment at the same time. This procedure allowed comparing the results, using as a reference the values of H16Ti.

4.2.2. Experimental of castings made with industrial furnace

After the characterization and testing presented above, new castings were performed, but this time in the industrial smelting furnace, with dimensions 200 mm x 200 mm x 1000 mm. The compositions obtained were to those presented in table 4.2.

The bars were heat treated in the industrial furnace and then quenched. Afterwards, a section of the top part of the bars was machined, about 100 mm in depth, in order to verify the occurrence of internal cracking.

4.3. RESULTS AND DISCUSSION

4.3.1. Chemical composition

The chemical composition of the steels produced is presented in Table 4.2. The production of all steel samples was whiting the specifications desired.

Table 4.2. Chemical composition of the AMS steels produced.

(%)	C	Mn	Cr	Mo	Ni	Si	P	S	Al	Ti	Nb
H16Ti-LC	**1.15**	17.01	1.14	0.10	0.18	0.51	0.034	0.003	0.015	0.506	--
H16Ti-Mo	1.40	17.16	1.65	**0.72**	0.22	0.69	0.038	0.001	0.010	0.278	--
H16Ti-Ni	1.39	16.49	1.44	0.09	**1.85**	0.52	0.035	0.001	0.016	0.450	--
H16Ti-Al	1.44	16.92	1.38	0.10	0.16	0.56	0.036	0.006	**1.347**	0.471	--
H16Nb	1.40	17.11	1.43	0.10	0.25	0.68	0.036	0.011	0.006	0.073	**0.67**

4.3.2. Results of the metallographic characterization of the H16Ti-Ni steel

Figure 4.2 show the micrographs of H16Ti-Ni. The as-cast condition presented perlite colonies and thick gran boundary carbides.

After solution treatment, the structure of H16Ti-Ni was almost free of primary carbides. Only re-precipitated carbides were visible along some parts of the grain boundary. Nonetheless, the network of carbides was not continuous.

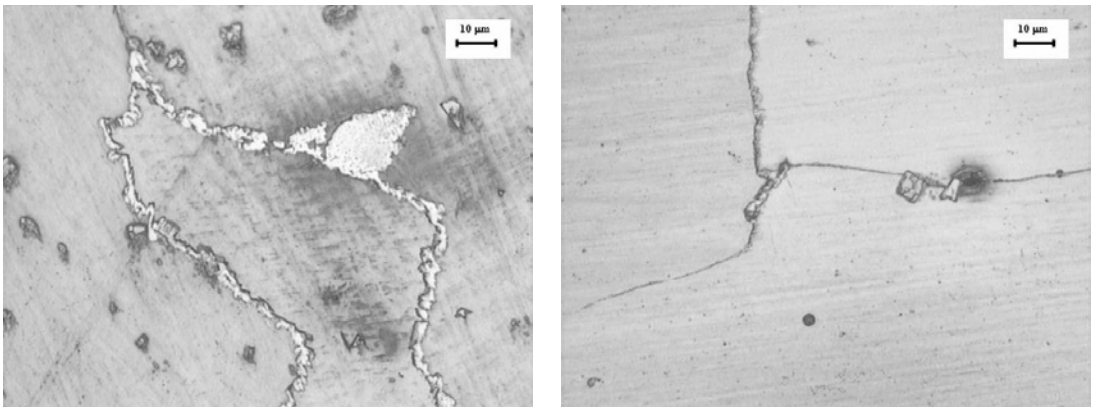

Figure 4.2. Micrographs of H16Ti-Ni (a) As-cast (b) solution treated

The SEM image of the as-cast condition of H16Ti-Ni is shown in Figure 4.3. The microstructure did not presented difference with the typical as cast condition presented in section 2.2.3. In the image, an eutectic carbide was analysed using EDS, and the presence of phosphorous detected.

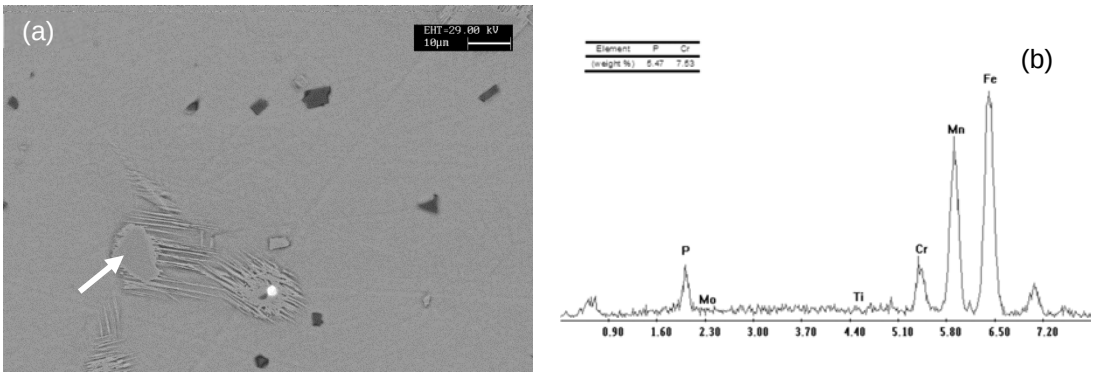

Figure 4.3. H16Ti-Ni in As-cast condition (a) SEM image, (b)EDS spectrum on region marked

The SEM image of the solution treated (austenitized) condition of H16Ti-Ni is shown in Figure 4.4. The microstructure did not presented difference with the solution treated condition presented in section 2.3.3. The eutectic carbides and the perlite colonies were not detected. The image shows a typical junction of three grain where thin grain boundary carbides were observed. These carbides were forming a network along all the grain boundaries of the microstructure. They contained some amount of Cr and Ni. Therefore, carbide reprecipitation effects were detected in this steels.

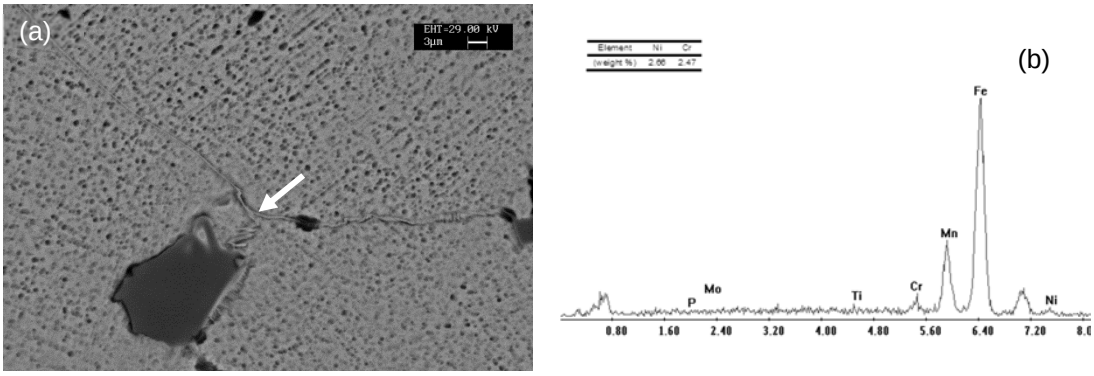

Figure 4.4. H16Ti-Ni in solution treated condition (a) SEM image, (b)EDS spectrum on region marked

4.3.3. Results of the metallographic characterization of the H16Ti-Mo steel

Figure 4.5 show the micrographs of H16Ti-Mo. The as-cast condition, as expected, presented perlite colonies and thick gran boundary carbides.

After solution treatment, the structure of H16Ti-Mo was free of primary carbides. Only re-precipitated carbides were visible along some parts of the grain boundary. Nonetheless, the network of carbides was not continuous.

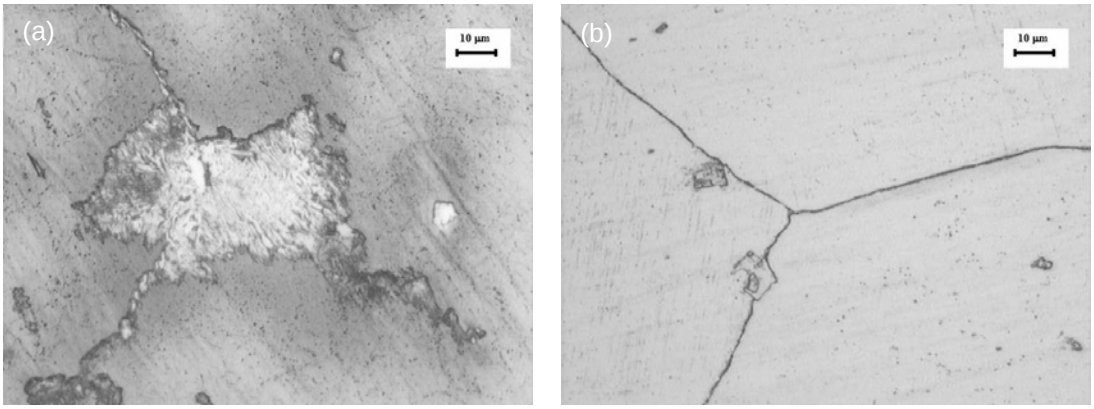

Figure 4.5. Micrographs of H16Ti-Mo (a) As-cast (b) solution treated

The SEM image of the as-cast condition of H16Ti-Mo is shown in Figure 4.6. The microstructure did not presented difference with the typical as cast condition presented in section 2.2.3. In the image, a eutectic carbide was analysed using EDS, and the presence of molybdenum was detected.

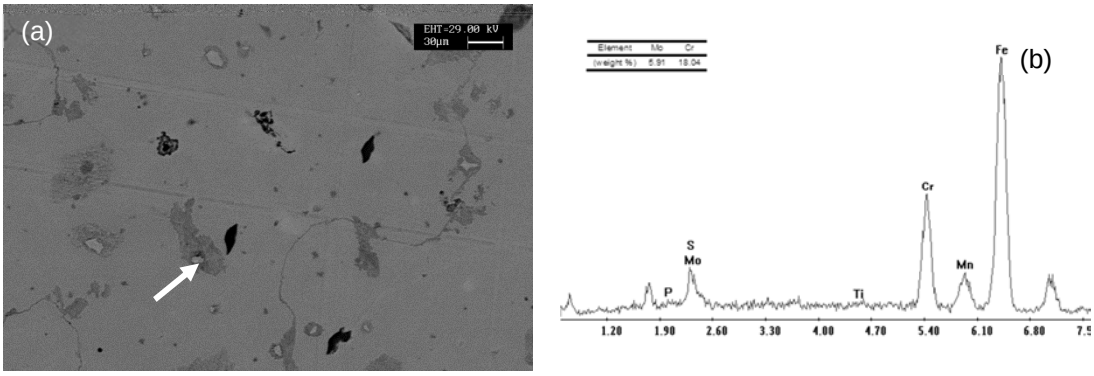

Figure 4.6. H16Ti-Mo in As-cast condition (a) SEM image, (b)EDS spectrum on region marked

The SEM image of the solution treated (austenitized) condition of H16Ti-Ni is shown in Figure 4.7. The microstructure did not presented difference with the solution treated condition presented in section 2.3.3. The eutectic carbides and the perlite colonies were not detected. The image shows a typical junction of three grain where thin grain boundary carbides were observed. These carbides were forming a network along all the grain boundaries of the microstructure.

Molybdenum content was detected along the titanium carbides. Possibly, Mo carbides associated with the TiC before solidification of the austenite matrix. In some carbide, EDS analysis confirmed a darker region, richer in Ti, and a clearer region with a higher amount of Mo.

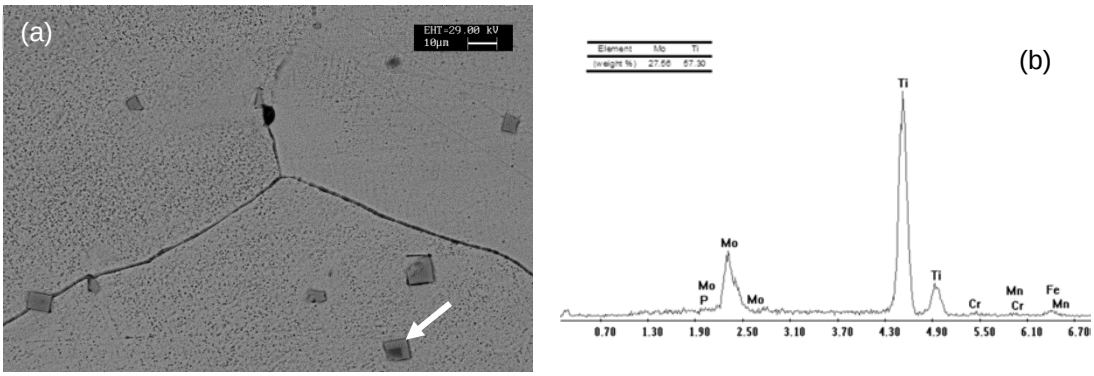

Figure 4.7. H16Ti-Mo in solution treated condition (a) SEM image, (b)EDS spectrum on region marked

4.3.4. Results of the metallographic characterization of the H16Ti-Al steel

Figure 4.8 show the micrographs of H16Ti-Al. The as-cast condition presented thick grain boundary carbides and phase unknown, possibly some type of pearlite colonies, but with a different morphology, which was difficult to characterize.

After solution treatment, the structure of H16Ti-Al was not free of primary carbides, thus the solution treatment was not entirely effective. In addition, re-precipitated carbides were visible along some parts of the grain boundary. The network of carbides was continuous, evidencing a considerable degree of reprecipitation.

Furthermore, black lines were observed in the microstructure, which sometimes followed the grain boundary, but sometimes did not.

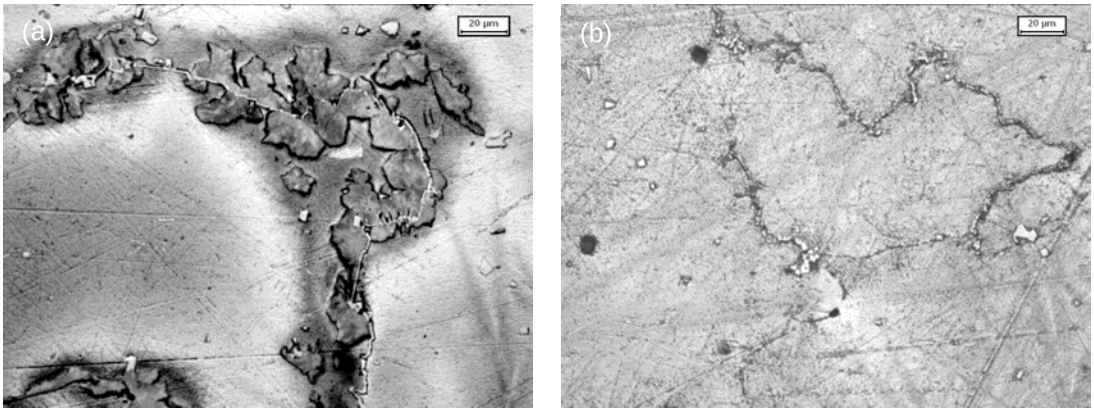

Figure 4.8. Micrographs of H16Ti-Al (a) As-cast (b) solution treated

The SEM image of the as-cast condition of H16Ti-Al is shown in Figure 4.9. The black lines seen in Figure 4.9 wer material oxidized, especially titanium. This oxidation occurred during the operation of casting. When the material contacted the mould a thin layer of oxide immediately formed, which was removed by more molten material entering the mould. The oxide ended up at the internal of casting. On the other hand, the new clear formations observed, were analysed by EDS and they presented a spectrum similar to the pearlite colonies showed in Figure 2.5.

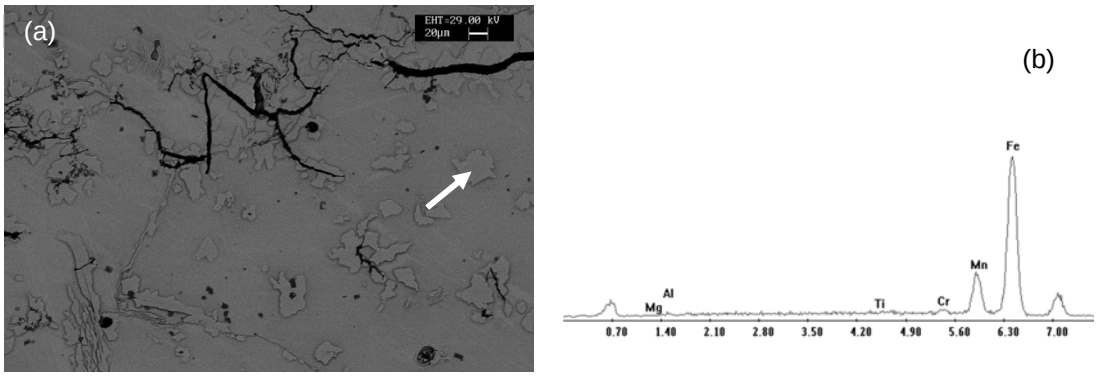

Figure 4.9. H16Ti-Al in As-cast condition (a) SEM image, (b)EDS spectrum on region marked

The SEM image of the solution treated (austenitized) condition of H16Ti-Al is shown in Figure 4.10. The microstructure presented the black lines, which contained Ti, as shown by the EDS spectrum.

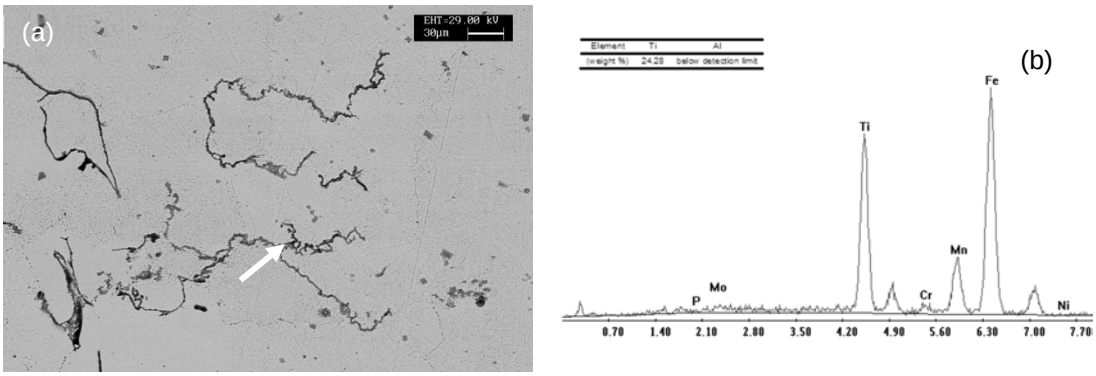

Figure 4.10. H16Al in solution treated condition (a) SEM image, (b)EDS spectrum on region marked

4.3.5. Results of the metallographic characterization of the H16Ti-LC steel

Figure 4.11 show the micrographs of H16Ti-LC. The as-cast condition presented small amount perlite colonies and thick gran boundary carbides.

After solution treatment, the structure of H16Ti-LC was free of primary carbides. Also, no sign of re-precipitated carbides were observed. The grain boundaries were free of carbides. These condition was considered an optimum austenitization.

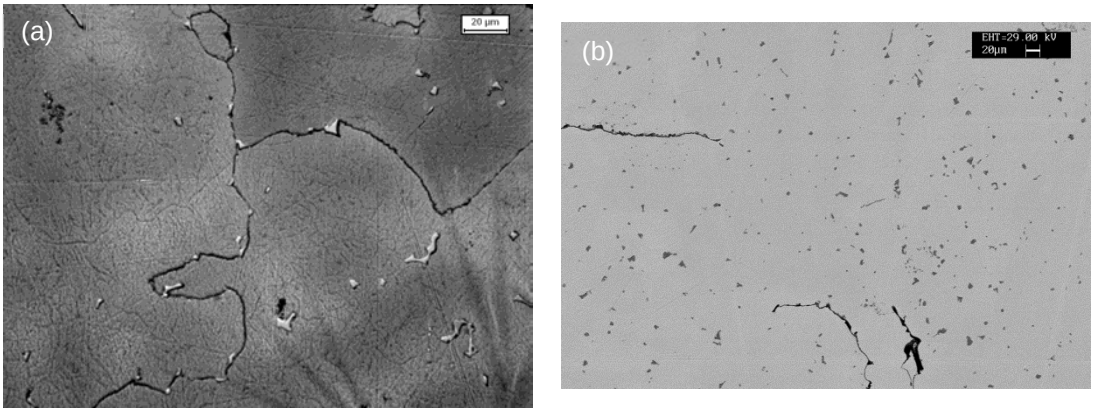

Figure 4.11. H16Ti-LC (a) Micrography of As-cast sample (b) SEM image of solution treated sample

4.3.6. Results of the metallographic characterization of the H16Nb steel

Figure 4.12 show the micrographs of H16Nb. The as-cast condition presented perlite colonies and thick gran boundary carbides. The NbC were clearly distinguished.

After solution treatment, the structure of H16Nb was free of primary carbides. Only re-precipitated carbides were visible along some parts of the grain boundary. Nonetheless, the network of carbides was not continuous.

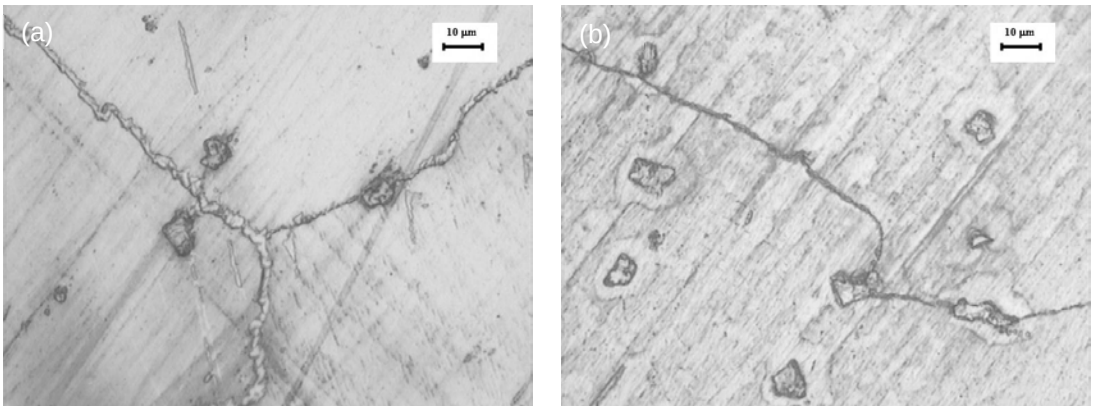

Figure 4.12. Micrographs of H16Ti-Nb (a) As-cast (b) solution treated

The SEM image of the as-cast condition of H16Nb is shown in Figure 4.13. The microstructure did not presented difference with the typical as cast condition presented in section 2.2.3.

The image shows a zone of the NbC and another one of TiC, firstly a darker central zone with more Ti content and then a lighter outer region with more Nb content.

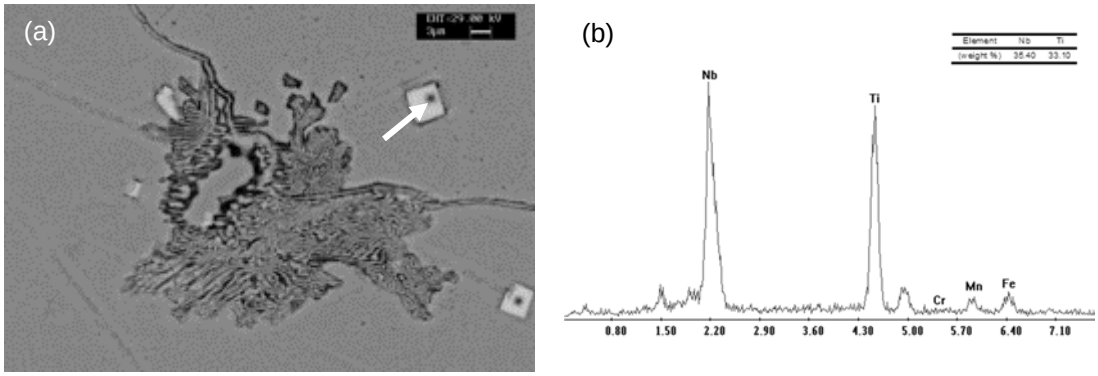

Figure 4.13. H16Nb in As-cast condition (a) SEM image, (b)EDS spectrum on region marked

The SEM image of the solution treated (austenitized) condition of H16Nb is shown in Figure 4.14. The microstructure did not presented difference with the solution treated condition presented in section 2.3.3. In most of the cases, only pure Nb carbides were observed. EDS analysis confirmed that the Ti content was small in many of the carbides. The presence of Ti was due to contamination from the steel scrap used for the production of the H16Nb steel.

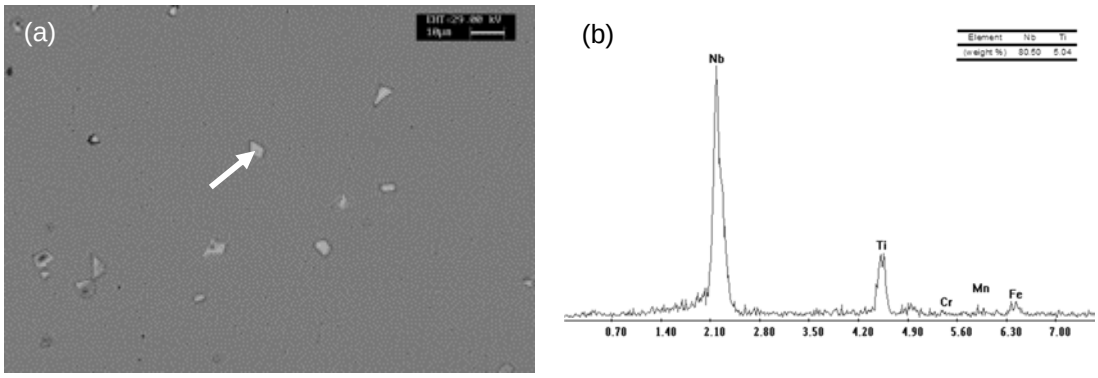

Figure 4.14. H16Nb in solution treated condition (a) SEM image, (b)EDS spectrum on region marked.

4.3.7. Results of Charpy tests and microhardness.

The results of the Charpy impact toughness test are presented in table 4.3. The biggest improvement in impact toughness was observed in H16Ti-LC, that showed an increase of 150%. Low Carbon AMS is well documented in literature; therefore high impact toughness was expected. The reason for such a high value was the complete austenitization of the structure (solution of precipitated phases) and the absence of carbide re-precipitation.

H16Ti-Ni presented an increase in impact toughness of 53%. Since the compositions of both H16Ti and H16Ti-Ni only differ in a content of 1.60% nickel, the increase in impact toughness might be attributed to the better microstructure achieved thanks to the addition of nickel.

H16Ti-Mo and H16Ti-Al presented a decrease of impact toughness of 23-27%, mostly due to the presence of carbide reprecipitation. Finally, H16Nb presented relatively the same impact toughness as H16Ti.

Table 4.3. Results of Charpy impact tests

	Mean (J)	SD
H16Ti	116.4	17.6
H16Ti-LC	290.7	6.4
H16Ti-Mo	90.1	3.2
H16Ti-Ni	177.6	0.5
H16Ti-Al	85.0	5.0
H16Nb	110.9	15.6

Table 4.4. Results of MicroHardness. (without workhardening)

	Mean (HV)	SD
H16Ti-LC	240	5,7
H16Ti-Mo	225	2,9
H16Ti-Ni	581	13,2
H16Ti-Al	258	16,2
H16Nb	259	11,5

The results of the micro hardness are presented in table 4.4. The only outstanding value was observed for H16Ti-Ni, that presented an increase of 78% in respect to H16Ti. Unfortunately, the values of the new steels after work hardening were not possible to measure, since the blow bars used for the wear tests were to be kept intact for further testing by the sponsor of this work.

4.3.8. Results of the wear test

The results of the wear tests are presented in Figure 4.15. The results show there are two groups of steels to be considered.

Firstly, the steels with low wear ratio, such as H16Ti-Ni, H16Ti-Mo and H16Nb, which presented values between 223 to 258 g/t. These values are similar to the wear rate of H16Ti, 244 g/t, already presented in section 3.5.3.

Secondly, the wear ratios of H16Ti-LC and H16Ti-Al were considered to be high, with values of 293 g/t and 316 g/t. Thus, the presence of low carbon in the LC case rendered the steel less resistant to wear. In the case of the Al steel, the problem of the low rear resistance may be originated by the poor microstructure presented in Figure 4.10.

Finally, none of the new steels tested showed an improvement in the wear rate of H16Ti, at best, they maintained it.

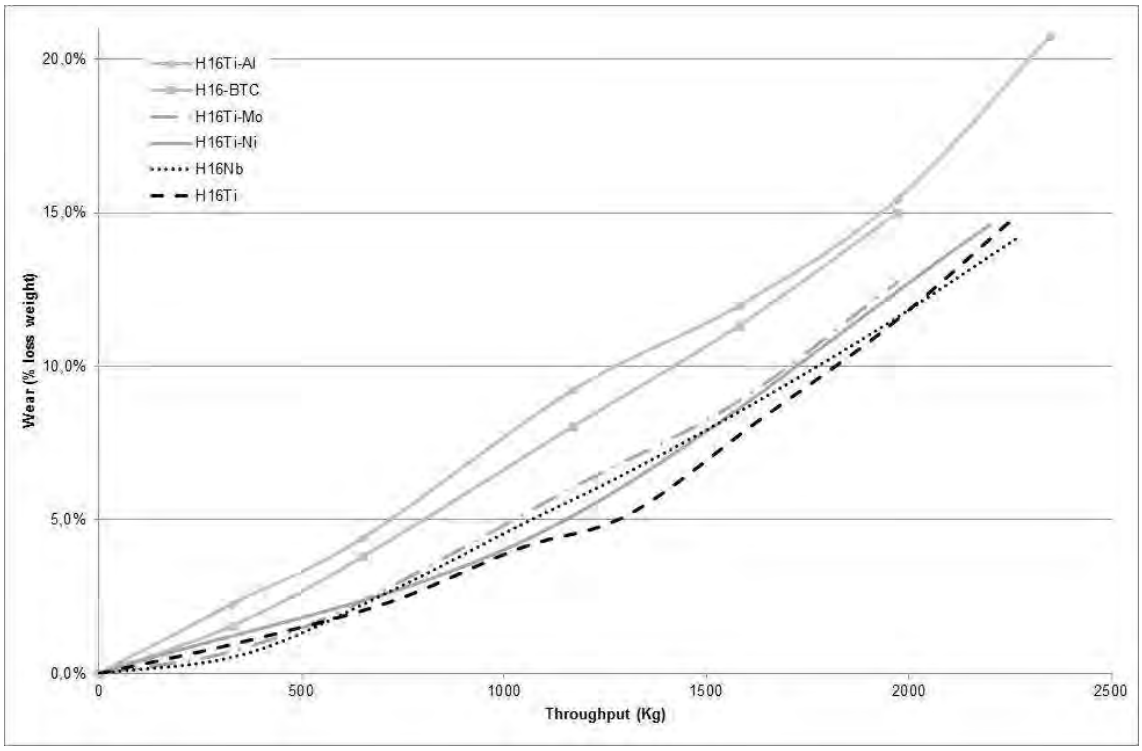

Figure 4.15. Results of wear tests for the new alloys.

4.3.9. Results of the inspection of large castings

The heat treatments of the bars showed cracking due to contraction in H16Ti-Ni, H16Ti-Mo, H16Ti-Nb. This cracking is frequently observed in casting in H16Ti and H12Ti. On the contrary, H16Ti-Al and H16Ti-LC instead, did not present cracking.

Further testing is needed to understand if Al addition helps to prevent internal cracking during heat treatment.

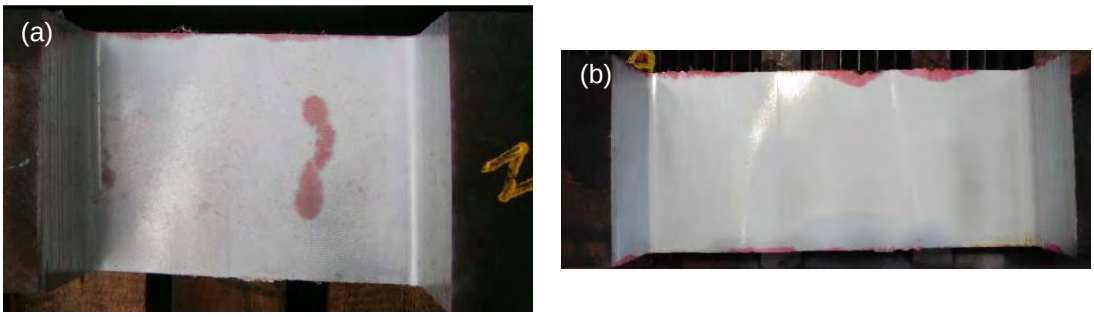

Figure 4.16. Images of steel bars with penetrating liquids. (a) H16Ti-Ni presented internal cracking. (b) H16Ti-Al did not resent any defect in the macrostructure.

The results of the HB measurements are presented in table 4.5. The values of HB do not correspond with the values measured in the microhardness. In general, Hardness Brinell was considered far less reliable than microhardness determinations.

Table 4.5. Results of Hardness Brinell.

	Mean (HB)	SD
H16Ti-LC	175.3	3.4
H16Ti-Mo	219.0	3.7
H16Ti-Ni	192.3	8.6
H16Ti-Al	189.1	2.5
H16Nb	196.4	1.9

The production of the new alloys at industrial scale did not require modification in the processes, although some precautions were taken in the introduction of Nb to the molten phase. In the case of Al, it was added at the last minute in the ladle, in order to avoid excessive oxidation.

4.4. CHAPTER CONCLUSIONS

The least successful of the trials was H16Ti-Al, which presented a poor microstructure, populated of defects formed during the process of pouring into the mould. The problems was in the timing of the addition of Al. These defects rendered the steel very low mechanical properties and decreased the wear resistance.

The case of H16Ti-Mo, the molybdenum carbides associated or bonded with the TiC, but the presence of this carbides neither improved mechanical properties nor contributed to wear resistance. Then again, the quantity of Mo added was relatively low. This test was considered not successful as well.

The production and testing of a high manganese and low carbon content steel, as in the case of H16Ti-LC, permitted to demonstrate the advantages and disadvantages of high C content. The mechanical properties (impact toughness) were largely improved, mostly due to the absence of reprecipitation. Nonetheless, wear resistance was decreased with the decrease of carbon content. Therefore, the utility of this steel is limited to thick casting in low abrasive materials such as the dolomite presented before.

The Nb test may be considered successful, since it was observed the formation of NbC that can easily substitute TiC. The wear and mechanical tests demonstrated that this replacement did not changed neither of the properties already observed in H16Ti. Therefore, H16Nb could be a good candidate for further testing and optimizations.

Finally, H16Ti-Ni presented the most promising results. The addition of Ni to the composition improved the austenitization effect, retaining more carbon in the austenite matrix that was not available to form carbides at grain boundary. The results of the impact toughness test demonstrated an improvement in the mechanical properties, mostly due to a better microstructure. Furthermore, the wear test demonstrated that Ni does not interfere with the workhardening effect.

CHAPTER V – COST ESTIMATIONS

5.1. INTRODUCTION

The replacement of wear consumables represents a minor, but nonetheless significant cost to the mining and minerals processing industries. These costs arise from [26]:

- The need to purchase replacement parts and equipment;
- Scheduled and unscheduled equipment downtime with attendant loss of production
- Labour and equipment costs expended during the replacement of worn equipment and component parts.

Of all the capital and operating expenses associated with these industries, the cost of downtime and lost production outweigh the cost of component replacement [30].

Although wear represents a minor portion of the operating expenses in minerals processing, it is uppermost in the minds of maintenance personnel, due to its recurring nature. Because of this, there is always a need for new materials and/or component designs that will last longer, be easier to install, and are more cost-effective than those currently in use. Other factors involved in wear material selection include availability and potential risk of catastrophic failure, which in the case of AMS are outstanding [30].

Crushing constitutes the second greatest source of wear in mineral processing, although the magnitude of loss is only about 7% as large as that for ore grinding per tonne. However, more minerals need to be crushed than ground. Maintenance, repair, and replacement of materials, including “downtime,” are responsible for a large portion of this cost. Design redundancies and excessive maintenance and inspection to minimize accidents and product liabilities also contribute to the expense. It is estimated that 20 to 30% of materials degradation costs could be avoided by the use of known technologies and other preventive measures [33].

In fact, wear from metal-to metal contact, abrasion, impact, and erosion in mining and minerals processing is greater than that of almost any other major industry. The experience gained through maintenance operations has allowed miners to develop extensive in-house information on wear materials for their unit operations. Those involved in the design and optimization of new liners are sometimes able to draw upon this extensive database when specifying wear materials and equipment, however, hard data are difficult to come by [26].

Optimization of wear materials, and in particular of AMS, usually leads to increasing the cost of process or materials in order to improve wear resistance. Two major constraints exist to restrict the specification and use of higher-cost wear consumables [30].

- Wear materials that offer improved performance, in general will cost more. Although such materials may be cost-effective in terms of the improved life obtained, their higher purchase price serves to increase capital requirements.
- In some cases, the original design for particular liners may not be optimal in terms of process performance. Such factors are usually addressed either during, or immediately following, the commissioning of new equipment. This may involve alterations to the design of particular

components, and under these circumstances the use of higher-cost and more durable wear materials in original equipment may not prove to be cost-effective in the longer term.

The potential savings from new materials, methodologies, and designs is often a distant second to purchase price as the main criterion. Service life, operating and maintenance costs are secondary considerations; despite the obvious shortcomings of this policy. For a new material to even be tested, it must meet the criteria of guaranteed increased performance and decreased cost whilst often located in a poorly understood (or regulated) chemical and physical environment, thus it is almost impossible to subject new material formulations to current/relevant environments [31].

If the initial capital outlay is amortized over operational time, the result can be lower lifetime costs for the more expensive (purchase price only) wear-resistant materials. These costs become even lower if potential loss of production and maintenance costs are added to the equation.

One of the most important material aspects of the crusher is its lining. If this fails, change-out can lead to many hours of downtime. In the past, it has sometimes been difficult to pinpoint problem areas amongst the many reasons for crusher stoppages. This situation was changed with the introduction of operations research-based statistical production packages that record all aspects of a mine operation [27].

Thus, one of the reasons that the wear resistance of the lining is so important is that it takes so long to re-line, especially if the equipment and personnel are not at hand. In many cases re-lining takes a median of 12 h and, with the cost of downtime per hour at around 500-1000 euro, the ultimate liner performance far outweighed the purchase price of the liner. [31]

Wear is a major cost factor in mining and mineral processing, although there are no hard data on the magnitude of these costs in individual plants. Whilst information is readily available from purchasing and/or production records; of the aggregate costs of replacement components, the related, and sometimes more significant, costs of labour and lost production associated with replacing worn items are not generally known. What is almost definitely certain, however, based on previously published experience, is that substantial savings are possible through the employment of known information about wear-resistant materials and products. In order to secure support for the implementation of appropriate programs to realise these savings, mine management is going to require convincing that wear is indeed a major cost. This will necessitate a detailed, systematic evaluation of wear problems and an assessment of the total costs (replacement items, labour, lost production) attributed to them [26].

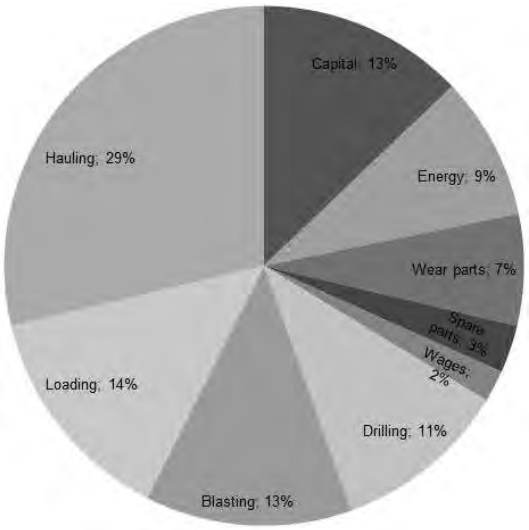

Figure 5.1. Example of Quarrying Cost [33]

For instance, in the typical quarrying operation the crushing and screening operations represent about 40% of total costs. As mentioned before, one of main components in the crushing and screening process is a cone crusher. While the message in Figures 5.1 is the relevance of wear part costs, it should be noted that costs are not the whole story; plant yield is also relevant. Higher costs can be justified if the resulting yield corresponds to higher levels of sales revenue. As demonstrated in chapter 3, liner wear is linked to quality of the product and therefore to plant yield [33].

From the mining engineering point of view, the optimization of AMS can be considered completed only if the improved new material possesses a cost that makes it profitable to use.

Manufacturing cost estimation of is a common practice in any foundry; however, the complete assessment of the steels can be only completed when the estimated cost is combined with the service performance of the liner.

Therefore, also a simulation of the liner's performance according to plant configuration, equipment design and material characteristics must be carried out. Finally with the final price of the liner estimated, plus the production performance of the liner simulated, the final performance cost can be calculated

5.2. METHODOLOGY

The cost estimation was carried out using the following guidelines:

- The chemical compositions of the steels used for the estimation are those presented in table 4.2. The recipe for H16Ti was modified to obtain the new steels.
- The production of the steels does not need modifications in the manufacturing process,
- The cost estimation was limited to variations in the chemical composition of the new alloys; all other processes are exactly equal (except for the steels termed H16Ti (TT)
- Under the item H16Ti (TT), a cost estimation of the steel H16Ti, with the classical chemical composition, was performed increasing the holding time of the heat treatment in a 50%.
- The recipe of steel constitutes the quantity and quality of raw materials that form the charge of the furnace.

- Quality of the raw materials remains the same as in the production of H16Ti.
- The smelting and casting temperatures remained fixed.
- New raw materials were introduced as well, as in the case of Nb.
- Timing of the raw materials addition to the charge is not important for the cost estimation, since there is no real process delay when adding them.
- Raw materials prices presented are accurate; they were extracted from production database in the period of 2013.
- The recipe and cost of H12Ti are also accurate.

The real costs cannot be published since it is information that compromises the market competitiveness of the sponsor of this work. Thus, an equivalence is presented, using as a reference point the true cost of H16Ti transformed to 100 euro. So, H16Ti's cost was selected as base = 100, and all other cost are referred to it. To obtain real values of each cost, one must multiply for a factor between 30 to 70 for the cone and 4 to 8 for the blow bar.

The cost were divided in three classifications

- Process costs: those cost related to the labour performed in each process.
- Charge costs: the raw materials cost
- Other cost: cost of recycling, energy, and ancillaries.

The estimation was performed for two items: a set of cone crusher liners as presented in section 5.3.1; and a set of blow bars as presented in section 5.3.2.

Using the information collected in the field test, plus the response of the new alloys to pilot scale test presented in section 4.3.8; the performance of these new alloys was simulated in a real industrial application. The results of these simulations for the cone crusher liner set and the blow bar set, the unitary cost of liner per processed ton was calculated.

5.3. RESULTS AND DISCUSSION

5.3.1. Blow bars cost estimation

Table 5.1. show the process costs for the production of the blow bars. H16Ti is the reference cost. The values of the steels, H12Ti, LC, Mo, Ni, Al and Nb did not changed. The only variable introduced in this table was the duration of the heat treatment in the case of H16Ti (TT). The cost per minute of the heat treatment for the blow bar is 0.48 euro. The value 33.36 min is the result of the division of the total length of the heat treatment by the quantity of pieces charged in the furnace for the heat treatment. The increase in 50% of the time (33.36 min to 50 min) resulted in an increase of the treatment cost from 2.26 euro per piece to 3.99 euro. The total cost only increased in 1.33 euros per piece processed.

Table 5.1. Estimation of the process costs

Process Costs	Cost per unit	H16Ti		H12Ti, H16Ti-LC, H16Ti-Mo, H16Ti-Ni, H16Ti-Al, H16Nb	H16Ti (TT)
		Quantity	Cost	Cost	Cost
	(€)	(min)	(€)	(€)	(€)
Pattern management			2,11	2,11	2,11
Steel plant			12,05	12,05	12,05
Moulding			14,32	14,32	14,32
Mould opening			0,97	0,97	0,97
Thermal treatment	0,48	33,36	2,66	2,66	3,99
Coarse Grinding			3,14	3,14	3,14
Precision grinding			6,12	6,12	6,12
Expedition			0,59	0,59	0,59
Sub - total			**41,95**	**41,95**	**43,28**

Table 5.2 shows the costs for the charge of raw materials necessary to produce each recipe. The cost of the scrap charge varied in the case of H12Ti, because less FeMn scrap was needed. In the case of H16Ti-LC, more of this scrap was needed.

For the ferroalloys, the cost changed in the case of H12Ti, since less FeMn electrolytic was needed. In the case of the LC, the carbon content was adjusted by charging less FeMnC. For the H16Ti-Mo, FeMo was added. For the alloys, there were only additions either of Al, Ni or Nb according to the steels. In this section, the highest changes in cost were observed. Raw materials were an important cost in the production of the blow bars, and the changes in the recipe did have an important impact in the final cost of some steels.

Table 5.2. Estimation of the raw materials costs

Charge costs		H16Ti		H12Ti	H16Ti-LC	H16Ti-Mo	H16Ti-Ni	H16Ti-Al	H16Ti-Nb	H16Ti (TT)
	Price	Quantity	Cost	Cost	Cost	Cost	Cost	Cost	Cost	Cost
	(€)	(Kg)	(€)	(€)	(€)	(€)	(€)	(€)	(€)	(€)
Scrap Charge										
Regular steel scrap	0,31	183,6	9,57	11,32	9,57	9,30	9,06	9,20	9,32	9,57
FeMn steel scrap	0,35	62,6	3,63	3,04	4,93	3,63	3,63	3,63	3,63	3,63
Pig iron	0,37	140,1	8,60	8,60	8,60	8,60	8,60	8,60	8,60	8,60
Sub - total		**386,30**	**21,79**	**22,96**	**23,10**	**21,53**	**21,29**	**21,42**	**21,54**	**21,79**
Ferro-Alloying										
FeMnC	0,914	42,9	6,51	6,51	3,09	6,51	6,51	6,51	6,51	6,51
FeSiMn	1,001	21,3	3,54	3,54	3,54	3,54	3,54	3,54	3,54	3,54
FeMn electr	1,244	32,2	6,65	1,79	6,65	6,65	6,65	6,65	6,65	6,65
FeCr	1,080	9,8	1,76	1,76	1,76	1,76	1,76	1,76	1,76	1,76
FeTi	3,493	6,4	3,71	3,71	3,71	3,71	3,71	3,71	3,71	3,71
FeMo	15,07	0	0,00	0,00	0,00	12,87	0,00	0,00	0,00	0,00
FeSi	1,132	0,4	0,08	0,08	0,08	0,08	0,08	0,08	0,08	0,08
Sub total		**113,00**	**22,23**	**17,38**	**18,82**	**35,10**	**22,23**	**22,23**	**22,23**	**22,23**
Alloying										
Al	1,950	0	0,00	0,00	0,00	0,00	0,00	2,30	0,00	0,00
Ni	14,50	0	0,00	0,00	0,00	0,00	23,44	0,00	0,00	0,00
Nb	25,00	0	0,00	0,00	0,00	0,00	0,00	0,00	19,87	0,00
Coke	0,320	0,4	0,02	0,02	0,02	0,02	0,02	0,02	0,02	0,02
Mn-N	2,920	0,6	0,29	0,29	0,29	0,29	0,29	0,29	0,29	0,29
Sub - total		**1,00**	**0,31**	**0,31**	**0,31**	**0,31**	**23,75**	**2,61**	**20,18**	**0,31**
Total weight charge		3400,7								

Table 5.3 present the estimation of other costs, such as the moulds and the slag forming materials. They did not change for any steel, since the materials needed in these processes are independent of the steel composition.

Table 5.3. Estimation of the other costs

Other costs	Price (€)	H16Ti Quantity (Kg)	H16Ti Cost (€)	H12Ti, H16Ti-LC, H16Ti-Mo, H16Ti-Ni, H16Ti-Al, H16Ti-Nb, H16Ti (TT) Cost (€)
Moulds				
Feeders and accessories			2,60	2,60
Olivine sand (contact and filler)			13,74	13,74
Sub - total			**16,35**	**16,35**
Slag forming elements				
Limestone	0,013	25,6	0,06	0,06
Lime	0,084	9,9	0,14	0,14
Deoxidant	0,875	0,4	0,06	0,06
Sub - total		**35,90**	**0,25**	**0,25**
Heating power				
Fuel oil	0,491	16,8	1,37	1,37
Grafite	0,250	23,5	0,97	0,97
Sub - total		40,30	2,34	2,34

The cost of all processes and raw materials was calculated in Table 5.4. The income from the recycling of the internal scrap, generated during the production of the piece, was discounted. Thus, the final production cost of the blow bar was calculated.

As can be seen, the total production cost of H12Ti and H16Ti-LC were lower than the reference. In contrast, the cost of addition of Ni and Nb represented cost around 20% higher.

Table 5.4. Estimation of the final costs of the castings

	H16Ti		H12Ti	H16Ti-LC	H16Ti-Mo	H16Ti-Ni	H16Ti-Al	H16Ti-Nb	H16Ti (TT)
	Quantity (Kg)	Cost (€)	Cost (€)	Cost (€)	Cost (€)	Cost (€)	Cost (€)	Cost (€)	Cost (€)
Total cost		**105,23**	**101,5**	**103,1**	**117,8**	**128,2**	**107,2**	**124,8**	**106,56**
Recycling									
scrap	137,32	-5,23	-5,23	-5,23	-5,23	-5,23	-5,23	-5,23	-5,23
Sub - total	137,32	-5,23	-5,23	-5,23	-5,23	-5,23	-5,23	-5,23	-5,23
Final Cost		**100,00**	**96,31**	**97,89**	**112,60**	**122,93**	**101,93**	**119,62**	**101,33**
Cost per Kilo		0,28	0,27	0,27	0,31	0,34	0,28	0,33	0,28

Figure 5.2. present a comparison of all the final production costs for the blow bar. Clearly, H16Ti-Ni and H16Nb stand out as the most expensive materials to produce. Contrarily, the change in the heat treatment barely increased the final cost of H16Ti (TT).

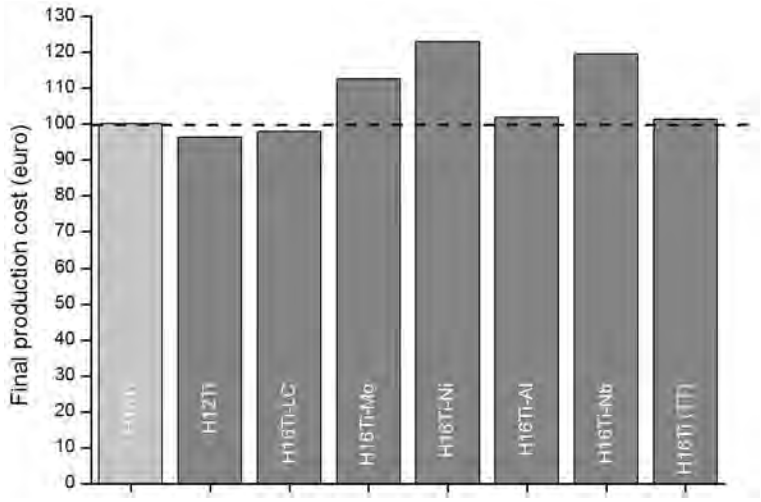

Figure 5.2. Final production costs

Table 5.5 shows the simulation of the performance of the steels based on the data extracted from the wear tests. The wear ratio is an important input for the model. Another important information resulting from the simulation is the quantity of re-linings (changes of liner) per year, which is an important factor for the operating and maintenance cost of a quarry.

Table 5.5. Estimation of the castings' cost performance

		H16Ti	H12Ti	H16Ti-LC	H16Ti-Mo	H16Ti-Ni	H16Ti-Al	H16Ti-Nb	H16Ti (TT)
Weight blw bars (x3)	(kg)	1089	1088,9	1088,9	1088,9	1088,9	1088,9	1088,9	1088,9
	(g)	1088940	1088940,0	1088940,0	1088940,0	1088940,0	1088940,0	1088940,0	1088940,0
Wear limit	(%)	20%	18%	20%	20%	20%	20%	20%	20%
Loss weight	(g)	217788	196009,2	217788	217788	217788	217788	217788	217788
Final weight	(g)	871152	892930,8	871152	871152	871152	871152	871152	871152
Wear ratio	(g/t)	28	33	34	30	28	37	26	28
Working days in quarry	(day)	200	200,0	200	200	200	200	200	200
Operating hours	(h/day)	4	4,0	4	4	4	4	4	4
Total rock processed	(t)	7905	5966,8	6353	7212	7845	5894	8322	7905
Throughput	(t/h)	85	85,0	85	85	85	85	85	85
Hours of work	(h)	93	70,2	75	85	92	69	98	93
Days of work per set	(day)	23	17,5	19	21	23	17	24	23
Sets changes per year	(#)	8,6	11,4	10,7	9,4	8,7	11,5	8,2	8,6
Price blow bars (x3)	(€)	300,00	288,9	293,67	337,80	368,80	305,78	358,85	303,99
Cost per ton	(€/t)	0,03795	0,04842	0,04622	0,04684	0,04701	0,05188	0,04312	0,03845
Percentage to H16Ti	**(%)**	**100%**	**128%**	**122%**	**123%**	**124%**	**137%**	**114%**	**101%**

Figure 5.3 presents the relationship of cost *vs.* performance. This value means the amount invested in the acquisition of the set of blow bars divided in the tonnage of rock processed in the service life of the set. Again, the value of reference is H16Ti, and the higher the values obtained, the more expensive the set, in term of performance. In other word, the higher the value, the poorer the performance of the steel.

H16Ti-Al presents the higher values, therefore is the worst steel to use in this application. In addition, H12Ti presented a relatively poor performance, which was already presented in section 3.9. The costs of Ni and Nb are amortized by their good performance.

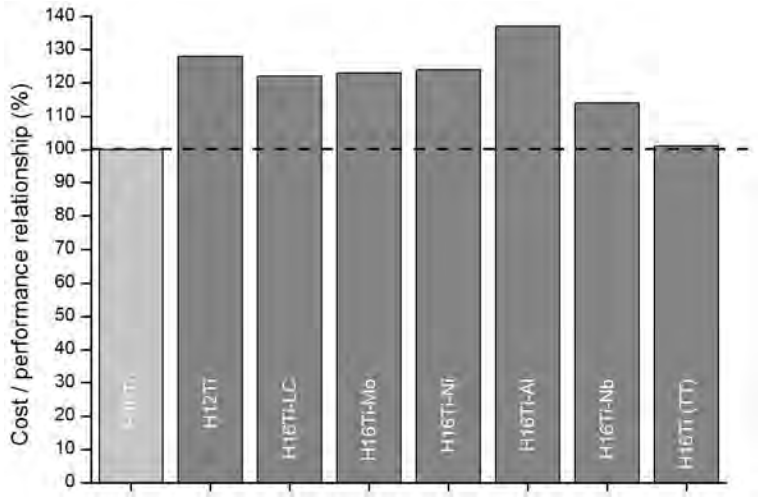

Figure 5.3. Relationship cost/performance

Additionally, other conclusion can be drawn from the simulation. H16Ti-Ni presents a relative higher cost/performance relationship, but its use could be justified when high impact toughness is needed. The LC steel presented good results in comparison with the alloyed steels. However, this does not mean the steel is applicable for high abrasive materials. The case of H16Ti (TT) demonstrated that an increment of the holding time in the heat treatment does not improve final performance, but it may improve reliability of the thick casts.

5.3.2. Cone liners cost estimation

Table 5.6. shows the process costs for the production of the set of cone liners. H16Ti is the reference cost. The values of the steels, H12Ti, LC, Mo, Ni, Al and Nb do not changed. The only variable introduced in this table was the length of the heat treatment in the case of H16Ti (TT). The cost per minute of the heat treatment for the set was 0.30 euro. The value 224.76 min is the result of the division of the total length of the heat treatment by the quantity of sets charged in the furnace for the heat treatment. The increase in 50% of the time (224.76 min) resulted in an increase of the treatment cost from 1.42 euro per piece to 2.13 euro. The total cost only increased in 0.76 euro per piece processed.

Table 5.6. Estimation of the process costs

		H16Ti		H12Ti, H16Ti-LC, H16Ti-Mo, H16Ti-Ni, H16Ti-Al, H16Ti-Nb	H16Ti (TT)
Process Costs	Cost per unit	Quantity	Cost	Cost	Cost
	(€)	(min)	(€)	(€)	(€)
Pattern management			1,02	1,02	1,02
Steel plant			12,81	12,81	12,81
Moulding			12,57	12,57	12,57
Mould opening			0,53	0,53	0,53
Thermal treatment	0,30553	224,76	1,42	1,42	2,13
Coarse Grinding			6,94	6,94	6,94
Precision grinding			10,49	10,49	10,49
Expedition			0,27	0,27	0,27
Sub - total			**46,05**	**46,05**	**46,76**

Table 5.7 shows the costs for the charge of raw materials necessary to produce each recipe. The cost of the scrap charge varied in many cases, because steel scrap and FeMn scrap quantities were used as a variable in order to compensate for the addition or subtraction of other materials. In the case of the set of cones, the quantities involved require a more complex adjustment than the one performed for the blow bar.

For the ferroalloys, the cost changed in the case of H12Ti, since less FeMn electrolytic was needed. In the case of the LC, the carbon content was adjusted by charging less FeMnC. For the H16Ti-Mo, FeMo was added.

For the alloys, there were only additions of Al, Ni or Nb according to the steels. In this section, the highest additional cost were observed.

Raw materials were an important cost in the production of the set of liners, and the changes in the recipe did have an important impact in the final cost of some steels.

Table 5.7. Estimation of the raw materials costs

Charge costs		H16Ti		H12Ti	H16Ti-LC	H16Ti-Mo	H16Ti-Ni	H16Ti-Al	H16Ti-Nb	H16Ti (TT)
	Price	Quantity	Cost	Cost	Cost	Cost	Cost	Cost	Cost	Cost
	(€)	(kg)	(€)	(€)	(€)	(€)	(€)	(€)	(€)	(€)
Scrap Charge										
Regular steel scrap	0,35	1251,00	8,95	10,58	8,95	8,70	8,48	8,61	8,72	8,95
FeMn steel scrap	0,34	497,10	3,49	3,49	4,57	3,49	3,49	3,49	3,49	3,49
Pig iron	0,35	1092,10	7,79	7,79	7,79	7,79	7,79	7,79	7,79	7,79
Sub - total		**2840,20**	**20,23**	**21,87**	**21,31**	**19,98**	**19,76**	**19,90**	**20,00**	**20,23**
Ferro-Alloying										
FeMnC	0,78	279,10	4,50	2,66	2,03	4,50	4,50	4,50	4,50	4,50
FeSiMn	0,84	117,20	2,04	1,04	2,04	2,04	2,04	2,04	2,04	2,04
FeMn electr	1,22	60,40	1,52	0,08	1,52	1,52	1,52	1,52	1,52	1,52
FeCr	1,05	52,00	1,13	1,13	1,13	1,13	1,13	1,13	1,13	1,13
FeTi	6,30	42,96	5,60	5,60	5,60	5,60	5,60	5,60	0,00	5,60
FeMo	13,16	0,00	0,00	0,00	0,00	9,52	0,00	0,00	0,00	0,00
FeSi	1,04	6,60	0,14	0,14	0,14	0,14	0,14	0,14	0,14	0,14
Sub total		**558,26**	**14,92**	**10,65**	**12,45**	**24,44**	**14,92**	**14,92**	**9,32**	**14,92**
Alloying										
Al	1,87	2,20	0,09	0,09	0,09	0,09	0,09	1,83	0,09	0,09
Ni	10,80	0,00	0,00	0,00	0,00	0,00	14,79	0,00	0,00	0,00
Nb	25,00	0,00	0,00	0,00	0,00	0,00	0,00	0,00	16,82	0,00
Coke	0,32	0,00	0,00	0,00	0,00	0,00	0,00	0,00	0,00	0,00
Sub – total		**2,20**	**0,09**	**0,09**	**0,09**	**0,09**	**14,87**	**1,83**	**16,91**	**0,09**
Total weight charge		3400,7								

Table 5.8 present the estimation of other costs, such as the moulds and the slag forming materials. They did not change for any steel, since the materials needed in this processes are the independent of the steel composition.

Table 5.8. Estimation of the other costs

Other costs	Price (€)	H16Ti Quantity (kg)	H16Ti Cost (€)	H12Ti, H16Ti-LC, H16Ti-Mo, H16Ti-Ni, H16Ti-Al, H16Ti-Nb, H16Ti (TT) Cost (€)
Moulds				
Feeders and accessories			2,43	2,43
Olivine sand (contact and filler)			17,45	17,45
Sub - total			**19,88**	**19,88**
Slag forming elements				
Limestone	0,0127	164,60	0,04	0,04
Lime	0,09	78,30	0,15	0,15
Deoxidant	0,88	2,90	0,05	0,05
Sub - total		**245,80**	**0,24**	**0,24**
Heating power				
Fuel oil	0,4476	113,60	1,05	1,05
Grafite	0,2500	151,10	0,78	0,78
Sub - total		**264,70**	**1,83**	**1,83**

The cost of all processes and raw materials were added in Table 5.9. The income from the recycling of the scrap, generated during the production of the piece, was discounted. Thus, the final production cost of the blow bar was calculated.

As can be seen, the total production cost of H12Ti and H16Ti-LC were lower than the reference. In contrast, the cost of addition of Ni and Nb represented cost around the 11-14%.

Table 5.9. Estimation of the final costs of the castings

	H16Ti		H12Ti	H16Ti-LC	H16Ti-Mo	H16Ti-Ni	H16Ti-Al	H16Ti-Nb	H16Ti (TT)
	Quantity (Kg)	Cost (€)	Cost (€)	Cost (€)	Cost (€)	Cost (€)	Cost (€)	Cost (€)	Cost (€)
Total cost		**103,24**	**100,6**	**101,8**	**112,5**	**117,6**	**104,6**	**114,2**	**103,95**
Recycling									
Scrap	922,66	-3,24	-3,24	-3,24	-3,24	-3,24	-3,24	-3,24	-3,24
Sub – total	**922,66**	**-3,24**	**-3,24**	**-3,24**	**-3,24**	**-3,24**	**-3,24**	**-3,24**	**-3,24**
Final Cost		**100,00**	**97,37**	**98,61**	**109,27**	**114,31**	**101,40**	**111,00**	**100,71**
Cost per Kilo		0,16	0,16	0,16	0,18	0,19	0,17	0,18	0,17

Figure 5.4. present a comparison of all the final production costs for the liner set. Clearly, H16Ti-Ni and H16Nb stand out as the most expensive materials to produce. The change in the heat treatment barely increased the final cost of H16Ti (TT).

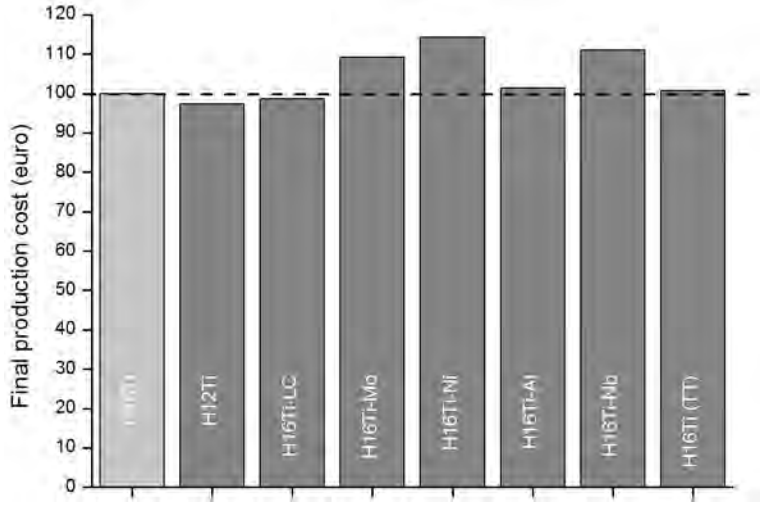

Figure 5.4. Final production costs

Table 5.10 shows the simulation of the performance of the steels based on the data extracted from the wear tests. The wear ratio is an important input for the model. Another important information resulting from the simulation is the quantity of re-lining (changes of liner) per year, which is an important factor for the operating and maintenance cost of a quarry.

Table 5.10. Estimation of the castings' cost performance

		H16Ti	H12Ti	H16Ti-LC	H16Ti-Mo	H16Ti-Ni	H16Ti-Al	H16Ti-Nb	H16Ti (TT)
Weight cone	(Kg)	2478	2478	2478	2478	2478	2478	2478	2478
	(g)	2478000	2478000	2478000	2478000	2478000	2478000	2478000	2478000
Wear limit	(%)	26%	28%	26%	26%	26%	26%	26%	26%
Loss weight	(g)	636846	691362	636846	636846	636846	636846	636846	636846
Final weight	(g)	1841154	1786638,0	1841154	1841154	1841154	1841154	1841154	1841154
Wear ratio	(g/t)	5,9	6,1	7,3	6,4	5,9	7,9	5,6	6
Working days in quarry	(day)	365	365,0	365	365	365	365	365	365
Operating hours	(h/day)	22,8	22,8	22,8	22,8	22,8	22,8	22,8	22,8
Total rock processed	(t)	108750	114000	87395	99195	107926	81090	114498	108750
Throughput	(t/h)	250	250,0	250	250	250	250	250	250
Hours of work	(h)	435	456	350	397	432	324	458	435
Days of work per set	(day)	19	20	15	17	19	14	20	19
Sets changes per year	(#)	19,1	18,3	23,8	21,0	19,3	25,7	18,2	19,1
Price set	(€)	100	97,4	98,61	109,27	114,31	101,40	111,00	100,71
Cost per ton	(€)	0,0009195	0,0008541	0,0011283	0,0011016	0,0010592	0,0012505	0,0009694	0,0009261
Percentage to H16Ti	**(%)**	**100%**	**93%**	**123%**	**120%**	**115%**	**136%**	**105%**	**101%**

Figure 5.5 presents the relationship of cost vs. performance. This value means the amount invested in the acquisition of the set of cone liner divided in the tonnage of rock processed in the service life of the set. Again, the value of reference is H16Ti, and the higher the values obtained, the more expensive the set, in terms of performance. In other word, the higher the value, the poorer the performance of the steel.

H16Ti-Al presents the higher values, therefore is the worst steel to use in this application. In addition, H12Ti presented a relatively poor performance, which was already presented in section 3.9. The costs of Ni and Nb are amortized by their good performance.

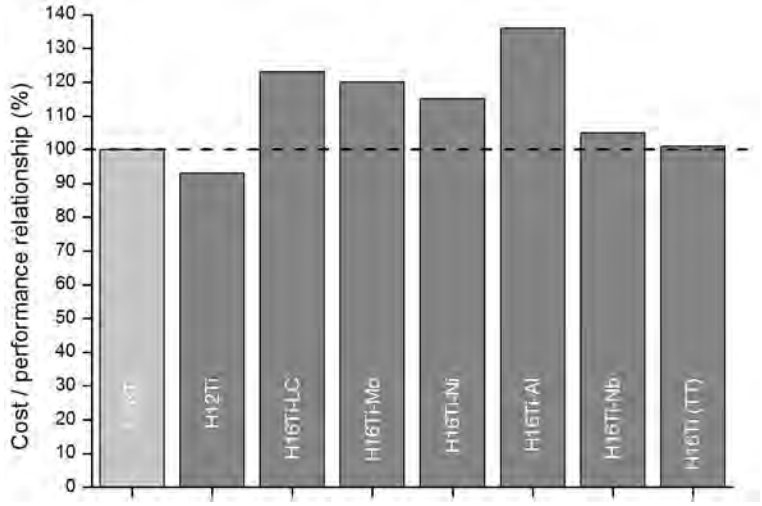

Figure 5.5. Relationship cost/performance

Additionally, other conclusion can be drawn from the simulation. H16Ti-Ni presents a relative higher cost/performance relationship, but its use could be justified when high impact toughness is needed. The case of H16Ti (TT) demonstrated that an increment of the holding time in the heat treatment does not improve final performance, but it may improve reliability of the thick casts.

5.4. CONCLUSIONS

The addition of Ni represent an increase in cost that should be carefully considered. Ni addition to H16Ti had demonstrated to have good effects in the mechanical properties, which may improve reliability of thick cast liners.

The good value of low cost/performance ratio does not seem to be reliable. The values obtained in the pilot scale test does not seem to reflect what is largely demonstrated in many industrial cases. Perhaps a better design of experiment is necessary to investigate the wear rate between regular carbon AMS (12%C) and the high carbon AMS presented here.

The addition of Al was clearly a disadvantage, because of the low wear rates obtained. However, this could be changed with improvements in the process of fabrication (better addition of the Al)

The case of addition of Mo did not show any improvement in the performance of the steel, perhaps more amount of Mo was needed.

In the case of Nb, the replacement of Ti did not showed any advantage in terms of performance, but it did increased the production costs.

Therefore, all materials proposed showed disadvantages in terms of cost. However, the Ni case seem to present the best opportunities for a cost/performance optimization.

CHAPTER VI - GENERAL CONCLUSIONS

The starting point of this work was H12Ti and H16Ti, which presented opportunities for improvement. Due to their high carbon content, both steels presented carbides in their microstructure, which rendered them brittle. The work of optimization focused on the chemical and microstructural characteristics of H12Ti and H16Ti, in order to increase their mechanical properties while, at least, maintaining their wear resistance.

The optimization of these steels started by improving the solution heat treatment, which was re-set at 1090°C and 120 min. This treatment proved to austenitize both steels successfully.

However, the problem of reprecipitation persisted, which was characterized by means of isothermal treatments. The phenomenon demonstrated to be critical in the temperatures between 950°C and 500°C.

In order to control re-precipitation, spheroidization of the pearlite was attempted, unsuccessfully. In addition, the quenching conditions were investigated, but the cooling rate of the casting for thick sections proved to be too slow to achieve good freezing of the microstructure in time to avoid reprecipitation.

Therefore, it was established that casting thicknesses above 100 mm were at risk of embrittlemnt due to reprecipitation. To minimize this risk, H16Ti was a better choice, since the higher content of manganese allowed more carbon to be retained in the austenite matrix, and thus be less available to migrate to grain boundary.

The wear test in pilot scale produce results with good validity. In particular, the impact crushing tests demonstrated to be representative and relatively easier to carry out. As a result of this representativity, reliable predictions were made regarding the performance of particular new materials under a range of in-service operating conditions.

In the case of the field tests, an appropriate data collection and experimental designs were needed, and, in some cases, extra monitoring of equipment would have been required. The extra resources needed, namely labor and measuring equipment, should be more than compensated for by better cost-efficient testing. The data collected could easily be used for more efficient maintenance programs in addition to wear assessment. Although the field tests possessed some shortcomings, reliable conclusions could be drawn:

- H16Ti is outranks H12Ti in any crushing application;
- There are applications were the presence of embrittling carbides (gbc) is not critical, such in the case of HSI. But there are crushing applications, namely cone crushers, were gbc is critical, especially when the abrasive material has a crushability index of difficult.
- H16Ti steel cannot yet match the performance of other wear resistance materials such as Chrome white irons and Low-alloy martensitic steels.

In consequence, H12Ti was not recommended for tick castings, and since the production cost of both steels does not differ too much, even it could be discarded altogether form the production of liners for crushing applications.

Furthermore, the use of H16Ti for the production of blow bars is not recommended with the current characteristics. Further improvements must be done in order to increase its wear resistance in impact crushing processes. Perhaps, the addition of higher amount of Nb may improve the wear resistance, by creating a hard ceramic phase of NbC. However, higher contents of Nb must be matched with higher carbon in the composition, which may increase the risk of reprecipitation.

Finally, the use of Ni seems to a partial solution to the formation of gbc. A certain amount of nickel proved to increase the mechanical properties, but also greatly increased the raw materials cost. Therefore, Ni addition must be consider in the case of very large castings (for primary crushing applications) were the final price of the piece is second to its reliability in service.

The author humbly proposes the following points as original contributions of his work to the science and technology of mining and metallurgy:

- A characterization of the grain boundary carbides re-precipitation phenomenon in high carbon austenitic manganese steels.
- A protocol to characterize and develop new steels, which integrates pilot scale wear testing with industrial experiments.

Proposal for future work

The work should continue by testing the new alloys in industry and assessing real cost per ton produced, eliminating the necessity of assumptions in the simulation.

Personal comments

Nowadays, Italian and European steelmakers of AMS for comminution applications face many challenges in the globalized market. The bigger threat comes from the developing economies, which traditionally have lower manufacturing costs, but now they are also producing with better quality.

The biggest opportunity for the Italian foundries is their global reputation of superior quality products and a long tradition of R&D. The future of AMS for comminution process may be the customization of products to meet specific demands of clients needing high wear resistance and high mechanical properties.

High production costs and therefore high price can be compensated with higher performance at the client operation. However, the path to successfully develop this kind of product lies in the close relation between foundry and mining operator. A relationship that seems natural, but that is not always ease to establish, because in most of the case the Original Equipment Manufacturer (OEM) stand in the middle, acting as a “middle man” and thus controlling the flow of information.

The role of application engineers, who understand the necessities of the mining client and feedbacks the foundry, in order to improve the production process of the steel, may be an economical and easy to implement first step to tailoring AMS for each costumer, according to their specific

necessities. The application engineer may be able to develop more representative experiments and protocols in order to improve the R&D as well.

AMS smelting is not a mass production operation. Small furnaces permit flexible production of steels, which must be accompanied with a good scheduling and logistics to provide the mining operator with tailored pieces in time.

In conclusion, the future of AMS production in Italy and perhaps western Europe may lay in maximization of knowledge and expertise of specific tailored steels, and in the full understanding of the comminution processes present in each site.

APPENDIX A: SIMULATION OF A COMMINUTION PROCESS

A.1. INTRODUCTION

In this work is presented a performance model that can be applied to different types of impact crushers. The goal is to predict the product size distribution, provided that the crusher's rotor velocity and radius as well as the feed rate and size distribution are known beforehand. The specific ore properties and the crusher's design are taken into account through a reasonable number of adjustable parameters. Furthermore, the development of the model contemplated the loss of quality of the product due to wear of the blow bars.

The starting point for the model's development is the model presented by Nikolov [28], which in turn is based on the standard model for cone and jaw crushers developed by Whiten and White [29]. A scheme of the model is presented in Figure A.1.

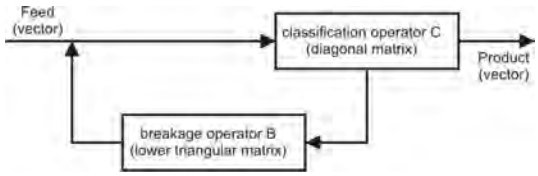

Figure A.1. Scheme of the breakage process in cone and jaw crushers. [29]

Nikolov's model proposed a modification to the White's model, considering high energy impact occurring in impact crushing. The equations are presented below:

$$C_i(d_i) = 1 - \exp\left[-\left(\frac{d_i - d_{\min}}{d_{\min}}\right)^k\right] \quad (A.1)$$

(Classification function proposed by Nikolov).

$$d_{\min} = d_{\max}.\exp\left\{-\left[c_0 + c_1.\ln\left(\frac{Q_0}{Q}\right)\right].\left(\frac{E}{E_0}\right)^n\right\} \quad (A.2)$$

(Breakage function proposed by Nikolov)

Where d_{min} is the minim breakage size, Q and E are the feed rate and the average impact energy per unit mass respectively. Q_0 and E_0 are reference feed rate and reference impact energy respectively. d_{max} (mm) is the maximum particle dimension in the feed; n is a material parameter; c_0 is a rate constant and c_1 accounts for the intensity of the particle–particle interactions.

As mentioned in Chapter 3, the loss of the geometry of the blow bars due to wear, generates a decrease in the quality of the product. Figure A.2. shows the change of the gap between the edge of the blow bar and the lower part of the impact shield.

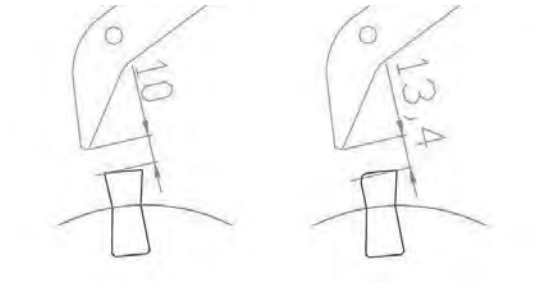

Figure A.2. Opening of the gap due to wear. Left, at the beginning of the service life of the blow bar. Right, at the end of the service life. [44] [45]

In order to simulate the effects of wear in the granulometric curve of the product, data from the crushing test presented in Chapter 3 were used [45].

The model predictions were compared with experimental data for granite treated in the pilot-scale HSI.

A.2. EXPERIMENTAL

Mathlab was used for programing the model. The input data for the model was sourced from the test results presented in Chapter 3. The list below present the data and parameters used:

Experimental data:

- Material: granite / Throughput: 80 kg/h
- Granulometric curve of feed: from test presented in section 3.5
- Initial height of the blow bar: 23 mm
- Rotor diameter: 255 mm / Velocity: 1957 rpm
- Gap at beginning of the test (gap 1): first shield, 8 mm / second shield, 3 mm
- Gap at 25% wear (gap 2): first shield, 10 mm / second shield, 5 mm
- Gap at 50% wear (gap 3): first shield, 12 mm / second shield, 7 mm
- Gap at end of the test (gap 4): first shield, 14 mm / second shield, 9 mm

Model parameters:

The parameters of the model were adjusted in order to match the values of the gaps used to predict the granulometric curves:

Table A.1. parameters of the model according to opening if the gap

Gap 1	d_{min}: 1.225	k=0.7	m=1.20	l = 0.95	c_0= 2.10
Gap 2	d_{min}: 1.225	k=0.67	m=1.20	l = 0.95	c_0= 2.05
Gap 3	d_{min}: 1.225	k=0.65	m=1.20	l = 0.95	c_0= 2.00
Gap 4	d_{min}: 1.225	k=0.63	m=1.20	l = 0.95	c_0= 1.60

A.3. RESULTS

The granulometric curves predicted by the model are presented in the figures below:

Figure A.3 shows the granulometric curve of the feed, which was input data. At the left, the curve of the product for the run with gap 1. The curves measured in the field and the curve predicted by the model matched almost completely.

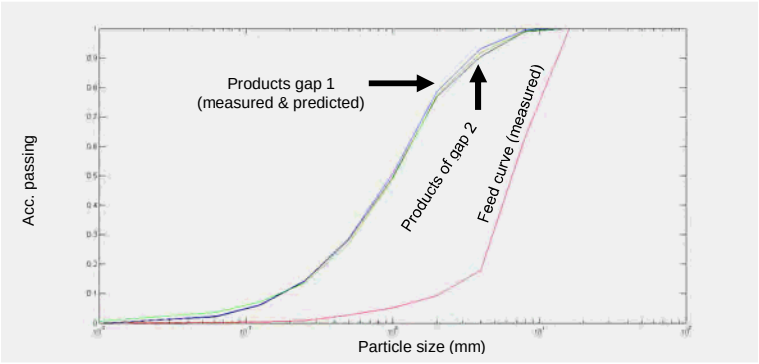

Figure A.3. Results of simulation for gap 1 and gap 2.

Additionally, the granulometric curves of the product of the run with gap 2 are presented in the same figure. The predicted and the measured curves almost matched. The products started to become slightly coarser.

Figure A.4 shows the result of for the run using gap 3. The

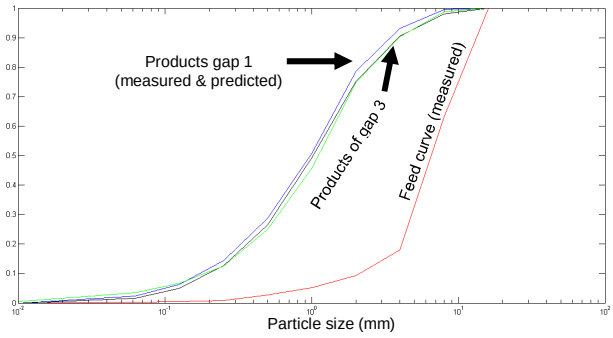

Figure A.4. Results of simulation for gap 1 and gap 3.

product progressively becomes coarser with the wear of the blow bars.

Finally, Figure A.5 presents the predicted and simulated curves for the run of the program with the gap 4. There was a much pronounced coarsening of the particles with this gap.

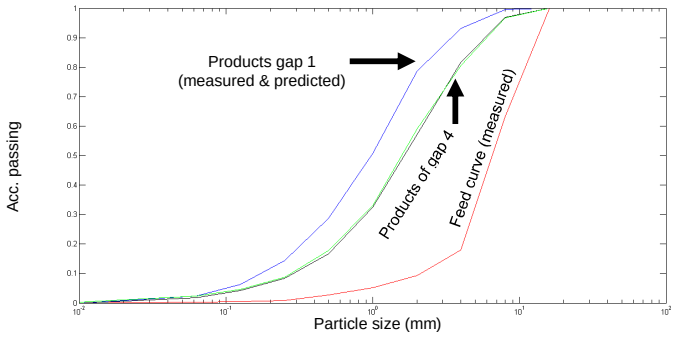

Figure A.5. Results of simulation for gap 1 and gap 4.

A.4. DISCUSSION

The mathematical model predicted the granulometric curve for each gap opening with good accuracy. The values collected in the test were reproduced by the program.

From the curve of gap 3 to the curve of gap 4 there was a dramatic loss of quality in the product of the machine. This sudden change was modelled by adjusting the parameter C_0. In order to reflect the change in the trend, two tipes of curves were combines. From the startin gap (gap 1) to gap 3, the trend was linear. From gap 3 to gap 4, the dramatic loss of quality was programmed using a hyperbolic curve.

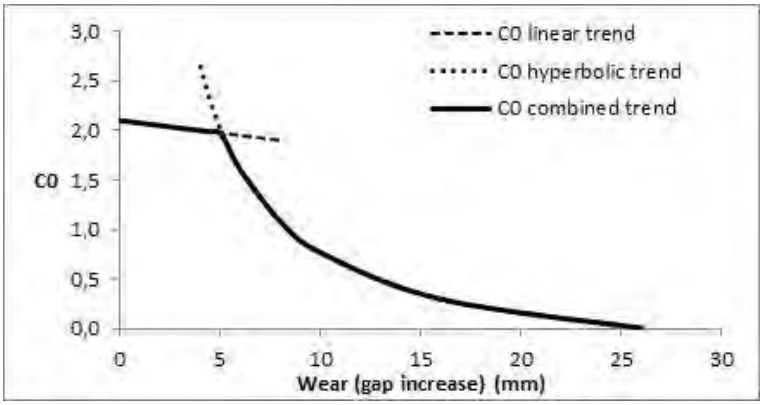

Figure A.6. The adjustment of C_0. [45]

The meeting point of the two curves represent the point where the front face of the blow bar has been rounded up by wear. This is the point that determines the end of the service life of the blow bar.

A.4. CONCLUSIONS

The model predicted successfully the values found in the tests. The matching of the curves measured and estimated was very good.

Additionally, a combination of two functions permitted to program the function of C_0 that is used to reflect the effects of wear in the quality of the product.

The model could predict intermediate values between gap 1 and 4 with accuracy, but values higher than gap 4, perhaps without much accuracy.

The model is only adjusted for this specific set of data, and would need further development if it was to be used for other systems.

APPENDIX B - COMMINUTION AND LEACHING EXTRACTION ENHANCEMENT USING AN ULTRASOUND TREATMENT

B.1. INTRODUCTION

In the field of mineral processing, and more particularly in hydrometallurgy, ultrasonically assisted reactions are well acknowledged in literature for having a positive impact on reaction kinetics and metal yield. Many researchers have reported an overall increase of metal extraction from different materials, such as silver, copper and nickel ores, using ultrasonic assisted leaching [46] [47] [48]. Effects of ultrasound assisted treatments originate from the cavitation bubbles collapsing into the medium (e.g. pulp). One of these effects is small particle size reduction, or micro-grinding. The results presented in this work show the response (in terms of particle size reduction) of rock particles, owing different petrographic and mineral characteristics, to an ultrasound treatment, focusing on three main variables: sonication time, sonication power and distance to the source. Additional studies check the effectiveness of this ultrasound treatment in enhancing the leaching rate of chromium in one of the rocks, which contains a considerable amount of this element.

Ultrasound frequencies start at 16 kHz, however they are usually used within the range from 20 kHz to 500 MHz. Frequency and power output are inversely proportional; therefore, high-intensity, low-frequency ultrasound, can modify the state of the medium. This is the type of ultrasound mostly used in mineral processing applications. Cavitation bubbles generated during the rarefaction (or negative pressure) period of sound waves are the source of the chemical and mechanical effects of ultrasound. Mechanical effects, such as particle erosion and particle fragmentation may be considered responsible for some enhancement of reaction kinetics, due to the generation of fresh surface area available for reaction. Moreover, deagglomeration and surface cleaning are other mechanical benefits commonly associated with ultrasound that also improve reaction rate [49]. In the case of chemical or sonochemical effects, benefits may be associated with the high temperatures and pressure spots generated during bubble collapse (up to 5000°K and 100 MPa during periods of microseconds) and with the reduction of the liquid boundary film surrounding the particle, thus improving mass transfer.

Cavitation conditions are governed by different parameters, including temperature and pressure. For instance, an increase in the ambient reaction temperature produces a decrease of the sonochemical effect, while an increase in the ambient reaction pressure usually intensifies the sonochemical effect. Nevertheless, one of the most important parameters to be considered is the power delivered to the pulp. As the power increases, the reaction kinetics increase to a maximum, followed by a decrease as the power continues to increase. Power intensity, which is defined as power delivered by the generator divided by the area of the probe, is another useful parameter for the adjustment of the treatment. The maximum ultrasonic intensity (I_{max}) is correlated to the pressure amplitude produced by collapsed bubble (P_A) by eq b.1:

$$I_{\max} = \frac{P_A}{2\rho C} \quad \text{eq.(b.1)} \qquad I = I_{\max} \exp(-2\alpha d_T) \quad \text{eq.(b.2)}$$

where ρ is the density of the liquid medium and C is the velocity of the sound in that medium. The intensity (I) present in a certain point in the medium will decrease as the distance (d_T) from the transmitting source increases as shown by eq b.2, where (α) is the attenuation coefficient of the medium [50].

The effect of cavitation on solid surfaces can be explained by two known mechanisms: micro-jetting and shockwave damage [51]. Micro-jetting can occur when a cavitation bubble is formed near a solid particle; the asymmetry of the liquid particle motion during cavity collapse provokes a strong deformation in the cavity. The bubble potential energy is then converted into kinetic energy with the production of a liquid jet, which can reach velocities of hundreds of meter per second. Due to the induced asymmetry, the jet often impacts the particle boundary, thus delivering immense energy densities at the site of impact. The other mechanism involves shockwaves produced by cavity collapse, which create agitation in the pulp, and therefore inter-particle collisions [52]. The impingement of micro-jets and shockwaves is responsible for ultrasonic cleaning and changes on particle surface, creating fissures and cracks. Inter-particle collision causes micro-grinding effects, thereby increasing the total surface area available for reactions, such as leaching or adhesion of surfactants. Moreover, these mechanisms allow the stirring of the pulp and avoid particle agglomeration.

Mineral materials possess natural internal cracks and fissures, and ultrasound energy may induce their propagation, thus creating fractures, and new smaller particles. These fractures may occur in the natural grain boundaries of the mineral [53]. Particle breakage is in part controlled by the physical characteristic of the rock, such as particle size, hardness, internal cracks, among others. The laws of comminution establish that the finer the particle, the higher the energy needed to further reduce its size [24]. Therefore fine comminution is an energy intensive process, and ultrasound assisted treatments may present, in certain cases, an option to conventional mechanical processes such as fine wet grinding. Additionally, conventional grinding mills have their capabilities restricted due to critical speed and limited size of the grinding media (i.e. if the ball are too small, their impact energy would be otherwise insignificant) [51]. As an alternative, fine comminution can be achieved by means of an ultrasonic assisted treatment. Furthermore, due to this process, new surface area is made available for the leaching reactions to take place. However, this method for reducing particle size is limited by a minimum particle mass at which the momentum of the particle is too small to create the impact required to cause particle fragmentation. Diverse studies have shown that the corresponding minimum particle size is around 10 - 20 microns [54].

B.2. EXPERIMENTAL

B.2.1. Materials and sample preparation

Three types of mineral materials were tested: quartzite and rhyolite rocks and steel furnace slag. The rocks were crushed, and afterwards sieved using four ASTM standard sieves (18#, 20#, 30# and 35#), as represented in Figure B.1. Two size classes were collected: the coarse fraction (-18# ÷ +20#), and the fine fraction (-30# ÷ +35#); particles outside these closed size ranges were discarded. Granulometric analysis, following the ASTM standard procedure [55], were performed before and after

each treatment in order to quantify grinding effects. The accumulated passing 80% (P80) was selected as the parameter for comparison between samples. Mean P80 size for the three coarse fractions was approximately 991 µm, and mean P80 size for the three fine fractions was approximately 574 µm. Additionally, Specific Surface Area (SSA) of the products were calculated using P90, P50 and P10.

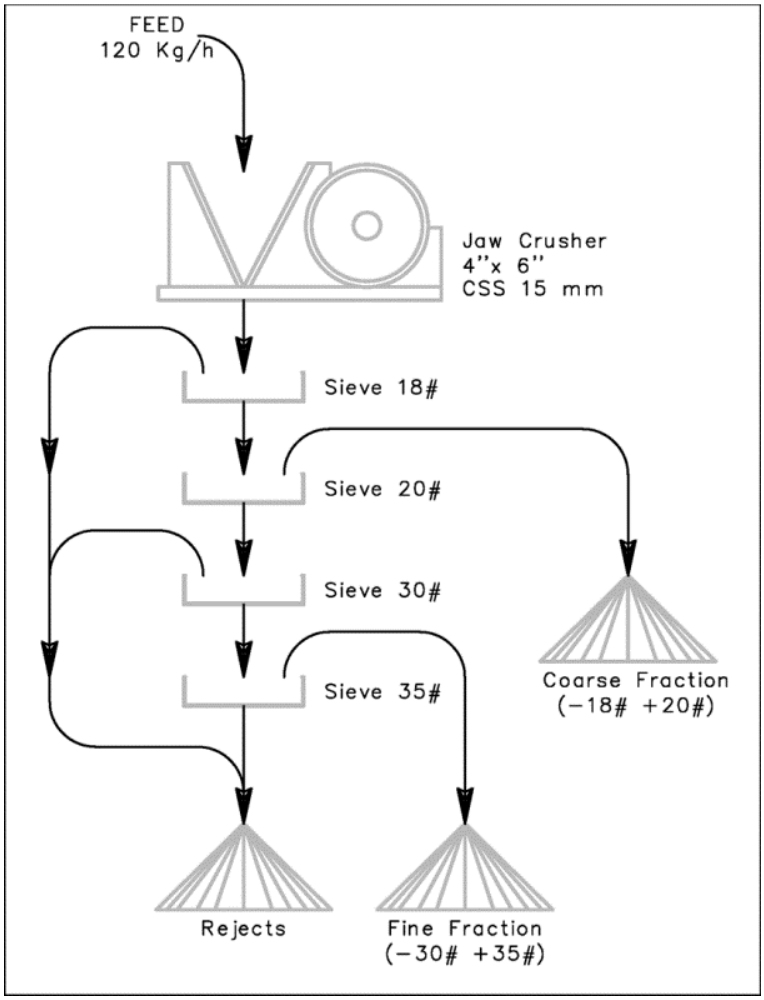

Figure B.1. Sample preparation process for coarse and fine fraction.

B.2.2. Micro-grinding treatment

The sonication of the three types of rocks, previously separated into coarse and fine fractions, was carried out in a 250 ml glass reactor, under atmospheric pressure. The schematic illustration of the experimental set-up is shown in Figure B.2. Low frequency (20 kHz) ultrasound was generated using a Bandelin UW2070 sonicator, equipped with a 13 mm diameter titanium probe (i.e. sonication with probe system). Power supply capacity of the generator was adjustable in a range of 0 – 70 W. In order to prevent the tip of the probe from premature pitting and erosion, the probe was periodically replaced and maintained. The ultrasonic power delivered to the pulp was measured by calorimetric method as reported in [50] and it was found to be approximately 50% less than the nominal power capacity produced by the generator. Temperature of the reactor content was controlled thermostatically at 40°C (± 2°C).

Each test used 30 g of rock sample in deionized water with pulp density of approximately 1.103 g l^{-1}. Small sample amount and low pulp density were selected in order to minimize attrition between particles. For that same purpose, no mechanical stirring was employed, and neither was gas injected to the pulp.

Three series of tests were carried out using the three types of rocks for each series. The parameter chosen for the first series (i) was the duration of the ultrasound treatment (sonication time). The second series (ii) used the power delivered by the ultrasound generator (sonication power). The third series of test (iii) looked at the distance from the tip of the probe to the bulk of the sample (sonication distance). All tests in each series were performed in duplicate.

The series (i) used sonication times of 120, 180 and 240 min while parameters of distance and power were fixed at 10 mm and 70W respectively. The series (ii) used sonication powers of 40, 55 and 70W, while the time was set at 120 min and distance was 10 mm. Finally, the series (iii) used 10 mm, 20 mm and 30 mm distances, whereas sonication time was of 120 min and sonication power of 70W.

A side series of tests (iv) was performed using a single coarse quartzite particle each time, which was attached to the bottom of the reactor, and placed just below the probe to prevent inter particle collision. This series used a 120 min sonication time, a 70W sonication power and a 10 mm sonication distance.

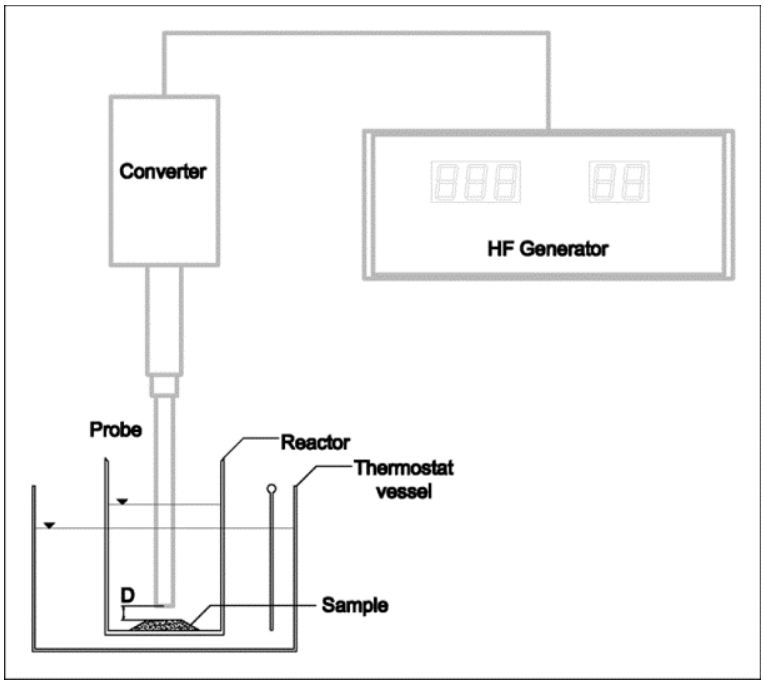

Figure B.2. Schematic diagram of experimental set-up.

B.2.3. Micro-grinding and leaching treatment

Fine fraction slag samples were leached using nitric acid at concentration of 63 g l^{-1}, with and without ultrasonic treatment. The set-up of the experiment remained equal to the micro-grinding test, and parameters were identical to those used in series (i). The chemical content of the ore, before and

after the leaching tests, was measured using a Thermo Scientific ARL Advant Sequential X-ray fluorescence (XRF) instrument. All tests were performed in duplicate.

B.3. RESULTS AND DISCUSSION

B.3.1. Micro-grinding treatment

The results of the series (i), sonication time, separated according to size fraction, are shown in Figure B.3. Coarse quartzite had the best response to treatment with a P80 size reduction of 7.9% at 120 min, from the original 991 µm size. However, from 120 min to 240 min, P80 only decreased of 1.3%. Coarse rhyolite had the second best response to treatment with a P80 size reduction of 2.1% at 120 min, from the original 991 µm size; at 240 min, P80 decreased to 5.5%. Coarse fraction slag instead, presented a weak response to treatment, showing a P80 size reduction of 0.2% after 120 min and 1.7% after 240 min.

For the fine particle fraction, rock response followed the same trend, with P80 of the quartzite reduced of 17.5% at 120 min, but only 19.8% size reduction after 240 min, with respect to the original 574 µm particle size. Fine rhyolite had a P80 size reduction response of 12.8% after 120 min to reach a maximum of 15.4% after 240 min. Finally, fine slag presented a size reduction of 8.6% at 120 min and attained 10.0% size reduction after 180 min. The difference of treatment response between the coarse and the fine fraction, at 240 min, was 9.8% greater for the rhyolite and 7.2% for the slag, while quartzite showed an increase of 10.6% (more than double of size reduction efficiency). Highest reduction ratio (RR) was of 1.25 for fine quartzite, while coarse slag presented the lowest RR at 1.02.
Most of the size reduction process seemed to occur before the 120 min treatment; afterwards time increase had less impact on the rock size. This may suggest that new fine particles came from sharp edges first. Once the original sample particles were rounded or smoothed, the energy necessary to chip away new particles increased, slowing down the process of size reduction.

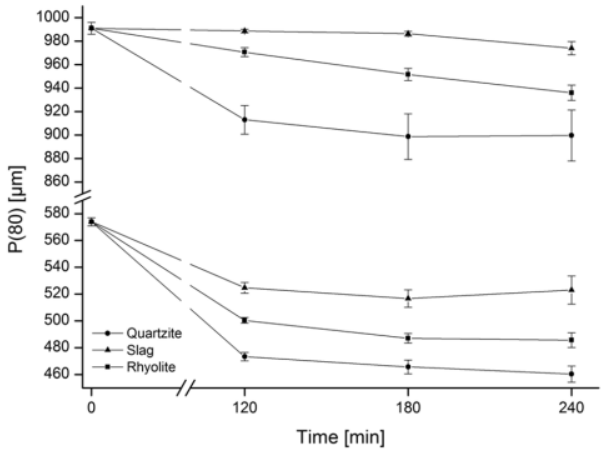

Figure B.3. Fine and coarse fraction response to ultrasound treatment as a function of time.

The effect of power applied to pulp, series (ii) of experiments, is shown in Figure B.4. Power levels of 40W and 55W were applied to coarse quartzite which only responded by a P80 decrease of

approximately 2% from the original 991 µm size in either case. When power was increased to 70W, size reduction efficiency considerably increased as P80 size reduction jumped from 2% to 7.9%. In the case of coarse rhyolite, the effect of power was only significant at 70W with a P80 reduction of 2.1%. Finally, the effect of power applied on coarse slag was noticeable at 70W only, with a P80 reduction of 0.5%. Quartzite and rhyolite fine particles presented a P80 reduction between 1.0% to 2.5% for a power of 40W and 55W and both showed a dramatic increase in efficiency when a power of 70W was applied, reaching values between 9% to 10%. Fine fractions of slag showed a change in response at 70W, compared to coarse fractions, with a P80 size reduction of 5.1% with respect to the 574 µm original size. The highest reduction rate (RR) was 1.21 for fine quartzite at 70W.

These results concur with the theory presented, since an increase on power intensity (power/area of probe) increased the probability of cavitation events per unit volume. Therefore, power increase is proportional to size reduction effects in the range of 40W to 70W.

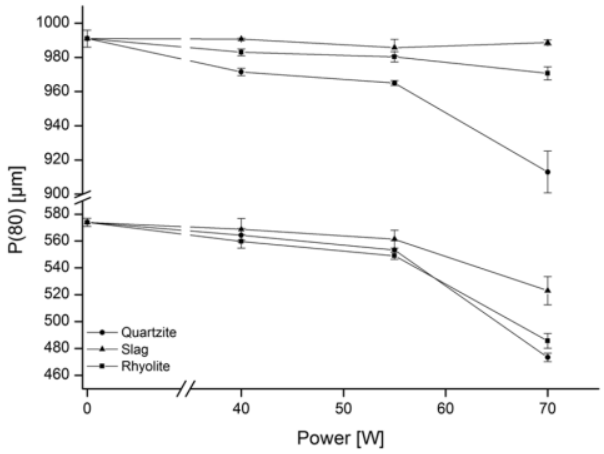

Figure B.4. Fine and coarse fraction response to ultrasound treatment as a function of power delivered by the ultrasound generator.

The effect of distance between probe and rock sample, corresponding to the series (iii) of test, is shown in Figure B.5. The best results were observed for a 10 mm distance, with a P80 size reduction of 17.5% and 12.8% for quartzite and rhyolite, and 8.6% for slag, with respect to the original size of 574 µm. A 20 mm distance showed results ranging from 5.1% to 2.8% P80 size reduction for the three materials. A further increase in distance to 30mm did not show any significant change in response. A distance of 10 mm had the best effect on size reduction and decreased as distance from the tip of the probe increased, explained by an ultrasonic intensity decrease with distance. The curve trend fitted with the ultrasonic intensity equation presented in eq. 2. Therefore, ultrasound treatment efficiency decreases with distance at an exponential rate. Distances smaller than 10 mm were found to be impracticable, due to the dynamics of the solid material movement.

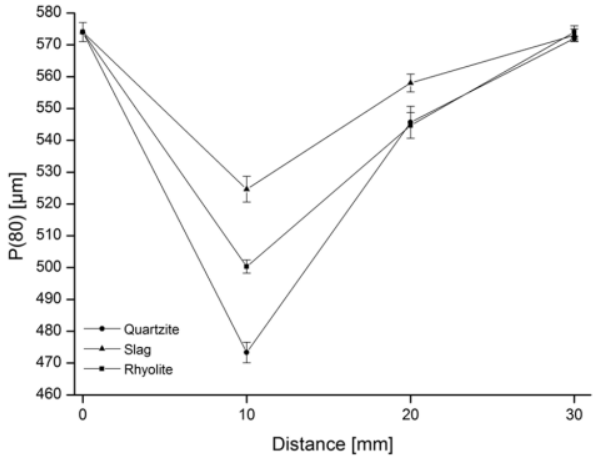

Figure B.5. Fine fraction response to ultrasound treatment as a function of distance to the tip of the probe.

Figure B.6 shows the new particles (passing 35#) generated from the coarse size fraction after sonication treatment. Quartzite presented some medium size particles and mostly fine new particles with round edges. Rhyolite appeared as relatively smaller new particles with round edges, meanwhile slag new particles were mainly a fine powder.

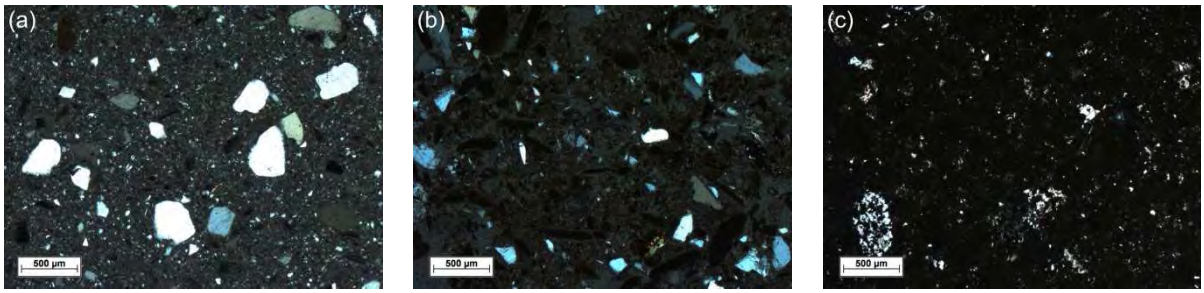

Figure B.6. Transmitted light microscopy images of (a) quartzite, (b) rhyolite and (c) steel furnace slag; fine new particles generated with ultrasound treatment. (cross-polarized light, 25x)

Figure B.7 shows coarse fraction particles of each rock after sonication treatment. Particles presented rounded edges for each material analysed. Moreover, there was no evidence of intra-particle fracturing.

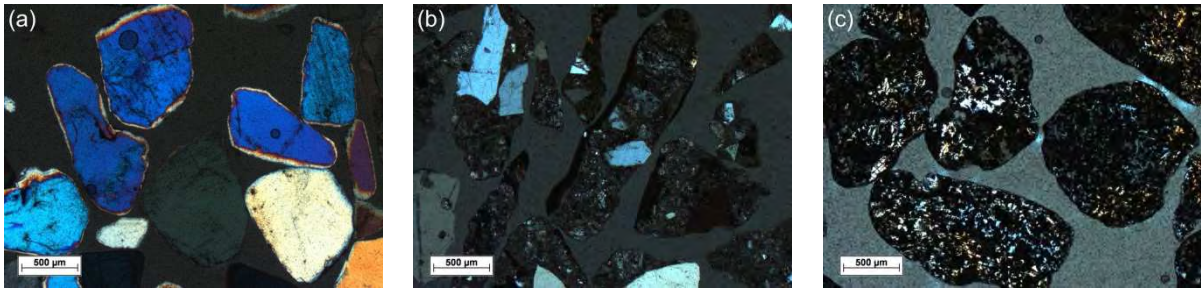

Figure B.7. Transmitted light microscopy images of (a) quartzite, (b) rhyolite and (c) steel furnace slag; coarse fraction particles smoothed after ultrasound treatment. (cross-polarized light, 25x)

The treatment was not effective enough to fracture entire particles; most of the new fine particles come from the erosion and chipping of the particle surface. Coarse particles mostly preserve their original size, but with their edges smoothed, rounded shapes mean less area exposed to sonication.

Finally, the results of the series (iv) of experiments are presented in the form of SEM images of the particle surface before and after treatment. In Figure B.8 the surface of a quartzite particle before and after the sonication treatment is shown. After treatment, surface of the rocks were smoothed, and edges chipped away.

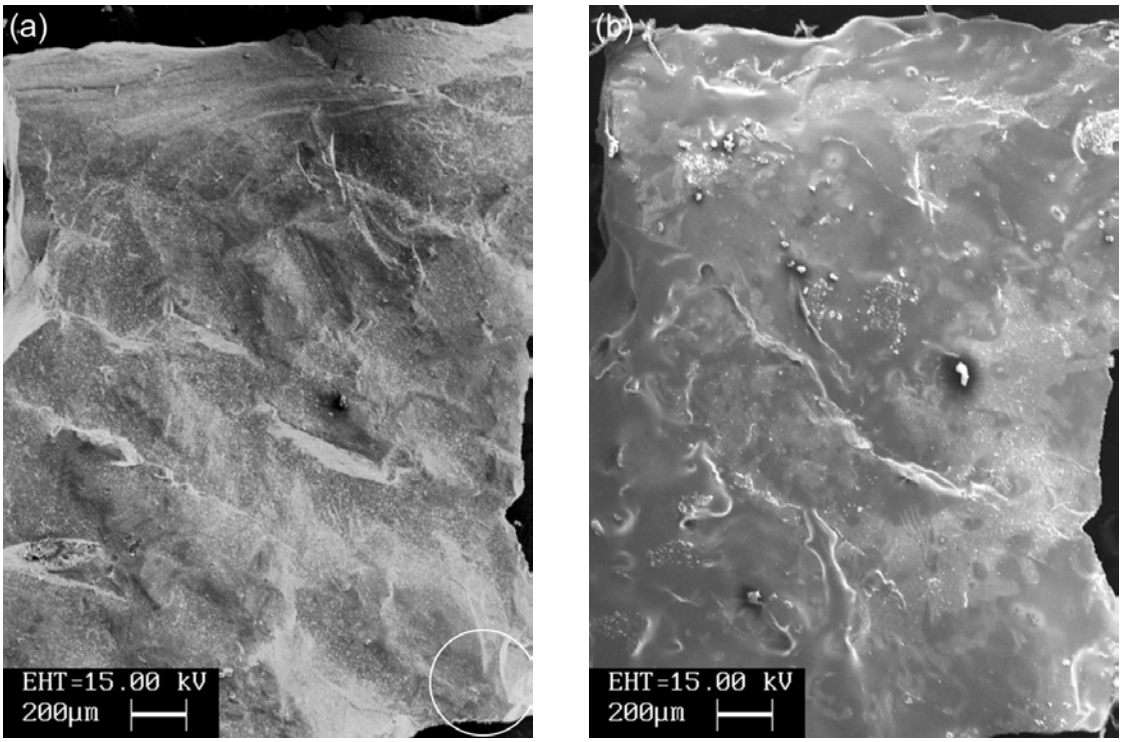

Figure B.8. SEM image of quartzite particle before (a) and after (b) ultrasonic treatment. Effects of micro-jetting on the surface of the particle.

Figure B.9 displays a closer view of the surface of the particle, where ultrasound treatment resulted in the removal of an edge.

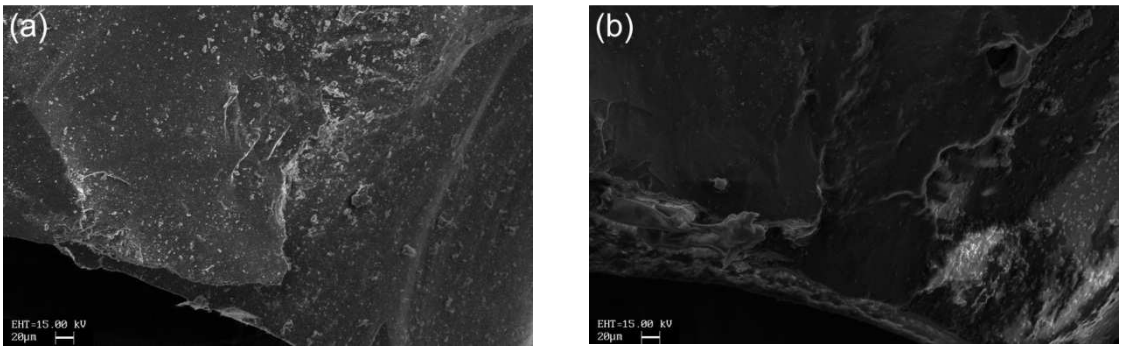

Figure B.9. SEM image of quartzite particle before (a) and after (b) ultrasonic treatment. The image corresponds to the area encircled in Figure A.8 and show the effects of micro-jetting on and edge of the particle.

The particles observed in Figure B.8 and Figure B.9 clearly demonstrates the effect of micro-jetting mechanism on the surface of the particle. Inter-particle collision (due to cavitation shockwave) could be ruled out because of the particular experimental set up, where the particle was fixed to the bottom of the reactor; therefore, only the impact of micro-jetting remained, leading to pitting and erosion of the particle surface. Micro-jetting effects were observed only in the surface, no deep cracks were observed towards the interior of the particles tested.

In general, rock response to micro-grinding treatment was consistent throughout all the experiments, series (i) to (iii): quartzite always had the highest reduction ratio; followed by rhyolite which had an intermediate response between the two other materials; and finally slag, which responded poorly to treatment, regardless of the variables tested. The response to treatment between the coarse and fine size fractions, presented in series (i) and (ii) of experiments, presented also a consistent trend during all the experiments: particle size reduction efficiency doubled in the case of treatment of fine particles.

Since the three rocks had very different physical characteristics (specific gravity, mineral composition, grain size, texture, cleavage, alterations and hardness) the responses to treatment cannot be explained using a simple correlation between one another. Quartzite's response (being quartzite a mono-mineral rock) may be mostly explained in terms of its cleavage, granular texture and brittleness. However, in the case of slag, such simplification may not be acceptable due to the presence of well-formed gehlenite crystals together with spinel and other species. Finally, rhyolite's phorphiric texture and perhaps the presence of the alterations around the grains, render difficult to correlate rock properties and ultrasound mechanisms contributing to the particle size reduction.

B.3.2. Micro-grinding and leaching treatment

Recovery rates are shown in Figure B.10 for slag samples with and without sonication treatment. Recoveries for the sonication treatment ranged from 13.6% to 15.6% for times between 120 to 240 min. SSA of the particles increased from the original 39 $cm^2\ g^{-1}$ to 59 $cm^2\ g^{-1}$ at 120 min, and subsequently, reached 68 $cm^2\ g^{-1}$ at 240 min. Recoveries for the leaching test without sonication ranged between 8.5% to 14.7% for the same time periods.

Ultrasonically assisted leaching gave better yields, thus confirming the properties of sonication as leaching reaction enhancer. The comparison of the two leaching treatments (traditional and

ultrasonically assisted) at different times showed different trends: for ultrasonically assisted leaching, overall recovery values were increased; however the trend seemed to decelerate with time. Meanwhile classical leaching showed an increasing trend, it could not be stated that a plateau would be reached. Two phenomena, not mutually excluding, may explain the trends obtained for ultrasonically assisted leaching. The first phenomenon may be related to the ratio of increment of SSA, which showed, from the initial tests, that the bulk of the new fine particles were generated within the first 120 min, therefore leaching ratio was directly correlated to particle size reduction. The second phenomenon may involve a side effect of cavitation in water: the generation of OH^- (and H^+), which may be causing the chromium ions to be reduced and re-deposited into the solid phase [56].

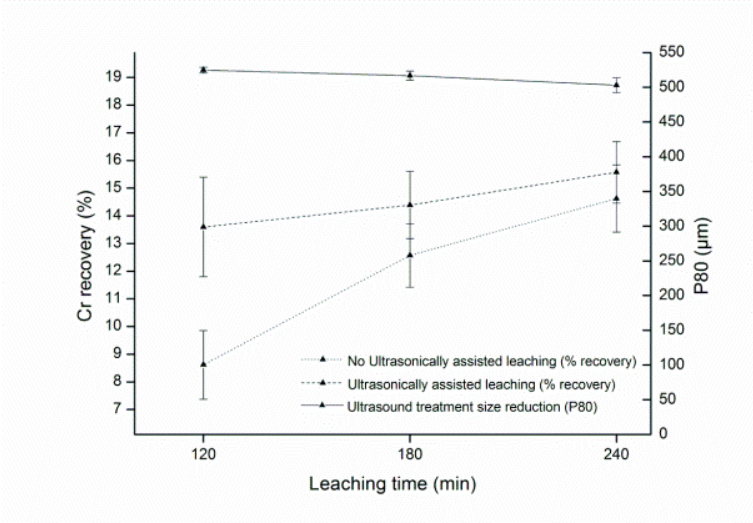

Figure B.10. Chromium recovery in leaching time with and without ultrasound.

B.4. CONCLUSIONS

An ultrasound treatment was performed to investigate the micro-grinding effects of micro-jetting and cavitation shockwave mechanism on three types of rocks. Successively, the treatment was combined with a leaching process, in order to correlate the micro-grinding effects (and area generation) to the sonochemical benefits.

Ultrasound treatment performance presented a considerable relationship with the complex mineral and petrographic features of the rock. Ultrasound introduced energy to the systems that, thanks to the mechanisms presented here, resulted in the size reduction of the particles suspended in the pulp. The magnitude of the response, however, was tied to different rock characteristics. In the conditions presented in this work, ultrasound treatment had a limited micro-grinding effect for coarse particles, but a better effect on finer particles. A particular observation of this work was that the ultrasound treatment created new small particles from sharp edges, but once particles had been smoothed, the generation rate of new particles decreased. Nevertheless, ultrasound treatment solely applied as a grinding process had very poor overall efficiency. The ultrasonic treatment may be only justified when used in combination with a leaching process, in order to obtain benefits both from sonochemical and mechanical effects of ultrasonic cavitation, as verified in this work, with the increase of chromium extraction rate from the slag.

GLOSSARY OF TERMS

- Wear rate is defined as mass of metal loss per mass of erodent crushed. [g of steel/t rock processed]
- Crushing chamber is the void between two crushing liners, where the action of crushing takes place.
- CSS: closed side setting is the gap between the two liners in a crusher. The CSS defines the particle size curve of the product.
- Reduction ratio: F80/P80 characterizes the degree of particle size reduction in a comminution process.

Nomenclature and Acronyms

- SEM: scanning electron microscopy
- EDS: energy-dispersive X-ray spectrometer
- EDM Wire: Electrical discharge machining wire.
- AG/SAG: Autogenous / semi-autogenous grinding mill
- HSI: Horizontal shaft impactor
- VSI : Vertical Shaft Impactor
- HPGR: High pressure grinding roll
- USGS: United State Geological Service
- P80: 80% passing size of product
- F80: 80% passing size of feed
- g.b.c.: grain boundary carbides
- rpm: rounds per minute
- min: Minutes
- s: Seconds
- °C: centigrades
- J: joules

REFERENCES

[1] C. Maranzana, Tesi di Dottorato:“Aspetti microstrutturali e tribologici di un acciaio austenitico al manganese modificato con ti”, Padova: UNIPD, 2006.

[2] F. Maratray, High Carbon Manganese Austenitic Steels, Paris: International Manganese Institut, 1995.

[3] N. Santos, D. Todorov, A. Cavalcanti and R. Fuoco, “Effect of Carbide Re-Precipitation on the Toughness of Hadfield Austenitic Manganese Steels,” *AFS Transactions,* no. 117, pp. 397-412, 2010.

[4] H. S. Avery e M. J. Day, «Austenitic Manganese Steels,» pp. 526-534.

[5] R. Lencina, C. Maranzana, K. Brunelli e M. Dabala, «Studio sull'influenza di un trattamento termico sull'usura e sulla tenacita di due tipi di acciai al manganese,» in *24° Convegno Nazionale Trattamenti Termici*, Piacenza, 2013.

[6] R. Lencina, C. Maranzana, K. Brunelli e M. Dabala, «Studio sulla dinamica di reprecipitazione dei carburi in due acciai al manganese,» in *24° Convegno Nazionale Trattamenti Termici*, Piacenza, 2013.

[7] S. Kuyucak and R. Zavadil, “On the Heat treatment of the Hadfield's Austenitic Manganese Steels - Impact Thoughness, Microstructure, Macro and Micro-segregation in Large Wedge-Block Castings,” *AFS Transactions,* pp. 1-14, 2003.

[8] S. Chakrabartti, «CAST AUSTENITIC MANGANESE STEELS».

[9] O. Aydin Ayasoy, «Effect of Alloying Elements and Heat Treatment on the structure and Properties of Hadfield's Austenitic Manganese Steels,» *Z. Metallkde,* pp. 463-471, 1983.

[10] N. Tsujimoto, «Casting Practice of Abraion Resistant Austenitic Manganese Steel,» *South East Asia Iron and Steel Institute Quaterly,* 1978.

[11] T. Gladman, The Physical Metallurgy of Microalloyed Steels, London: The Institute of Materials, 1997.

[12] F. Haakonsen, Optimizing of Strømhard austenitic manganese steel, Trondheim: Norwegian University of Science and Technology, 2009.

[13] N. V. P. D. E.G. Moghaddama, «On the comparison of microstructural characteristics and mechanical properties of high-vanadium austenitic manganese steels with the Hadfield steel,» *Materials Science and Engineering A,* p. 260– 266, 2012.

[14] A. Secondin, Tesi di Laurea:"Caratterizzazione di acciai al cromo manganese por l'industria mineraria", Padova: UNIPD, 2005.

[15] S. Amarena, Tesi di Laurea "Caratterizzazione della resistenza ad usura de un acciaio austenitico modificato con l'aggiunta di titanio", Padova: UNIPD, 2004.

[16] A. Capoferri, Tesi di Laurea:"Studio dell'inflienza del titanio sulle propietà meccaniche di acciai austenitici al manganese", Padova: UNIPD, 2003.

[17] K. D. Ashok Kumar Srivastava, «Microstructure and abrasive wear study of (Ti,W)C-reinforced high-manganese austenitic steel matrix composite,» *Materials Letters,* p. 3947–3950, 2008.

[18] E. G. Moghaddama, N. Varahrama e P. Davami, «On the comparison of microstructural characteristics and mechanical properties of high-vanadium austenitic manganese steels with the Hadfield steel,» *Materials Science and Engineering A,* n. 532, p. 260– 266, 2012.

[19] K. D. Ashok Kumar Srivastava, «Microstructural characterization of Hadfield austenitic manganese steel,» *J Mater Sci,* p. 5654–5658, 2008.

[20] S. Kuyucak, V. Y. Gertsma e R. Zavadil, «On the Heat Treatment of Hadfield's Austenitic Manganese Steels: Part VIII: Studies on Microcharacterization,» *AFS Transactions,* pp. 1-10, 2004.

[21] S. Kuyucak and R. Zavadil, "On the Heat treatment of Hadfield's austenitic manganese steels - Part IV: Microstructure vs Impact toughness relationship.," *AFS Transactions,* vol. 02, no. 116, pp. 1-18, 2002.

[22] P. Detrez, «L' acier moulé austénitique au manganese,» *Matériaux et Techniques,* pp. 27-32, 1977.

[23] C. Cason, Tesi di Laurea "Studio sulla dinamica di precipitazione di carburi in un acciaio al manganese", Padova: UNIPD, 2012.

[24] B. A. Wills e T. Napier-Munn, Mineral Processing Technology, Oxford: Elsevier Science & Technology Books, 2006.

[25] M. Yao e N. W. Page, «Influence of comminution products on abrasive wear during high pressure crushing,» *Wear,* p. 105–113, 2000.

[26] J. A. Hawk e R. D. Wilson, «Tribology of Earthmoving, Mining, and Minerals Processing,» in *Modern tribology handbook*, Columbus, Bharat Bhushan, 2001, pp. 1331 - 1400.

[27] A. Gupta e D. S. Yan, Mineral Processing Design and Operation, Perth, 2006.

[28] S. Nikolov, "A performance model for impact crushers," *Minerals Engineering,* no. 15, p. 715–721, 2002.

[29] W. J. Whiten e M. E. Whiten, «Modeling and simulation of high tonnage crushing plants,» *Proceedings of the 12th International Mineral Processing Congress,* vol. 2, p. 148–158, 1979.

[30] I. Sare and A. Constantine, "Development of methodologies for the evaluation of wear-resistant materials for the mineral industry," *Wear,* no. 203, pp. 671-678, 1997.

[31] I. Sare and J. Mardel, "Wear-resistant metallic and elastomeric materials in the mining and mineral processing industries—an overview," *Wear,* no. 250, pp. 1-10, 2005.

[32] A. Garcia, A. Varela, L. Garcia, M. Rio, S. Naya e M. Suarez, «Comparing the tribological behaviour of an austenitic steel subjected to diverse thermal treatments,» *Wear,* n. 258, p. 203–207, 2005.

[33] J. Eloranta, “Improving cost efficiency and aggregate quality in crushing plants,” Metso Minerals, 2004.

[34] Mineral Research and Test Center, “Rock test report,” Metso Minerals, Tampere, 2003.

[35] V. Ratia e I. Miettunen, «Surface deformation of steels inimpact-abrasion: The effect of sample angle and test duration,» *Wear,* pp. 94-101, 2013.

[36] A. Garcıa, A. Varela, L. Garcıa, M. C. Rıo e S. Naya, «Comparing the tribological behaviour of an austenitic steel subjected to diverse thermal treatments,» *Wear,* p. 203–207, 2005.

[37] F. Pitard, «Practical and Theoretical Difficulties when Sampling Gold,» in *Mineral Processing Plant Design, Practice and Control*, Littleton, Colorado, Society for Mining, Metallurgy and Exploration Inc. (SME), 2002, pp. 77-98.

[38] F. Pitard, Pierre Gy's Sampling Theory and Sampling Practice, Boca Ratons: CRC Press LLC, 1993.

[39] P. V. R. Salminen, “Rock Drillability Study,” Helsinki University of Technology, Helsinki, 1985.

[40] C. Maranzana, K. Brunelli and L. Peruzzo, “Influence of hardening by heat treatment and rock characters on wear resistance of White Cast Iron 25%Cr under repeated-impact abrasion,” in *Proceedings of Abrasion*, Trento, 2008.

[41] B. S. D. ,. L. W. C. ZUIDEMA, “The Effect of Aluminum on the Work Hardening and Wear Resistance of Hadfield Manganese Steel,” *METALLURGICAL TRANSACTIONS A,* vol. 18A, pp. 1629-1639, 1987.

[42] J. Leaver, Austenitic Manganese Cast Steels, B.S.C.R.A., 1966.

[43] J. Tasker, Austenitic Manganese Steel – Fact and Fallacy, The Frog, Switch and Manufacturing Co. U.S.A..

[44] M. Zuliani, Tesi di Laurea:"Studio di un processo di frantumazione in un mulino HSI", Udine: UNIUD, 2011.

[45] R. Marchetto, Tesi di Laurea:"Studio e simulazione del processo di usura di un acciaio Hadfield utilizato nel campo della frantumazione di inerti", Padova: UNIPD, 2013.

[46] A. Bese, “Effect of ultrasound on the dissolution of copper from copper converter slag by acid leaching,” *Ultrasonics Sonochemistry,* p. 790–796, 2007.

[47] M. Oncel, M. Ince and M. Bayramoglu, “Leaching of silver from solid waste using ultrasound assisted thiourea method,” *Ultrasonics Sonochemistry 12,* p. 237–242, 2005.

[48] K. Swamy, K. Narayana and V. Misra, “Bioleaching with ultrasound,” *Ultrasonics Sonochemistry,* p. 301–306, 2005.

[49] H. Kyllonen, P. Pirkonen, V. Hintikka, P. Parvinen, A. Gronroos e H. Sekki, «Ultrasonically aided mineral processing technique for remediation of soil contaminated by heavy metals,» *Ultrasonics Sonochemistry,* p. 211–216, 2004.

[50] L. H. Thompson and L. K. Doraiswamy, “Sonochemistry: Science and Engineering,” *Ind. Eng. Chem. Res.,* pp. 1215-1249, 1999.

[51] Y. Wang and E. Forssberg, “Enhancement of energy efficiency for mechanical production of fine and ultra-fine particles in comminution,” *China Particuology,* pp. 193-201, 2007.

[52] U. Teipel, K. Leisinger and I. Mikonsaari, “Comminution of crystalline material by ultrasonics,” *Int. J. Miner. Process,* p. 183–190, 2004.

[53] L. Gaete-Garreton, Y. Vargas-Hermandez and C. Velasquez-Lambert, “Application of ultrasound in comminution,” *Ultrasonics; Elsevier Science B.V.,* p. 345–352, 2000.

[54] K. Swamy and K. Narayana, “Ultrasonically Assisted Leaching,” in *Advances in Sonochemistry; Vol 6*, Amsterdam, Elsevier Science B.V., 2001, pp. 141-179.

[55] L. Pope, C. Ward e (Ed.), Manual on test sieving methods, ASTM manual series, West Conshohocken, PA: ASTM, 1998.

[56] H. Li, Z. Zhang, S. Tang, Y. Li and Y. Zhang, “Ultrasonically assisted acid extraction of manganese from slag,” *Ultrasonics Sonochemistry,* pp. 339-343, 2008.